Modelling sand-mud dynamics in Delft3D

January, 2024; Modelling sand-mud dynamics in Delft3D

TKI MUSA project

Author(s)

Roy van Weerdenburg, ir.

Ana Colina Alonso, ir.

Bas van Maren, dr.

Modelling sand-mud dynamics in Delft3D

TKI MUSA project

Client	MUSA consortium
Contact	Leo van Rijn and Ymkje Huismans
Reference	
Keywords	Sand, mud, numerical modelling, Delft3D, process formulations, digital flume

Document control	
Version	Version 1
Date	31-01-2024
Project nr.	11204950
Document ID	11204950_TKI-MUSA_04
Pages	68
Status	Final

Doc. version	Author	Reviewer	Approver	Publish
Draft	Roy van Weerdenburg, ir. Ana Colina Alonso, ir. Bas van Maren, dr.	Thijs van Kessel, dr.ir.		

About the MUSA project

Estuaries and tidal basins form the transition zones between land and sea. They provide important habitats for flora and fauna and are extensively used by people, like for navigation. For ecological and navigational purposes, it is important to understand and predict the evolution of channels and shoals, including sedimentation rates and the composition of the bed sediments. The bed material of large estuaries and tidal basins largely consists of mixtures of mud and sand, with predominantly sandy channels and mainly muddy intertidal areas. The interaction between sand and mud, in combination with currents and waves, leads to complex dynamics in these areas, with migrating channels and shoals.

Much is known about the behaviour of the individual sediment fractions, but the knowledge and understanding of sand-mud interaction remains limited, as do the available tools and models to accurately predict the bed evolution and sediment transport rates in sand-mud areas. Existing models, like the ones by Van Ledden (2003), Soulsby & Clarke (2005) or Van Rijn (2007) have only limitedly been verified with observations due to a lack of good quality observational data. Also, none of the available approaches cover the complete spectrum of sand-mud interaction, which includes settling, erosion processes induced by the combination of waves and currents, and the bed shear stress. Therefore, in practice sand and mud fractions are often treated separately. This decoupled approach limits the predictive capacity of numerical models, and therefore the impact assessment of human intervention such as deepening of channels and port construction on maintenance dredging volumes and other morphological changes.

In the MUSA-research project, a consortium of contractors, consultants and research organizations join forces to increase the understanding of sand-mud dynamics by means of fieldwork campaigns and laboratory experiments, and to implement this knowledge in engineering tools and advanced models for the prediction of mud and sand transport and associated morphology in tidal conditions with both currents and waves.

Modelling sand-mud dynamics in Delft3D

31 January 2024

Summary

In the MUSA project, laboratory experiments and field measurements have been carried out to better understand the dynamics of sand-mud mixtures. The work that is described in this report focusses on the reproduction and application of two of the most intriguing findings in numerical models. Hereto, we make use of Delft3D.

The first part of this study focusses on the erosion rates of sand-mud mixtures that were derived from long bed experiments. Based on OBS measurements, erosion rates were determined for different hydrodynamic forcing and different bed composition. An inverse relation was found between the erosion rates and the mud content in the sediment bed. We have reproduced these experiments in a Delft3D model that we refer to as the digital flume, to better understand the obtained data and to evaluate the performance of process formulations in Delft3D in reproducing the observed behavior.

Our model results show that in order to correctly reproduce the observed erosive behavior (decreasing erosion rates for increasing mud contents for a range of $0.13 < p_{mud} < 0.3$), we must account for sand-mud erosion interaction (as defined in van Ledden's (2003) model) in the model set-up. Moreover, we have seen that suspended sand concentrations reach an equilibrium concentration within a short time span, while suspended mud concentrations build up over time. The timing and sequence at which measurements of absolute suspended mud concentrations are taken therefore largely influences the results, and erosion rates should be derived from continuous measurements.

The second part of this study focuses on the dependency between the dry bulk density of sediment mixtures and their critical shear stress for erosion. Short bed erosion tests have shown that starting from pure sandy beds ($p_{mud} = 0\%$, $\rho = 1600$ kg/m^3) the strength of the bed (i.e., the critical shear stress for erosion) increases with increasing mud content up to a certain point (around $\rho \approx 1200$ kg/m^3), after which it decreases again. A formulation that described this behavior was developed in a previous phase of the MUSA project. Here, we have implemented this formulation in Delft3D and we have evaluated its performance on morphological model predictions, for which we used a schematized model of a tidal basin.

In general, it is very difficult to model long-term morphodynamic development including mudflat formation with mudflats that are capable of surviving episodic storms; mud is either too mobile to survive a storm or too immobile to be transported towards the flats. However, when applying the new density-erodibility formulation, which results in a space- and time varying mobility of mud, we are able to reproduce this behavior in a Delft3D model.

To support applications of sand-mud formulations in Delft3D, we have included instructions on practical aspects of working with these formulations in this report. Besides, we discuss in which engineering applications these formulations may be of crucial importance.

Modelling sand-mud dynamics in Delft3D

31 January 2024

Contents

Modelling sand-mud dynamics in Delft3D

31 January 2024

Modelling sand-mud dynamics in Delft3D

31 January 2024

MUSA

1   Introduction

1.1   Motivation

The main objective of the MUSA project is to improve and develop the engineering tools and numerical models that are needed to deal with sand-mud mixtures in estuarine and coastal systems. This requires fundamental knowledge on the behaviour of sand-mud mixtures. In previous phases of the MUSA project, lab- and field experiments have been executed to better understand the erosion behaviour of sand-mud beds, the deposition fluxes and the accompanied settling velocities, and the bed density. This work builds upon the findings of these experiments (see Boechat Albernaz, et al., 2022, 2023a), with a primary focus on the erosive behaviour, by means of numerical modelling.

Several formulations exist in literature describing the separate and combined sand-mud transport. In previous work, sand-mud interaction formulations were implemented in Delft3D and tested with a schematized model of a tidal basin (Colina Alonso, et al., 2020; see also: van Ledden (2006) and Scheel, et al. (2012) for earlier tests with sand-mud interactions in tidal basins). This work showed that including sand-mud interaction in numerical models largely influences the long-term morphodynamic development, altering bed level evolution and sediment composition. Although these formulations were based on experimental findings, the resulting erosion rates have not been extensively validated against experimental data. In addition, experimental data from previous phases of the MUSA project has resulted in a new formulation for the erosive properties of sand-mud mixtures, but the performance of this formulation in numerical models has yet to be investigated.

1.2   Objectives and approach

This report focuses on the reproduction of two types of results of earlier MUSA phases in numerical models. We define a specific objective and approach for each of these two results:

1)   **Sand-mud erosion rates derived from the long bed experiments.**
The long bed experiments and the corresponding insights that were obtained in previous phases of the MUSA project (see for the latter also: van Rijn et al., 2023b) are reproduced in Delft3D to:
- better understand the data of the concentration and erosion rate measurements;
- evaluate the performance of Delft3D in reproducing the observed behavior;
- determine what sand-mud erosion formulations (related to sand-mud interaction) are necessary to reproduce the observed behavior, and identify improvements.

Hereto, a model is set up ('*digital flume*') aiming at closely resembling the experiments.

2)   **The dependence of sediment erodibility on the dry bulk density, as derived from the short bed experiments.**
Analysis from short bed experiments has resulted in a new formulation for the dependence of the erodibility (τ_{cr}) of sand-mud mixtures with the dry bed density (see van Rijn et al., 2023b). Typically, τ_{cr} is a fixed parameter in morphodynamic models — unless consolidation modules are applied, which are usually numerically expensive (depending on the level of detail that is included) — which introduces limitations for modelling morphodynamic evolution of muddy systems including high-energetic storm conditions.

The new density-erodibility formulation is implemented in Delft3D to:
- evaluate its performance on long-term morphodynamic simulations;
- determine its potential for modelling the effects of storms.

This formulation is tested on a case of morphodynamic evolution of a schematized tidal basin ('*tidal basin model*').

Modelling sand-mud dynamics in Delft3D

31 January 2024

1.3   Outline

The outline of this report is as follows: In Chapter 2 we briefly summarize the flume experiments and the corresponding findings. Herein, Chapter 2.1 focusses on the first aspect (findings on erosion rates, based on the long bed experiments) and Chapter 2.2 on the second (density-erodibility formulation derived from short bed experiments). In Chapter 3 we introduce our model set-up and settings of the digital tidal flume and the tidal basin model. The modelling results of the digital tidal flume are presented in Chapter 4 and those of the tidal basin model in Chapter 5. In Chapter 6 we discuss these findings and reflect on the relevance of sand-mud modelling in engineering projects. Lastly, concluding remarks are presented in Chapter 7.

2 Laboratory experiments and findings

The flume experiments and the results that were obtained in previous phases of the MUSA project are briefly introduced in this chapter, after which these will be used in the next few chapters to 1) evaluate the performance of the digital flume in Delft3D in reproducing the observed behavior and 2) to evaluate the performance of newly proposed formulations for the erodibility of sand-mud mixtures. Section 2.1 of this chapter is a summary of the long bed experiments with currents and waves described in much greater detail by Boechat Albernaz et al. (2023) and extended with additional analyses on concentration profiles and erosion rates. Section 2.2 provides an overview of the short bed experiments with currents only (described in Boechat Albernaz et al. (2022)) and the results of the extended analyses on the sediment erodibility based on these experiments.

2.1 Long bed experiments

2.1.1 Setup of the long bed flume experiments

The long bed flume in the laboratory of WaterProof is 13 m long and 0.4 m wide. The maximum water depth is 0.6 m. The flow in the flume is generated by a centrifugal pump; given a certain water depth, the pump discharge generates a certain flow velocity in the flume. A mechanical wave maker at the upstream end of the flume is used to generate regular waves. A wave damping ramp at the downstream end of the flume prevents reflection of the waves as much as possible. The pictures in Figure 2-1 show the flume for wave-current experiments.The water in the flume is (re)circulated from the downstream to the upstream end of the flume through a pipeline system. Bedload sediment is trapped in a sediment trap at the downstream end of the flume.

The experiments that are reproduced by the digital flume in Delft3D are the long bed experiments with waves and currents and with sediment samples that contain sand and mud. The sediment samples in these experiments are 3 m long and were placed in the center of the flume. The thickness of the sediment samples is in the order of 5-7 cm. The resistance against erosion is tested by increasing the hydrodynamic forcing over time. The water depth in the flume is approximately 0.25 m. As listed in Table 2-1, the successive forcing conditions are characterized by an increasing wave height for a certain depth-averaged flow velocity, after which the flow velocity is also increased in steps. Each hydrodynamic condition is applied for approximately 15 minutes up to 1 hour. The wave length varies between 1.3 m and 3.0 m for the different conditions, such that the maximum wave length is as long as the sediment sample in the flume.

Table 2-1 Hydrodynamic forcing conditions that are applied in the long bed wave-current experiments.

Condition	1	2	3	4	5	6	7
Depth-averaged velocity (U [m/s])	0	0	0	0.2	0.2	0.35	0.75
Wave height (H [m])	0.06	0.08	0.12	0.08	0.12	0.08	0.06
Wave period (T [s])	2.0	1.5	1.0	1.5	1.0	1.2	1
Wave length (L [m])	3.0	2.2	1.3	2.2	1.3	1.7	1.3

The flow velocities in the flume are measured by an ADV instrument (Vectrino ADV Nortek). Wave characteristics are measured using wave gauges for measuring instantaneous water level elevations. An OBS optical sensor is used to measure suspended sediment concentrations in the flume at a temporal resolution of 1 Hz. The OBS instrument is mounted on the wall of the flume, just downstream of the 3 m long sediment sample (see Figure 2-1). The output signal of the OBS (in NTU) is converted to a concentration by using a calibration curve that is based on several sediment dilutions of Noordpolderzijl

Modelling sand-mud dynamics in Delft3D

31 January 2024

MUSA

samples (Boechat Albernaz et al., 2022). This calibration curve is used for each of the experiments. Concentration profiles of sand and mud are determined by collecting (water-sediment) samples from the flume at different heights in the water column. These samples are washed over a sieve of 63 µm to determine the sand concentration, after which small subsamples were filtered to determine the mud concentration.
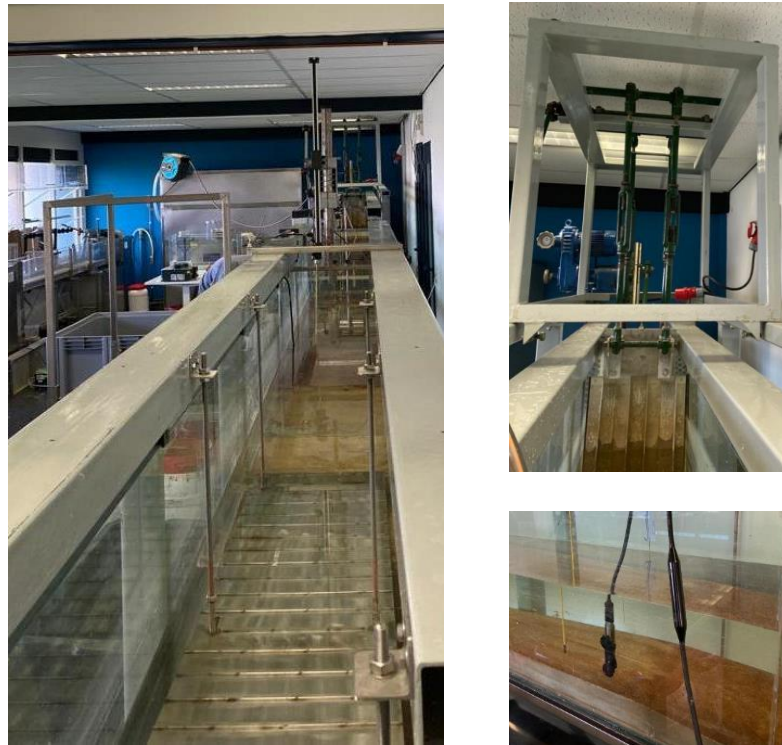

Figure 2-1 Wave-current flume in the laboratory of WaterProof. Left: Flume as seen from the downstream end. Top right: Mechanical wave maker at the upstream end. Bottom right: OBS instrument attached to the wall of the flume, downstream of the sediment sample.

Four different sediment samples are considered in the long bed experiments in the digital flume. The sand-mud mixtures are created by mixing fine sand (d_{10} = 0.05 mm, d_{50} = 0.13 mm and d_{90} = 0.22 m) thoroughly with remoulded (muddy) sediment that was collected in Noordpolderzijl in the Dutch Wadden Sea (p_{mud} = 55%; ρ_{dry} = 780 kg/m³). Adding different amounts of sand to the natural sediment leads to sediment samples with a different mud fraction (Table 2-2). The long bed experiments with 90% mud from Bengal Bay (Boechat Albernaz et al., 2023) are not considered in the digital flume, in order to focus on the transition zone between non-cohesive and cohesive sediment mixtures that is expected around a critical clay content of 5-10% (Van Ledden, 2003). The long bed experiments with only sand are only used to study modelled sand concentration profiles.

Table 2-2 Mud content and dry density in long bed experiments with currents and waves.

	A	I	J	K
p_{mud} [-]	0	0.18	0.13	0.30
ρ_{dry} [kg/m³]	1600	1205	1260	1150

Modelling sand-mud dynamics in Delft3D

31 January 2024

MUSA

2.1.2 Concentration profiles

The collection of samples from the flume at different heights in the water column provides concentration profiles for sand and mud. These are illustrated for the different forcing conditions in Figure 2-2 (mud concentrations) and Figure 2-3 (sand concentrations). Not all hydrodynamic conditions (Table 2-1) are applied for all sediment samples (Table 2-2), such that not all the different sediment samples are represented in the different windows in Figure 2-2 and Figure 2-3. The sediment concentrations were negligibly small for Condition 1, such that no data were obtained.

The measured sediment concentrations reflect instantaneous values, although the experiments ran with constant hydrodynamic conditions for durations up to approximately 1 hour. However, the concentrations are expected to increase in time as long as the erosion rate is larger than the amount of deposition in the flume. The measured concentration profiles may therefore not be representative for the entire experiment. This is studied further by using model simulations, as discussed in Chapter 4.

In general, the measured sediment concentrations near the bottom of the flume increase up to 200 mg/L for mud and up to 500 mg/L for sand. Measured concentrations are generally lower towards the water surface. However, measured sediment concentrations for Condition 7 increase towards the water surface, for which the reason is not completely clear. The increase in concentrations over time is probably the main cause, as the samples from different heights in the water column were taken in series, such that the concentration in the flume had increased by the time the next sample was taken.

Further analysis of the measured concentration profiles is discussed by Boechat Albernaz et al. (2023). Regarding the digital flume that is discussed in this report, the concentration profiles are used to study the results from the Delft3D model (Chapter 4).
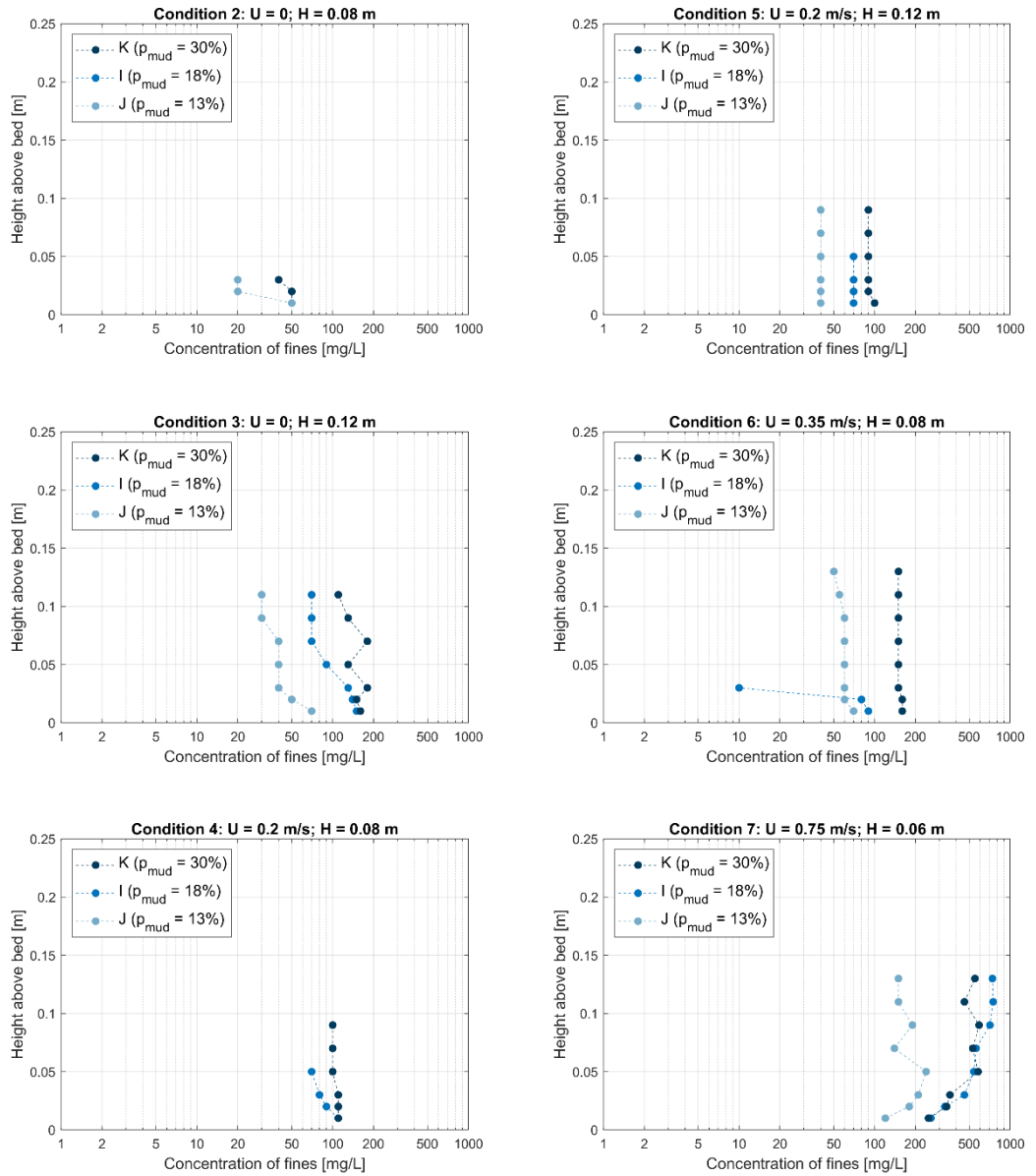
MUSA

Figure 2-2 Measured concentration profiles of fines during long-bed experiments with currents and waves.

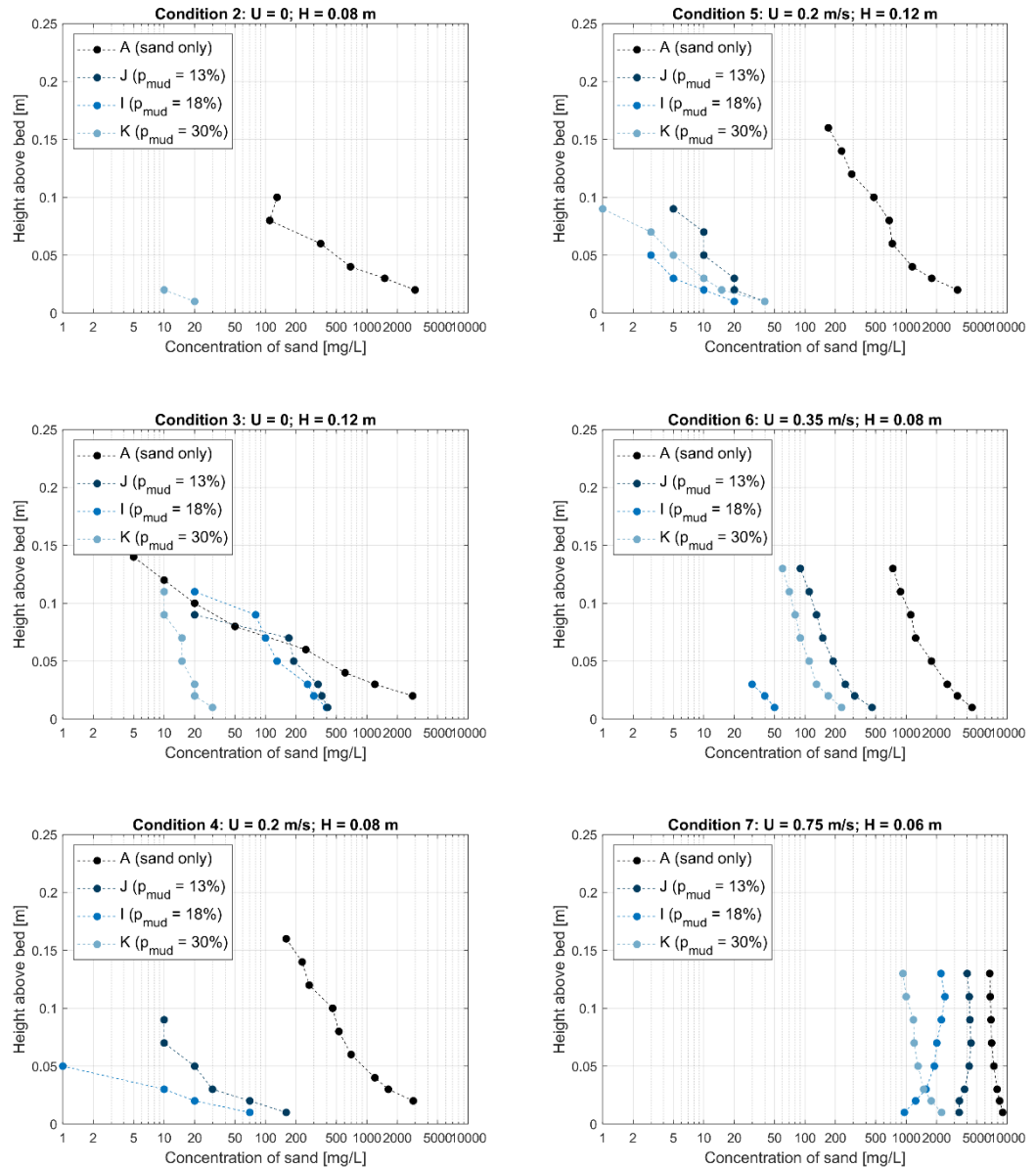Modelling sand-mud dynamics in Delft3D

31 January 2024

Figure 2-3 Measured concentration profiles of sand during long-bed experiments with currents and waves.

2.1.3 Erosion rates

The OBS measurements of suspended sediment concentrations in the flume are used to determine the average erosion rate of sand-mud mixtures during the experiments. The results from the experiments are discussed in this section before they are compared with model results in Chapter 4.

2.1.3.1 Method

Suspended sediment concentrations (SSC) in the flume were measured during the flume experiments by an OBS instrument at 7 cm above the bed. The way in which the change in SSC is used to estimate the average erosion rate is explained below and illustrated for the experiment with sample I, a wave height of 0.12 m and without a current (i.e., Condition 3 of Table 2-2).

Timeseries of the measured SSC have a temporal resolution of 1 second. A moving average over 120 seconds is determined to find a trend in the SSC signal. The moving average is illustrated by the red line on top of the measured concentration data (i.e., data points) in Figure 2-4.
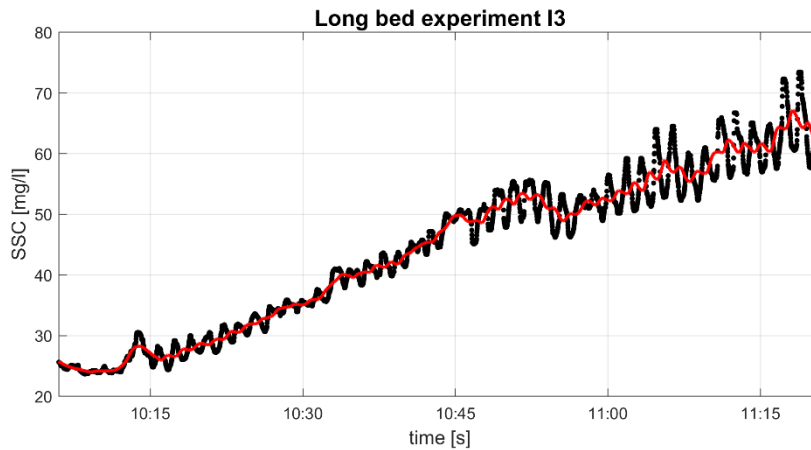

Figure 2-4 Timeseries of the SSC signal (black dots) obtained during experiment I3 (18% mud; H = 0.12 m and no current) and moving average over 120 seconds (red line).

The increasing trend in the SSC signal over the duration of the experiment is used to estimate the average erosion rate. Therefore, it is assumed that the measured signal is representative for the average concentration in the flume. By accounting for (1) the total volume of water in the flume system (V_W = 2.78 m³), (2) the surface area of the sediment sample (A_S = 1.2 m²) and (3) the duration of the flume experiment (T), the increase in SSC (in [kg/m³]) is converted into an average erosion rate (E_{mud} in [kg/m²/s]) following conservation of mass:

$$E_{mud} = \frac{\Delta SSC * V_w}{A_S * T}$$

In this approach, it is assumed that only the mud fraction is observed by the OBS instrument, since the OBS is less sensitive to the sand concentration and most sand is transported in the layer below the OBS level. Basically, it is valid that:

$$E_{tot} = E_{mud} + E_{sand} \tag{2.1}$$

with:

$$E_{mud} = p_{mud} E_{tot} \tag{2.2}$$

and

$$E_{sand} = (1 - p_{mud}) E_{tot} \tag{2.3}$$

Thus, scaling the erosion rate of mud (E_{mud}) with the availability of mud in the bed (p_{mud}) yields:

$$E_{tot} = \frac{E_{mud}}{p_{mud}} \tag{2.4}$$

For the example of experiment I3, the increase in SSC is 37 mg/L over a time interval of 75 minutes. Accounting for the total volume of water in the flume gives an average erosion rate of mud of 1.9e^{-5} kg/m²/s (Table 2-3). Scaling with the availability of mud (p_{mud} = 18%) yields an average total erosion rate of 1.1e^{-4} kg/m²/s.

The OBS instrument was not or at least not successfully used in all the experiments. Therefore, the average erosion rate could only be determined for a selection of the experiments.

2.1.3.2   Results

Without sand-mud interaction, the erosion rate of fine sediments would increase with more mud in the bed (because more mud is available for erosion). The observed critical bed shear stress was similar for experiments I, J and K ($\tau_{crit} \approx 0.3$ Pa; Boechat Albernaz et al., 2023). Therefore, any change in erodibility is caused by the erosion rate parameter M. Interestingly, the relation between M and p_{mud} is opposite to what is expected based on sediment availability.

The estimated erosion rates for different experiments are listed in Table 2-3 and visually presented in Figure 2-5 and Figure 2-6. The hydrodynamic conditions are characterized by the total bed shear stress (Table 2-4). The wave bed shear stresses in Table 2-4 only represent the shear stress by orbital velocities, although we recognize that wave-induced deviator stresses that originate from water pressure gradients on the bed may plan an important role as well (Van Kessel., 1997).

Despite the limited number of data points in Figure 2-5, it follows from this figure that the erosion rate of mud decreases for increasing mud content; the highest erosion rates were generally found for experiment J with $p_{mud} = 13\%$. This relationship becomes more pronounced after scaling the erosion rate with the availability (Figure 2-6). The long bed experiments therefore suggest that the erosion rate decreases with increasing mud content through a reduction in the erosion parameter M, and not an increase of the critical bed shear stress for erosion. Earlier studies (e.g. Jacobs et al., 2011; Mitchener & Torfs, 1996; van Rijn et al. 2020) suggested sand-mud interaction reduces erosion rates through an increase in the critical bed shear stress (and not in M). This behavior is analyzed further by using the digital flume simulations, as discussed in Chapter 4.

Table 2-3 Estimated mean erosion rate during long-bed experiments. Hydrodynamic conditions that were not applied for a certain sample or for which no OBS data was collected during the experiments lead to N/A. The erosion rate of mud (E_{mud}) is scaled by the availability of mud (p_{mud}) to determine E_{tot}.

Condition	Experiment I ($p_{mud} = 18\%$)	Experiment J ($p_{mud} = 13\%$)	Experiment K ($p_{mud} = 30\%$)
Condition 1 $u_c = 0$; $H = 0.06$ m	N/A	N/A	N/A
Condition 2 $u_c = 0$; $H = 0.08$ m	N/A	$E_{mud} = 6.7^{e-6}$ kg/m^2/s $E_{tot} = 5.2^{e-5}$ kg/m^2/s	$E_{mud} = 4.7^{e-6}$ kg/m^2/s $E_{tot} = 1.6^{e-5}$ kg/m^2/s
Condition 3 $u_c = 0$; $H = 0.12$ m	$E_{mud} = 1.9^{e-5}$ kg/m^2/s $E_{tot} = 1.1^{e-4}$ kg/m^2/s	$E_{mud} = 1.8^{e-5}$ kg/m^2/s $E_{tot} = 1.4^{e-4}$ kg/m^2/s	N/A
Condition 4 $u_c = 0.2$ m/s; $H = 0.08$ m	N/A	$E_{mud} = 4.0^{e-6}$ kg/m^2/s $E_{tot} = 3.1^{e-5}$ kg/m^2/s	N/A
Condition 5 $u_c = 0.2$ m/s; $H = 0.12$ m	N/A	N/A	N/A
Condition 6 $u_c = 0.35$ m/s; $H = 0.08$ m	$E_{mud} = 3.7^{e-6}$ kg/m^2/s $E_{tot} = 2.1^{e-5}$ kg/m^2/s	$E_{mud} = 4.3^{e-6}$ kg/m^2/s $E_{tot} = 3.3^{e-5}$ kg/m^2/s	N/A
Condition 7 $u_c = 0.75$ m/s; $H = 0.06$ m	$E_{mud} = 1.6^{e-4}$ kg/m^2/s $E_{tot} = 8.8^{e-4}$ kg/m^2/s	$E_{mud} = 3.5^{e-4}$ kg/m^2/s $E_{tot} = 2.7^{e-3}$ kg/m^2/s	N/A

MUSA

Table 2-4 Total bed shear stress and wave bed shear stress for the different hydrodynamic conditions (Boechat Albernaz et al., 2022).

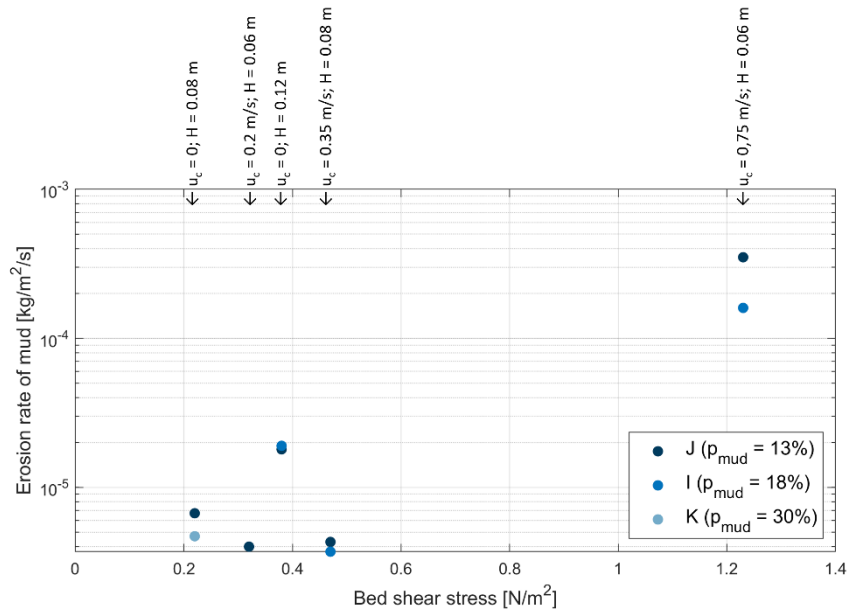| Condition	1	2	3	4	5	6	7
Total bed shear stress according to formulations by Van Rijn (1993) [Pa]	0.13	0.22	0.38	0.32	0.48	0.47	1.23
Wave bed shear stress according to formulations by Van Rijn (1993) [Pa]	0.13	0.22	0.38	0.22	0.38	0.22	0.13

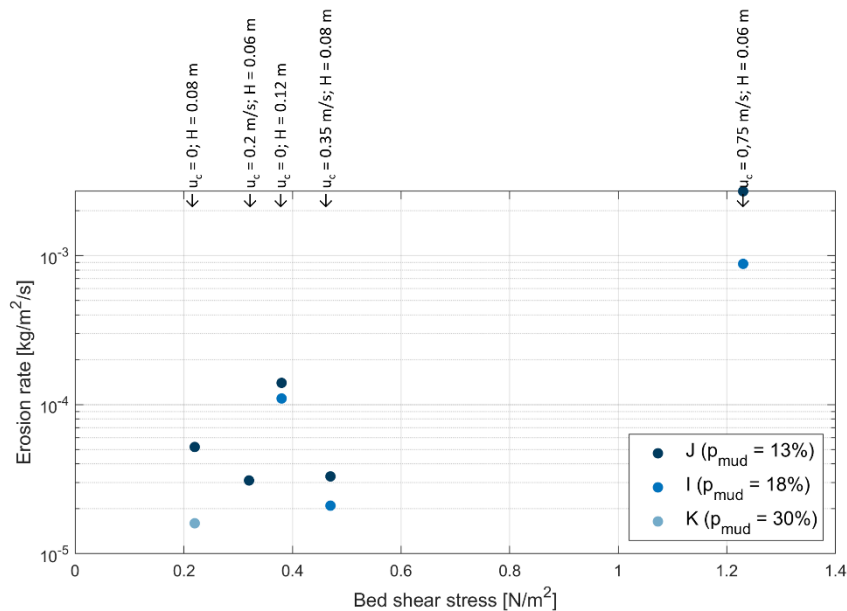*Figure 2-5 Estimated erosion rate of mud during long-bed experiments.*

Figure 2-6 Estimated total erosion rate during long-bed experiments, determined by scaling the erosion rate of mud by the availability of mud.

Modelling sand-mud dynamics in Delft3D

31 January 2024

2.2 Short bed experiments

2.2.1 Setup of short bed flume experiments

Next to the long-flume experiments with currents and waves that were described in the previous section, also experiments have been carried out in a small flume with currents only (see Boechat Albernaz et al., 2022; van Rijn et al., 2023b). The small flume around 5 m long and 0.3 m wide and is illustrated in Figure 2-7. Mud samples are prepared in trays of approximately 15 cm x 10 cm and placed in the central section of the flume. During the experiments, the flow velocity in the flume was increased in steps of 5 cm/s while observing the erosive behavior of the sediment within the compartment. The critical bed shear stress for surface erosion is determined based on visual observations, which are validated by analyzing OBS measurements of suspended sediment concentrations in the flume for a few of the flume experiments (Van Rijn et al., 2023b).

The short bed flume experiments that are most relevant in this report are the experiments with remolded sediment beds. Sediment samples were collected in the Wadden Sea, Western Scheldt and Scheldt River, Plymouth Estuary and Bengal Bay. In the preparation of samples, the sediment was remolded and after filling the sediment trays the top layer was scraped off, such that the sediment surface was levelled with the bottom of the flume. Additional variations in bed density were induced by diluting some of the sediment samples (Boechat Albernaz et al., 2022).

Figure 2-7 Small flume in the laboratory of WaterProof. The flow direction in the flume is from left to right in the picture. The sediment sample is placed in the central section of the flume.

2.2.2 Erodibility as function of the sediment density

The results from the short bed experiments, as well as those documented in previous studies (e.g., Jacobs et al. 2011), show that the dry bed density is a key parameter defining the sediment characteristics that influence the erosion of sand-mud mixtures. While the long-bed experiments showed hardly any variation in the critical bed shear stress, the short-bed experiments covered a wide range of densities and showed that there is a distinct relation between the critical bed-shear stress of the samples and their dry bulk density (see Figure 2-8). For an extensive description of these results, we refer to van Rijn et al. (2023b).

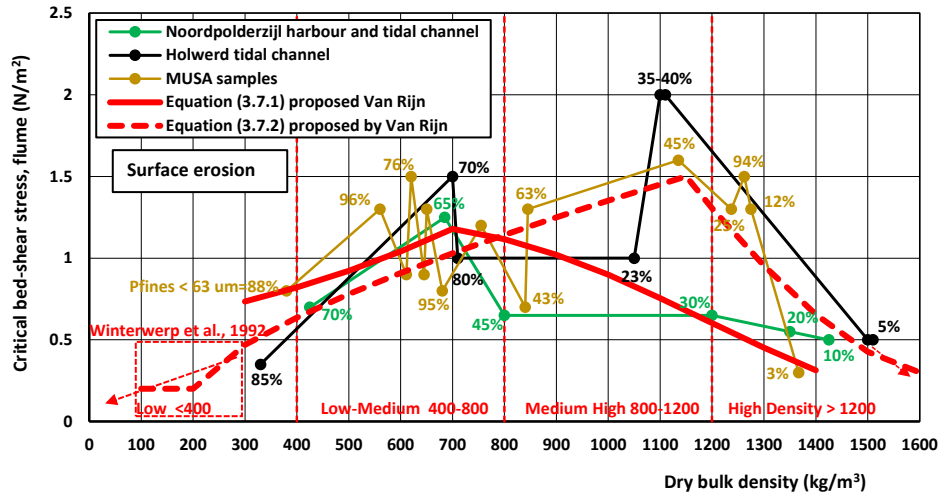Modelling sand-mud dynamics in Delft3D

31 January 2024

Figure 2-8 Measured and computed relation between the critical bed-shear stress of the fine fraction and the dry bed density (van Rijn et al., 2023).

Based on the results of these laboratory experiments, a formulation was developed to determine the critical bed-shear stress for a sediment bed with a certain density (van Rijn et al., 2023), which is as follows:

$$\tau_{cr,fines} = \tau_{cr,min1} + [(\rho_{dry} - \rho_{dry,min})/(\rho_{dry,*} - \rho_{dry,min})]^{\alpha 1}(\tau_{cr,max} - \tau_{cr,min1}) \quad \text{for } \rho_{dry} < \rho_{dry,*} \tag{2.5}$$

$$\tau_{cr,fines} = \tau_{cr,min2} + (\rho_{dry,max} - \rho_{dry})/(\rho_{dry,max} - \rho_{dry,*})^{\alpha 2}(\tau_{cr,max} - \tau_{cr,min2}) \quad \text{for } \rho_{dry} > \rho_{dry,*} \tag{2.6}$$

with:

$\tau_{cr,fines}$ = critical bed-shear stress of fines at dry bulk density ρ_b

$\tau_{cr,min1}$ = critical bed-shear stress of fines (about 0.1 to 0.2 N/m²) at dry bulk density $\rho_{dry,min}$

$\tau_{cr,min2}$ = critical bed-shear stress of fines (about 0.2 to 0.3 N/m²) at dry bulk density $\rho_{dry,max}$

$\tau_{cr,max}$ = maximum critical bed-shear stress of fines (about 1 to 2 N/m²) at dry bulk density $\rho_{dry,*}$

ρ_{dry} = dry bulk density depending on p_{fines}, p_{silt} and p_{sand}

$\rho_{dry,min}$ = minimum dry bulk density (about 200 kg/m³)

$\rho_{dry,max}$ = maximum dry bulk density (of about 1600 kg/m³)

$\rho_{dry,*}$ = dry bulk density (range of 1000- 1200 kg/m³) for which the critical bed-shear stress is maximum

$\alpha 1$, $\alpha 2$ = coefficients (0.5 to 1.5).

The results from this formulation are shown in Figure 2-9, for various combinations of input values.

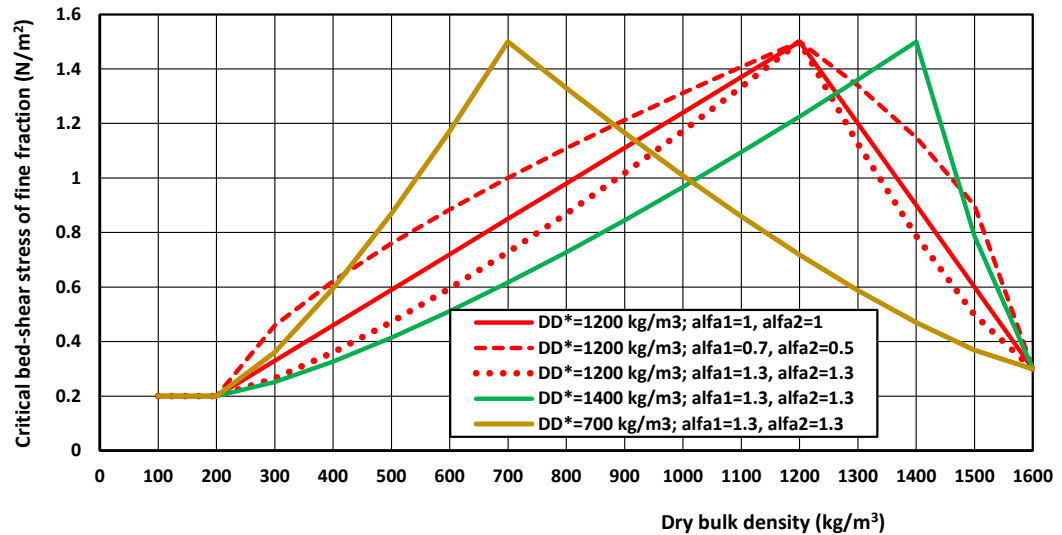Modelling sand-mud dynamics in Delft3D

31 January 2024

Figure 2-9 Proposed relation between the critical bed-shear stress of the fine fraction and the dry bed density (van Rijn et al., 2023). DD=dry bulk density.

2.2.3 Implementing the dry density effect in numerical models

Implementing the dry density effect on erodibility in numerical models may provide an important advancement in morphodynamic modelling. In general, it is very difficult (if not impossible) to model long-term morphodynamic development including mudflat formation with mudflats that are capable of surviving episodic storms. When a high critical bed shear stress for mud erosion is applied, the mud fraction is often too immobile to be transported towards the flats, resulting in modelled morphologies with muddy channels (which are not representative for the conditions in tidal basins like the Wadden Sea). Modelling mudflat formation thus requires lower critical bed shear stresses, but when these are applied, the mud is immediately eroded during a storm event. Yet field observations (such as those by Colosimo et al, 2023) have shown that some mudflats in the Wadden Sea are very well capable of withstanding storms (with bed shear stresses of over 10 Pa). Applying a variable critical bed shear stress that depends on the bulk density (which varies along the simulation) may solve this problem.

Numerical models such as Delft3D usually do not directly compute or consider the density of the sediment bed, and only do so indirectly when computing consolidation effects via a consolidation model or module (e.g., Zhou et al., 2016; Winterwerp et al., 2018), which results in a large increase of the computation time. Yet, some of the input parameters in sediment transport computations do depend on the sediment density (e.g., τ_{crit}), such that their values can be based on their relation to the dry bed sediment density. Even though, the dry bed density is not a parameter in Delft3D, the bed sediment composition is, which holds a direct relation with the bed density. In other words: in case the dry bed density of the modelled system is unknown, it can be estimated based on the sediment composition, following relations such as those previously established by Mulder (2005) or Rijn and Barth (2019) for sediment samples from Dutch intertidal areas, in which a certain degree of consolidation is expected. Both formulations give reasonable estimates of the dry density for MUSA data (see Figure 2-10 and Figure 2-11). The relation by Mulder (2005) slightly underestimates the dry bed density compared to van Rijn & Barth (2019). Note that the silt-rich samples from Bengal Bay are however outliers; neither of the relations are capable of giving a good estimate of their densities.
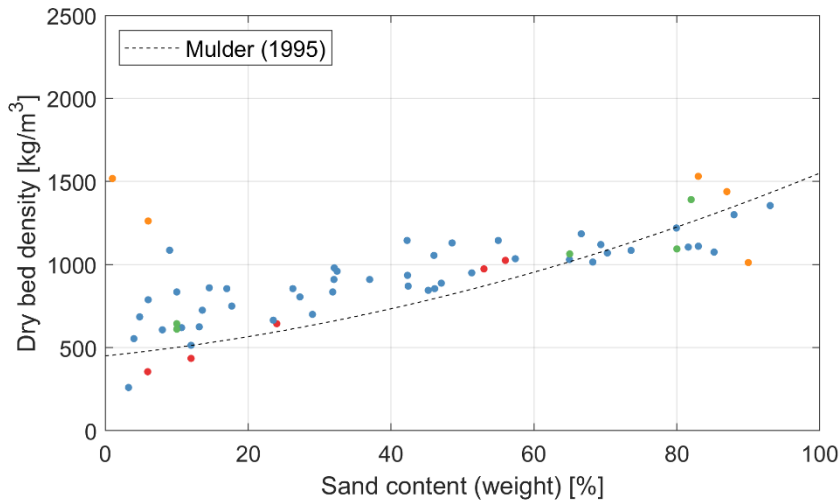
MUSA

Figure 2-10 Relation between the sand content and the dry bed density of sand-mud mixtures based on Mulder (2005). The dots show the sediment samples analyzed within the MUSA project.
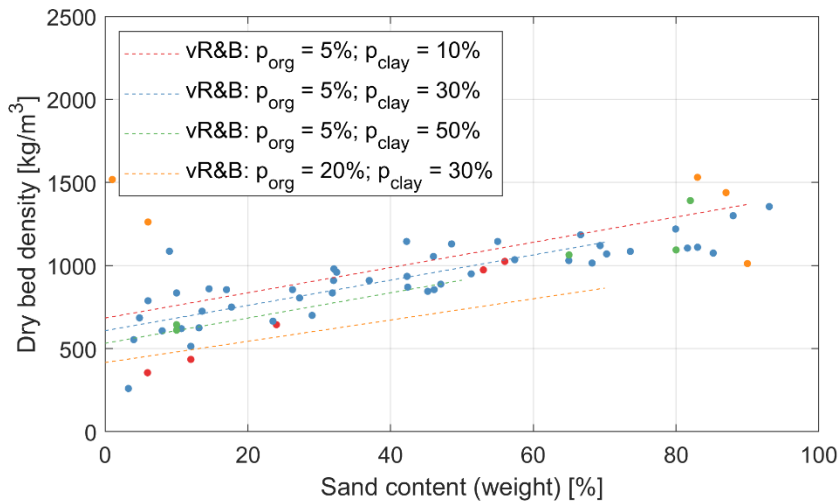

Figure 2-11 Relation between the sand content and the dry bed density of sand-mud mixtures based on van Rijn & Barth (2019). In this relation $p_{clay} + p_{silt} + p_{sand} = 100\%$, which implies that the percentage of organic materials and the percentages of clay, silt and sand are determined from two separate subsamples. The dots show the sediment samples analyzed within the MUSA project.

Modelling sand-mud dynamics in Delft3D
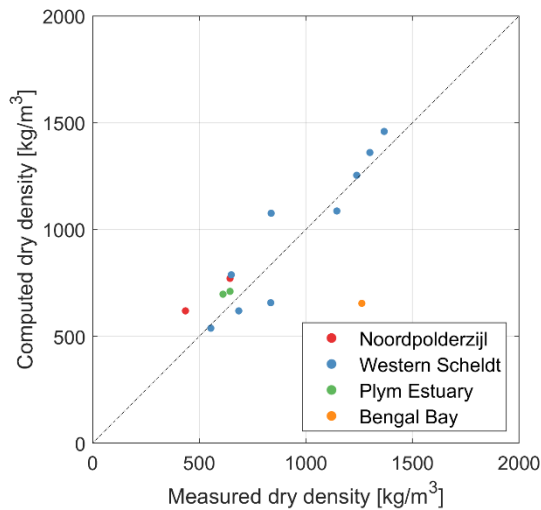
31 January 2024

MUSA

Figure 2-12 Comparison between the measured dry density of the MUSA sediment samples and the computed densities (using van Rijn & Barth, 2019) based on their sediment composition.

These relations between p_{mud} and ρ_{dry} enable an indirect implementation of the effect of the bulk dry density on erodibility (τ_{crit}). Since in Delft3D we typically use CdryB = 500 kg/m^3 for the mud fraction and CdryB = 1600 kg/m^3 for the sand fraction and we don't distinguish clay and silt, for now the dry density may be estimated as:

$$\rho_{dry} = 500\ p_{mud} + 1600\ p_{sand.} \tag{2.7}$$

in which p_{mud} and p_{sand} are volume fractions (i.e. in contrast to the weight fractions in the formulations by Mulder (2005) and Van Rijn & Barth (2019)) and $p_{mud} + ps_{and} = 1$. This equation provides a rough estimate of the dry bulk density; a comparison with measured dry bed densities is illustrated in Figure 2-13. These rough estimates of the dry bulk density disregard a wide body of literature on sediment packing and consolidation. At a later stage, more advanced computations of the dry bed density may be adopted in Delft3D.

The dry bed density is calculated every time step, such that it changes depending on the sediment composition of the bed. Subsequently, the computed density is used in Equations 2.5 and 2.6 (which have also been implemented in Delft3D) to calculate τ_{crit} of the mud fractions and depending on the input settings also that of the sand fractions.
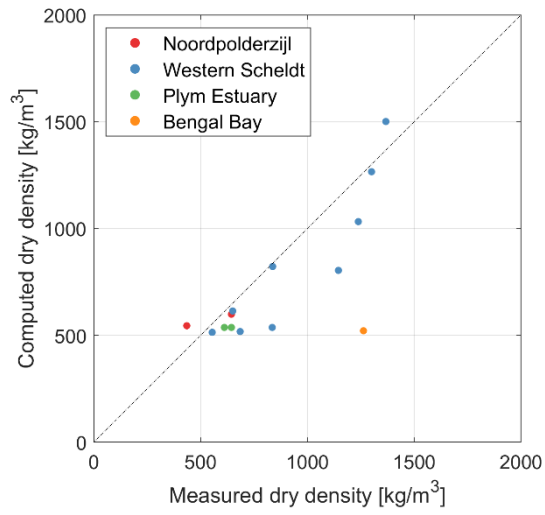
Figure 2-13 Comparison between the measured dry density of the MUSA sediment samples and the computed densities (using Equation 2.7) based on their sediment composition in volume fractions.

Modelling sand-mud dynamics in Delft3D

31 January 2024

3 Delft3D model set-up and formulations

3.1 Part 1: Digital flume

3.1.1 Model schematization and hydrodynamic conditions

The flume of 13 m long and 0.4 m wide is schematized into a digital flume in Delft3D by 65 grid cells of 0.2 x 0.4 m. The vertical direction is schematized by 20 equidistant σ-layers. The recirculation of water is generated in the digital flume by using a coupled intake and outfall. The intake is located in the most downstream grid cell and the outfall is located in the most upstream grid cell. In this way, flow velocities in the digital flume are regulated by the imposed discharge at the intake and outfall. Generating the recirculation by means of such a coupled intake and outfall is preferred over hydrodynamic up- and downstream boundary conditions because the intake and outfall allow suspended sediment concentrations to recirculate through the flume.

The initial water level in the flume is set to 0.25 m. The four most energetic hydrodynamic conditions that were executed in the laboratory flume (3, 5, 6, and 7, see Table 2-1) are modelled in the digital flume. The discharges through the coupled intake-outfall (Table 3-1) are determined based on the flow velocity of a certain hydrodynamic condition and the dimensions of the flume (i.e., 0.4 m wide and a water depth of 0.25 m).

The set-up of the digital flume is illustrated in Figure 3-1 by means of a side view on flow velocities through the flume. The intake is in the rightmost grid cell and the outfall is in the leftmost grid cell. The withdrawal of discharge at the intake and the inflow of discharge at the outfall are uniformly distributed over the water depth. Therefore, the flow velocity profile is developing towards a logarithmic velocity profile over the length of the flume.

Waves are included in the digital flume by a coupling to a Delft3D-WAVE model. The boundary conditions imposed to each of the boundaries of the wave model are constant and uniform and are corresponding to the wave conditions in the laboratory flume experiments (see Table 3-1). Waves are propagating in the direction of the flume ($\varphi = 270°$).

The digital flume is used to model the erosion of sand and mud at time scales of minutes to hours for different hydrodynamic forcing conditions. The hydrodynamic conditions reach a steady state within several minutes. The total simulation time is set to 24 hours. Other settings of the Delft3D model are listed in Table 3-2.
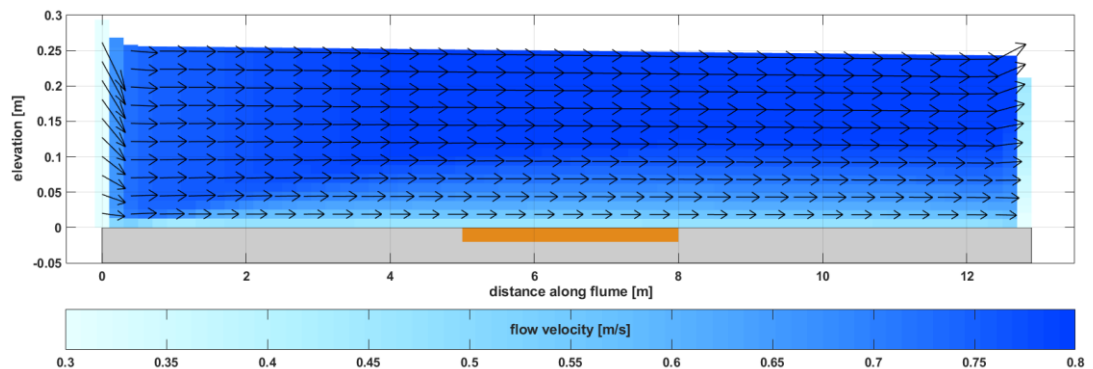

Figure 3-1 Side view of flow velocities in the digital flume in Delft3D for hydrodynamic condition 7 (see Table 3-1). The flow through the flume is generated by the coupling between an intake in the rightmost grid cell and an outfall in the leftmost grid cell.

Table 3-1 Hydrodynamic conditions that are simulated in the digital flume in Delft3D.

Condition	3	5	6	7
Depth-averaged velocity [m/s]	0	0.2	0.35	0.75
Discharge through intake-outfall [m³/s]	0	0.02	0.035	0.075
Significant wave height [m]	0.12	0.12	0.08	0.06
Peak wave period [s]	1.0	1.0	1.2	1
Total bed shear stress in Delft3D computations [Pa]	0.36	0.45	0.50	1.43

Table 3-2 Settings of the Delft3D model of the digital flume.

Parameter	Keyword	Setting
Uniform bottom roughness (White-Colebrook)	Ccofu / Ccofv	0.0005 m
Uniform horizontal eddy viscosity	Vicouv	0.1 m²/s
Uniform horizontal eddy diffusivity	Dicouv	10 m²/s
Type of turbulence closure model	Tkemod	K-epsilon
Bottom stress formulation due to wave action	Rouwav	VR04

Flow regimes

The spatial scale of the digital flume is smaller than in typical applications of Delft3D (open channel flow in rivers and coastal environments which are always turbulent), and under these conditions the flow may become laminar (conditions for which Delft3D may not be applicable). We therefore evaluate the flow regimes for the different hydrodynamic conditions using the formulations by Soulsby and Clarke (2005). The Reynolds number for flow is computed as:

$$Re_c = \frac{Ud}{\nu}$$

in which U is the depth-averaged flow velocity, d is the local water depth and v is the kinematic molecular viscosity of water. The critical Reynolds number for laminar flow is 2000. Given the local water depth of 0.25 m and a kinematic molecular viscosity of $1e^{-6}$ m²/s, a flow velocity of 0.008 m/s leads to the critical Reynolds number of 2000.

In case of combined flow and waves, waves are affecting the critical Reynolds numbers for flow and both the critical Reynolds numbers for flow and waves should be considered (Soulsby and Clarke, 2005). Flow is turbulent as long as $Re_c > Re_{c,cr}$ and $Re_w > Re_{w,cr}$, where:

$$Re_{w,cr} = 1.5 * 10^5$$

$$Re_{c,cr} = 2000 + (5.92 * 10^5 Re_w)^{0.35}$$

The Reynolds number for waves is determined as:

$$Re_w = \frac{U_{orb}A_{orb}}{\nu}$$

in which U_{orb} is the wave orbital velocity, A_{orb} is the wave orbital excursion and v is the kinematic molecular viscosity of water.

Table 3-3 lists the actual and critical Reynolds numbers for each of the hydrodynamic conditions that are simulated in the digital flume. For conditions 5, 6 and 7, the Reynolds number for flow exceeds the critical

Modelling sand-mud dynamics in Delft3D

31 January 2024

MUSA

value, such that the flow regime is turbulent. The Reynolds number for waves, in contrast, is always below its critical value. For condition 3, in which there is no current, the flow regime is therefore laminar. As Delft3D is assuming the flow regime to be turbulent, flow conditions for condition 3 may therefore be different in the digital flume than in the laboratory flume. This will be taken into account by the interpretation of model results for condition 3 in comparison to observed concentrations and erosion rates.

Table 3-3 Actual and critical Reynolds numbers for flow and waves for each of the hydrodynamic conditions.

Condition	3	5	6	7
Reynolds number for flow (Re_c)	NA	50000	87500	187500
Critical Reynolds number for flow ($Re_{c,cr}$)	NA	4615	4323	3609
Reynolds number for waves (Re_w)	9815	9815	6997	2454
Critical Reynolds number for waves ($Re_{w,cr}$)	150000	150000	150000	150000

3.1.2 Sediment transport settings and formulations

Two sediment fractions are included in the digital flume in Delft3D: one sand fraction and one cohesive mud fraction. The sediment properties of both fractions (Table 3-4 and Table 3-5) are based on the laboratory flume experiments (Boechat Albernaz et al., 2023). The erosion parameter M is used as a calibration parameter to reproduce the observed erosion rates, as will be discussed in more detail in Chapter 4.

A 3 m long erodible sediment bed is located in the middle of the flume (see Figure 3-1). Identical to the flume experiments, there is no initial sediment prescribed in the bed up- and downstream of this sediment sample. The total thickness of the initially prescribed sediment layer in the middle of the digital flume is 0.1 m with a mud content equal to the laboratory flume experiments (Table 2-2). As the amount of erosion during the simulation time is negligibly small in terms of the loss of thickness of the sediment layer, the bathymetry is not updated during the simulation.

Table 3-4 Sediment properties and transport formulation of the sand fraction in the digital flume in Delft3D.

Sand	
D50 (median sediment diameter)	130 μm
Van Rijn (2007) formulations with default settings, unless stated otherwise	

Table 3-5 Sediment properties and transport formulation of the mud fraction in the digital flume in Delft3D.

Mud	
w_s (settling velocity)	0.5 mm/s
τ_{cr} (critical bed shear stress for erosion)	0.3 Pa
Parteniades-Krone formulations	

Modelling sand-mud dynamics in Delft3D

31 January 2024

MUSA

The effect of sand-mud interaction (van Ledden, 2003) on the erosion of sand and mud is going to be studied by different model simulations with different sediment transport formulations and settings. In the reference scenario, sand and mud erode independently according to the Van Rijn (2007) transport formulations for the sand fraction and the Partheniades formulations for the mud fraction. The erosion rates are subsequently scaled with the sand and mud availability in the bed such that the erosion rates without interaction between sand and mud are:

$$E_{sand} = p_{sand}E_{sand;0}$$
$$E_{mud} = p_{mud}E_{mud;0}$$

in which $E_{sand;0}$ is the erosion rate of pure sand, calculated following Van Rijn (2007), and $E_{mud;0}$ is the erosion rate of pure mud, calculated following the Partheniades formulation.

Although erosion rates of sand and mud are not mutually dependent in this approach, following Van Rijn (2007), the presence of mud in the bed does slightly influence the erodibility of sand, following this relation:

$$\tau_{cr;sand} = (1 + p_{mud})^{\beta}\tau_{cr;sand;0}$$

in which $\tau_{cr;sand}$ is the adapted critical bed shear stress for erosion of sand within a sand-mud mixture, p_{mud} is the mud content, $\tau_{cr;sand;0}$ is the critical erosion bed shear stress for pure sand and β is an empirical coefficient which depends on the packing of the bed and is by default set to $\beta = 3$. When accounting for sand-mud interaction (see below), it is however advised to set β to 0.75-1.25 (see also Colina Alonso, et al, 2020).

Following van Ledden (2003), the erosional behavior of sand and mud within sand-mud mixtures is mutually coupled: this is what we refer to as *sand-mud interaction* or *sand-mud erosion interaction*. According to this approach, sand-mud mixtures can be either non-cohesive or cohesive, depending on the composition of the sediment mixture. The transition between the non-cohesive and cohesive regime depends on the clay content $p_{cl,cr}$ which typically is 5-10%. Assuming a constant clay/silt ratio, which is generally valid for Dutch estuarine systems, a critical mud content ($p_{m,cr}$) can be determined at which the transition takes place. For the Dutch estuarine systems, a relatively constant clay/silt ratio of 0.25 leads to a critical mud content of 20-40%.

From experimental and theoretical studies, it follows that the erosion fluxes of sand and mud are proportionally coupled. Herein, erosion of both sand and mud depend on the erosion properties of the non-cohesive or cohesive mixture (Mitchener & Torfs, 1996; Winterwerp & van Kesteren, 2004; van Ledden, van Kesteren, & Winterwerp, 2004; Jacobs et al., 2011; Le Hir et al., 2011). In the schematization following Van Ledden (2003), erosion fluxes of sand and mud both depend on the erosion behavior of the sand fraction in case the mixture is non-cohesive, whereas in a cohesive mixture, sand and mud erosion depends on the erosion behavior of the mud fraction, such that the following relations hold when accounting for sand-mud interaction:

Non-cohesive regime:

$$E_{sand} = p_{sand}E_{sand;0}$$
$$E_{mud} = p_{mud}E_{sand;0}$$

Cohesive regime:

$$E_{sand} = p_{sand}E_{mud;0}$$
$$E_{mud} = p_{mud}E_{mud;0}$$

Here, E_{mud} and E_{sand} in the cohesive regime are derived from a logarithmic interpolation of τ_{cr} and M between $p_{mud} = p_{m,cr}$ and $p_{mud} = 1$. This is straightforward for single sand and mud fractions as in van Ledden (2003), but becomes more complex when applied with multiple sand and mud fractions. Van Kessel, et al. (2012) extended the interpolation of E_{mud} for multiple fractions in the cohesive regime and implemented this version in Delft3D. Here, E_{mud} and E_{sand} in the cohesive regime are also based on an interpolation between their values at $p_{mud} = p_{m,cr}$ and at $p_{mud} = 1$. For details see Van Kessel, et al. (2012) and Colina Alonso, et al. (2020).

MUSA

3.1.3   Application of sand-mud erosion interaction in Delft3D

To include sand-mud erosion interaction in the Delft3D simulations, the $p_{m,cr}$ input variable is required in the *.sed file, such that the top of the *.sed file would for example look like what is listed below.

```
[SedimentOverall]
   Cref            = 1.6000000e+003 [kg/m3]
   IopSus          = 0
   PmCrit          = 0.3
```

In addition, the parameter `BetaM` (β) can be defined in the *.tra file when the Van Rijn formulations are used to determine the transport of sand, such that the *.tra file would for example look like what is listed below.

```
[TransportFormulaFileInformation]
   FileCreationDate = Thu Jul 20 2023, 10:07:00
   FileVersion = 01.00
[TransportFormula]
   Number = -2
   Name = #Van Rijn (2004)#
   BetaM = 1.0
```

MUSA

3.2 Part 2: Tidal basin model

3.2.1 Model schematization and hydrodynamic conditions

The proposed formulation for erodibility as function of the sediment density (Equations 2.5-2.7) is tested for a case study of a schematized tidal basin. Hereto, we make use of the model of Colina Alonso et al (2023, see Figure 3-2). This 2DH (depth-averaged) model is inspired by the tidal basins of the Wadden Sea. The domain consists of a tidal inlet in between two islands and a back-barrier basin with dimensions of 15 x 10 km. The computational grid is regular with a resolution of 100 x 100 m. We work with a stratified bed consisting of an active transport top layer with a thickness of 0.1 m and 20 Eulerian bed layers with a thickness of 1 m underneath. Starting from a sloping bathymetry and a uniform sediment composition (p_{sand} = 0.95, p_{mud} = 0.05), we simulate a full hydrodynamic year with a MorFac of 50, such that the morphodynamic evolution is simulated for a period of 50 years. The mud concentration at the offshore open boundary is set to 5 mg/l, which is representative for offshore concentrations in the North Sea.

During the first 11 hydrodynamic months (corresponding to ~45 morphological years), the model is forced by a semi-diurnal tide with an amplitude of 1.5 m (S2 + S4) entering from the (only) open boundary at the North (located 15 km from the inlet), and a wave-climate created by locally generated wind-waves of varying strength (with wind speeds of 4–8 m/s) and direction (SW-NW). During the last hydrodynamic month (corresponding to ~5 morphological years), we also simulate occasional storms with wind speeds of up to 16 m/s (the 95th percentile of the wind velocities measured in the Dutch Wadden Sea lies between 12-14 m/s, the median lies around 6m/s, see https://systeemrapportage.nl/wadden/).
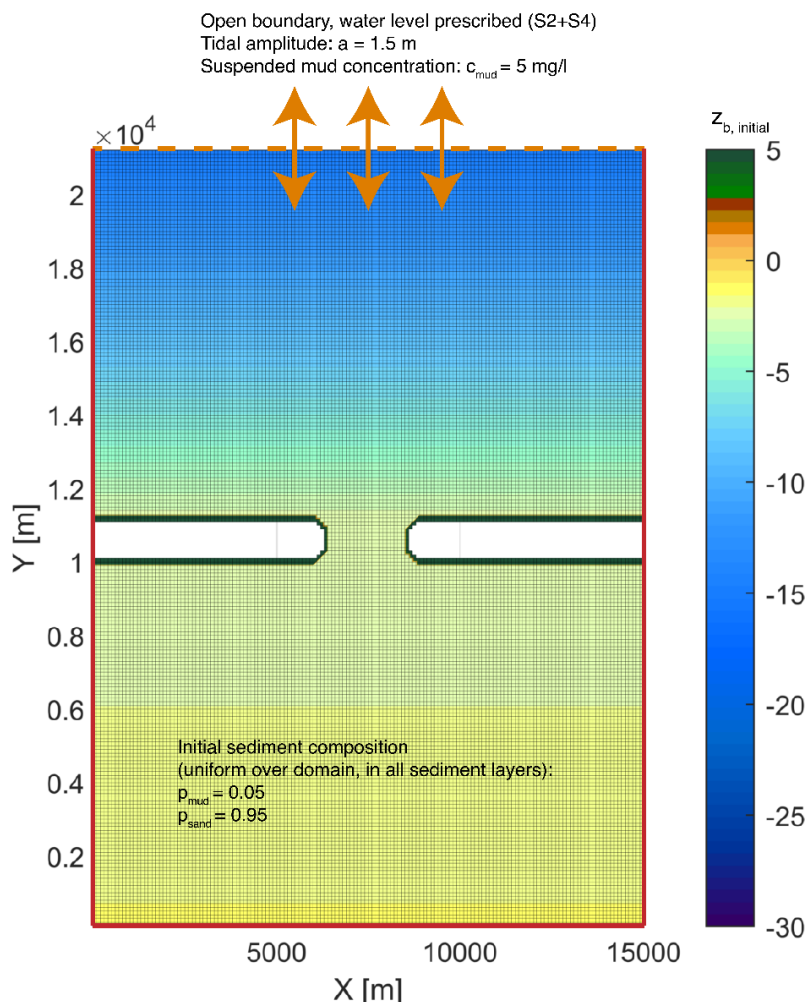

Figure 3-2 *Overview of the model set-up, showing the initial bathymetry, the closed boundaries (red lines), the open boundary (orange dashed line) and the computational grid (for both flow and wave computations, with a resolution of 100 x 100 m.)*

Modelling sand-mud dynamics in Delft3D

31 January 2024

3.2.2 Sediment transport settings and formulations

Simulations are carried out with one medium fine sand fraction (D50 = 250 µm) and one mud fraction. Sand transport is calculated with the Van Rijn transport formulations (van Rijn, 1993) and mud transport with the Partheniades erosion formulation (Partheniades, 1965).

We compare simulations with and without the effect of the dry bulk density (indirectly via the sediment composition as explained in Section 2.2) on the sediment erodibility. When accounting for the density effects, every timestep the dry bed density ρ_{dry} is calculated for every grid cell, and based on the local values, the local erodibility of the mud fraction (τ_{crit}) is computed. Depending on the user settings, the computed τ_{crit} can also be applied to the sand fraction: τ_{crit} is by default only applied to the mud fraction, unless stated otherwise.

In the simulations where the density effect is excluded, the type of mud differs between scenarios, ranging from mud that is easily eroded ($\tau_e = 0.25$ Pa) to consolidated mud ($\tau_e = 1.0$ Pa), and sand erodibility mainly depends on the grain size (following van Rijn, 1993), which is equal for all scenarios.

3.2.3 Application the density effect on sediment erodibility in Delft3D

To include the effects of the sand-mud density on the erodibility of the sediment in the Delft3D simulations, the keyword `IErosion = 5` should be added to the `[Underlayer]` part of the *.mor file, such that the top of the *.mor file would for example look like what is listed below. Below, under the `[Erosion]` section, the values of the user-defined parameters can be set. In case these values are not defined by the user, computations will be executed with the default values, which are the values listed in the overview below.

```
[Underlayer]
   IErosion      = 5
[Erosion]
   rho_min       = 200 [kgm-3]  Min. dry bed density ρdry,min when using IErosion = 5
   taucr_min1    = 0.2 [Pa]   Critical bed shear stress τcr,min1 at minimum dry bed
                   density when using IErosion = 5 (MUSA)
   alpha1        = 1.0  [-]   Non-linearity coefficient α1 when using IErosion  = 5
   rho_star      = 1200[kgm-3]   Dry bed density ρdry,* associated with maximum critical
                   bed shear stress when using IErosion = 5
   taucr_max     = 1.50 [Pa] Max. critical bed shear stress τcr,max when using IErosion =5
   alpha2        = 2 [-] Non-linearity coefficient α2 [-] when using IErosion = 5
   rho_max       = 1600 [kgm-3]  Max. dry bed density ρdry,max [kgm-3] when IErosion = 5
   taucr_min2    = 0.2 [Pa] Critical bed shear stress τcr,min2 at maximum dry bed density
                   when using IErosion = 5
   taucr_min2    = 0.2 [Pa] Critical bed shear stress τcr,min2 at maximum dry bed density
                   when using IErosion = 5
```

To also apply the calculated erodibility of the sediment on the sand fraction, the keyword `ITauCr = 2` should be added to the `[Sediment]` part of the *.sed file in which the sand settings are specified (`SedTyp = sand`), as listed in the overview below.

```
[Sediment]
    Name          = #Sedimentsand#  Name of sediment fraction
    SedTyp        = sand [-]   Must be "sand", "mud" or "bedload"
    ITauCr        = 2 Overrule standard taucr1
```

Modelling sand-mud dynamics in Delft3D

31 January 2024

4 Modelling results part 1: Digital flume

This chapter includes a discussion of model results in comparison to the data that was obtained during the long bed flume experiments that were introduced in Chapter 2. Firstly, in Section 4.1, the reproduction of concentration profiles of sand and mud are discussed. The computed sand concentration profiles are also compared to what is computed by the SEDCON Engineering Tool. In the second part of this chapter, the reproduction of erosion rates with different types of formulations is discussed in detail.

4.1 Concentration profiles

4.1.1 Sand concentration profiles

The sand concentrations in the long bed experiments with sand only (sample A) are reproduced by different models. The measured sand concentrations for condition 6 (0.35 m/s flow velocity and 0.08 m wave height) are illustrated in Figure 4-1, together with computed concentrations by the TR2004 sediment transport model (Van Rijn, 2007) and the SEDCON engineering tool (Van Rijn, 2023). Important settings of the TR2004 and SEDCON models are listed in Table 4-1. With these settings, the sand concentrations for a pure bed can be represented reasonably well (withing a factor of 2) by the models. In the specific case of experiment A6 in Figure 4-1, the sand concentrations are better reproduced by the TR2004 model than by the SEDCON model, which makes sense because SEDCON basically is a simplified version of the detailed TR2004 sediment transport model. In general, the SEDCON model produces somewhat smaller sand concentrations than the TR2004 model (Van Rijn, 2023).
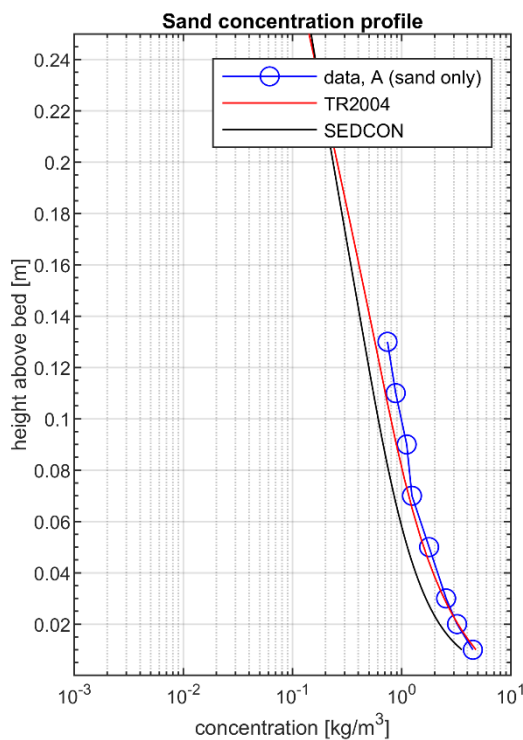

Figure 4-1 Measured and computed sand concentration profiles for the long bed experiment with sand only and hydrodynamic condition 6 (U = 0.35 m/s; H = 0.08 m).

Table 4-1 Settings of the TR2004 and SEDCON sediment transport models to reproduce the computed sand concentration profiles in Figure 4-1. Empty fields imply that the parameter is not a relevant input field for either TR2004 or SEDCON.

	TR2004	SEDCON
settling velocity		10 mm/s
D10	97.5 µm	
D50	130 µm	
D90	195 µm	
bed roughness	0.02 m	0.02 m
critical bed-shear stress		0.15 Pa
reference height	0.01 m	0.01 m
scaling coefficient reference concentration	2	2
scaling coefficient current-related mixing		1.5
scaling coefficient wave-related mixing		1

The implementation of the Van Rijn (2007) sediment transport model in Delft3D is largely based on the original TR2004 model Van Rijn (2004). Using this transport model, the sand concentrations in the digital flume are modelled. The first results are illustrated in Figure 4-3. The TR2004 settings in Table 4-1 were also applied in the Delft3D simulation. In addition, the vertical mixing distribution of the Van Rijn sediment transport model was applied (keyword EpsPar = true in *.mor file).

With this model set-up, the sand concentrations in the digital flume are lower than the concentrations that were measured and computed by the other two transport models. The vertical velocity gradient in Delft3D is small compared to the TR2004 and SEDCON results, such that the flow velocity is larger near the bottom and smaller near the water surface. This is largely due to the different implementation of vertical mixing in Delft3D (i.e. the k-ε turbulence model). The discontinuity in the sand concentration profile near the bed is caused by the fact that in Delft3D, the sediment source and sink terms for suspended sand transport are applied in the first layer above the reference height, as illustrated schematically in Figure 4-2. The reference height in the digital flume is set to 0.01 m and the thickness of each of the layers is approximately 0.0125 m, such that the sink and source terms are applied in the second vertical layer from the bed.
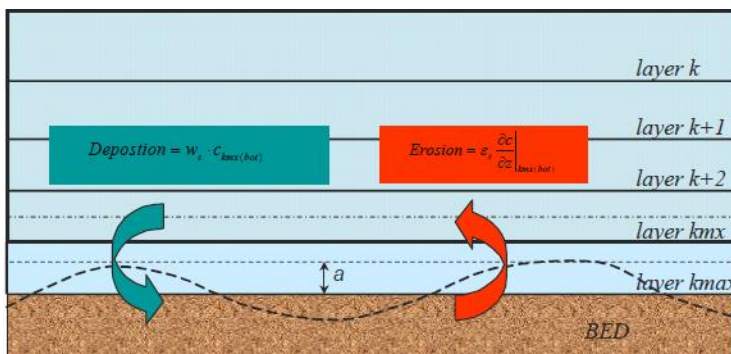

Figure 4-2 Schematic diagram illustrating the application of the source and sink terms for suspended transport of non-cohesive sediments in Delft3D in the first layer above the reference height a.
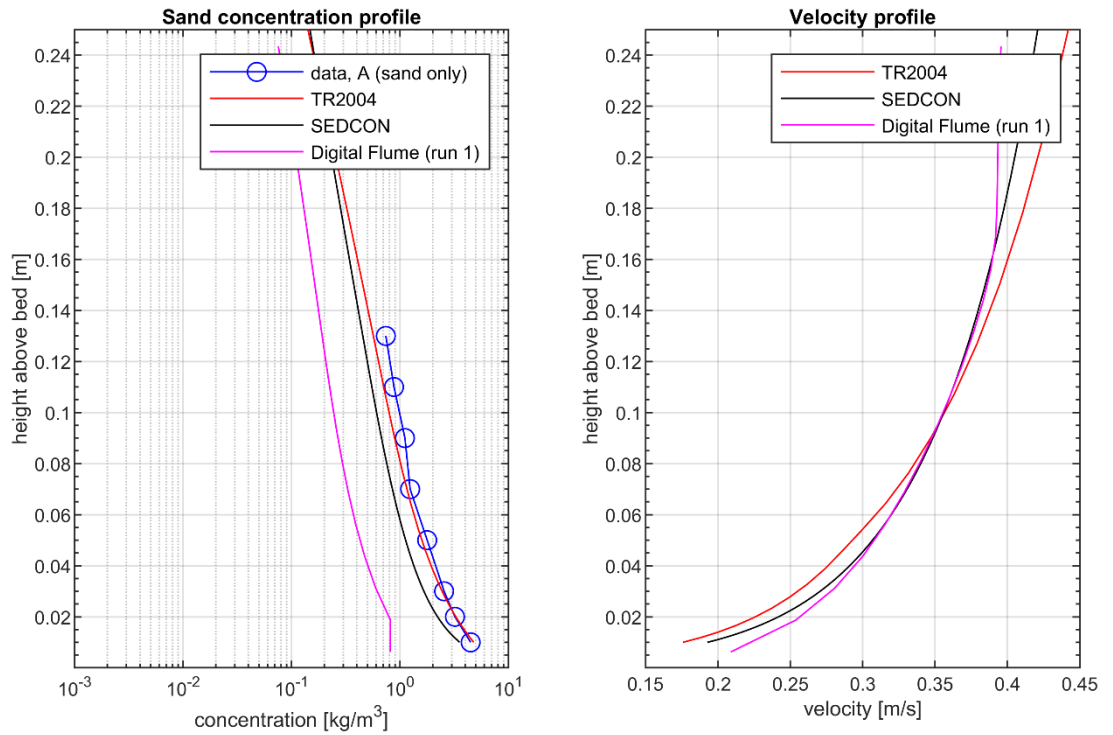
Modelling sand-mud dynamics in Delft3D

31 January 2024

Figure 4-3 Left: Computed sand concentration profiles for the long bed experiment with sand only and hydrodynamic condition 6 (U = 0.35 m/s; H = 0.08 m) compared to measured sand concentrations. Right: Computed velocity profiles.

The underestimation of sand concentrations in Delft3D compared to TR2004 is largely caused by different methods to determine the orbital velocity near the bed. Two important differences are:

1. In contrast to Van Rijn (2007), the root-mean square wave height (H_{RMS}) and not the significant wave height (H_S) is used in Delft3D to determine the sediment transport rate. H_{RMS} is $\sqrt{2} \approx 1.41$ times smaller than H_S, such that the orbital velocity that is used to determine the sediment transport rate is $\sqrt{2}$ times smaller.

2. In Delft3D, the average orbital velocity near the bed is computed based on linear wave theory by

$$u_b = \frac{\sqrt{\pi}}{2} * \frac{\pi f_p H_{RMS}}{\sinh{(kh)}}$$

This formulation follows from the assumption that the probability density function of the wave spectrum follows a Rayleigh distribution. The orbital velocity u_b is therefore $\frac{\sqrt{\pi}}{2}$ times as large as the orbital velocity of a regular sinusoidal wave, for which:

$$u_b = \frac{\pi f_p H_{RMS}}{\sinh{(kh)}}$$

Assuming a Rayleigh distributed wave height thus yields an orbital velocity in sediment transport computations in Delft3D that is $\frac{\sqrt{\pi}}{2} = 0.89$ times as large as in TR2004 and SEDCON.

One way to correct for these two differences in the sediment transport computations is by upscaling the wave height in the digital flume by $\sqrt{\frac{8}{\pi}}$. Doing this for the long flume experiment that was discussed before yields the sand concentrations that are illustrated in Figure 4-4. The computed sand concentrations are now in the same order of magnitude as the results from TR2004. Remaining differences are mostly explained by the different vertical mixing profile and the effect of upscaling the wave height on the flow velocity profile.

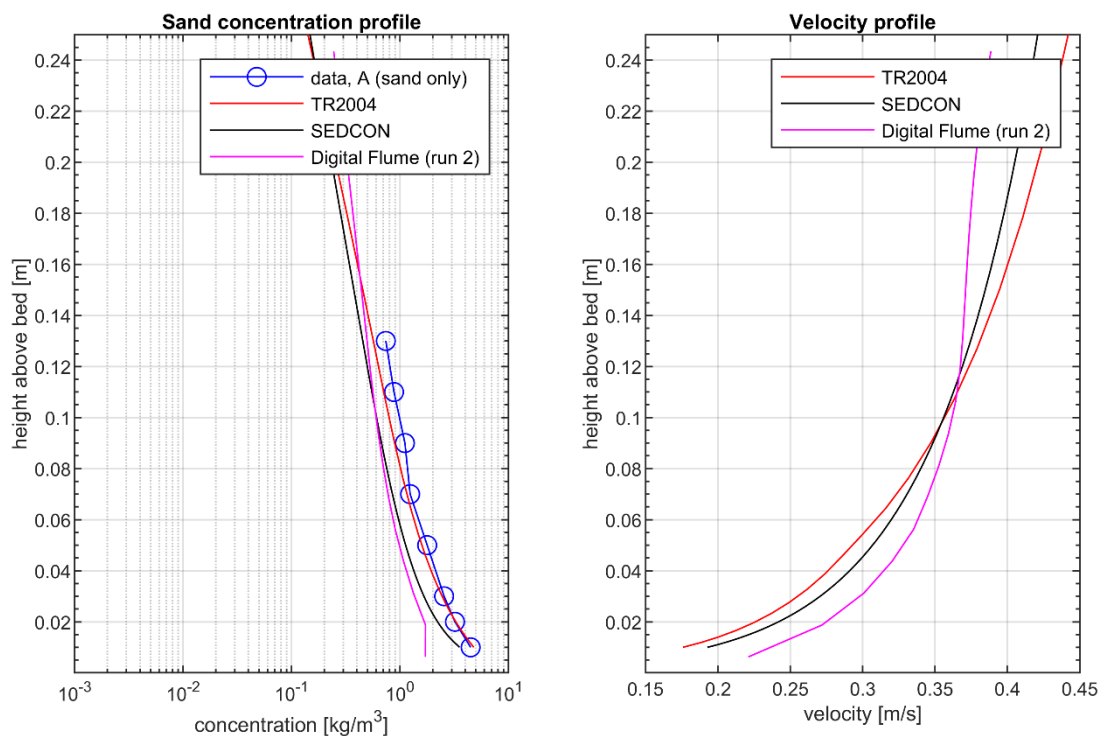Modelling sand-mud dynamics in Delft3D

31 January 2024

MUSA

Figure 4-4 Computed sand concentration (left) and velocity (right) profiles after upscaling the wave height in the digital flume with $\sqrt{\frac{8}{\pi}}$ compared to the results in Figure 4-3.

In Delft3D, the vertical mixing profile in 3D simulations is usually determined by using the k-ε turbulence model. For sand transport computations, however, one can specify to either use the k-ε turbulence for vertical mixing of sediment or to use the vertical mixing distribution according to Van Rijn (2007; `EpsPar = true` in *.mor file)[1]. Figure 4-5 illustrates that the vertical sediment diffusion is much higher in case the Van Rijn (2007) formulations are used. The development of the vertical velocity profile over the length of the flume causes the amount of turbulence in the k-ε model and therefore the vertical eddy diffusivity to increase in downstream direction. In the laboratory experiments, however, the amount of turbulence may already be high at the upstream end of the flume. The vertical mixing is independent of the vertical velocity profile according to Van Rijn (2007) formulations. The impact on the sediment concentrations is illustrated in Figure 4-6: the Van Rijn (2007) formulations yield significantly larger sand concentrations. In this specific case the concentrations are several times larger near the bottom. The difference in sediment concentration increases up to approximately one order of magnitude near the water surface.

―――――――――――――――――――――

[1] By specifying the background vertical eddy viscosity and vertical eddy diffusivity in Delft3D via keywords Vicoww and Dicoww in the *.mdf file, these background values are used for the vertical eddy viscosity and the vertical eddy diffusivity in case they are larger than the values that follow from the k-ε model. However, the background values are not copied to the sediment transport diffusivity, such that the sediment diffusion may be smaller than the background diffusivity.
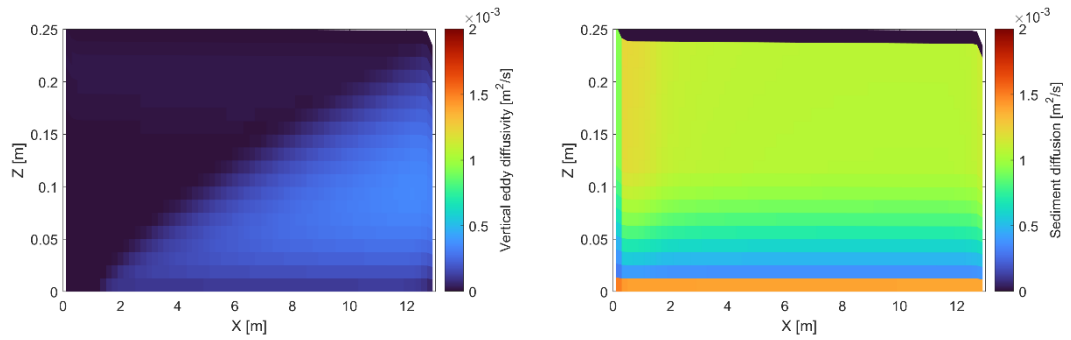
Modelling sand-mud dynamics in Delft3D

31 January 2024

MUSA

Figure 4-5 Vertical eddy diffusivity in the digital flume for Condition 6 (U = 0.35 m/s; H = 0.08 m) when using the vertical mixing from the k-ε turbulence model (left) and when using the vertical mixing distribution according to Van Rijn (2007) (right).
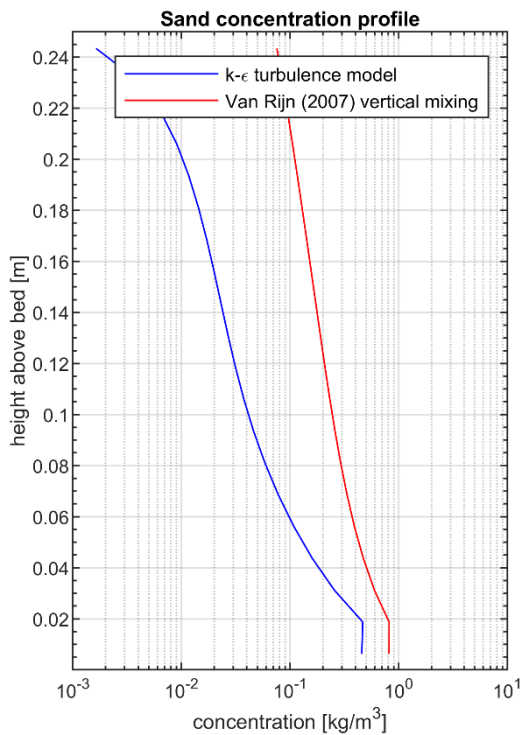

Figure 4-6 Computed sand concentration profiles by application of the k-ε turbulence model or the Van Rijn (2007) formulations for vertical mixing in the digital flume in Delft3D, without correction of the orbital velocity.

Effect of mud on sand concentration profiles

The measured sand concentration profiles for experiments with different samples illustrate that sand concentrations in the flume generally decrease for increasing mud content in the bed (see Figure 2-3). This is illustrated again for Condition 6 in *Figure 4-7*. It is not clear why the number of data points in the concentration profile for the experiment with sample I is different. Anyway, the measured concentrations for this experiment are relatively low and do not follow the general trend of the effect of a mud fraction on the sand concentration profile. In experiments J and K, the sand concentrations decrease by approximately a factor of 10 (experiment J, p_{mud} = 13%) and a factor of 20 (experiment K, p_{mud} = 30%) compared to experiment A. The effect of a certain mud fraction in the bed on the sand concentration profiles is accounted for in the Van Rijn (2007) sediment transport formulations in two ways. Firstly, the reference concentration is scaled by the availability of sand in the bed (i.e., multiplication by (1 - p_{mud})). Secondly, the mud fraction is affecting the critical bed shear stress for erosion of the sand fraction (see

Modelling sand-mud dynamics in Delft3D

31 January 2024

MUSA

Section 3.1.2). We used the digital flume in Delft3D to explore the results of the sediment transport formulations. The same effects of including a mud fraction are expected in the SEDCON model and in the original TR2004 model.
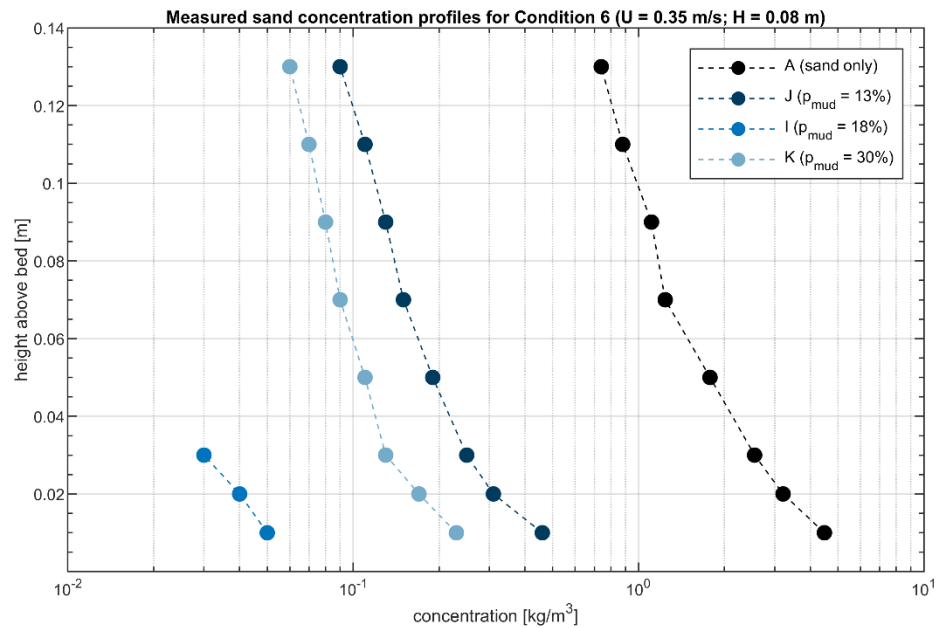

Figure 4-7 Measured sand concentration profiles for sediment samples with different p_{mud} (see also Figure 2-3).

As discussed earlier in this chapter, the concentrations in the digital flume underestimate the measured sand concentrations. We therefore focus on the relative effect of including a mud fraction. The effect of scaling the reference concentration by the availability of sand in the bed is illustrated in *Figure 4-8*. In this case, scaling the reference concentration by 70% (i.e., from sample A (sand only) to sample K (p_{mud} = 30%)) causes sediment concentrations to be approximately 10% lower. For a smaller reduction on the reference concentration (i.e., for experiments J and I), the reduction of the sediment concentrations is also smaller.

The effect of mud on the critical bed shear stress for erosion of sand following the methodology of van Rijn (2007) (see also section 3.1.2) has a much larger effect on the sediment concentrations than scaling the reference concentration, as is illustrated in *Figure 4-9*. For sample K, for example, the sediment concentrations reduce by a factor of 5-6 due to the increase in the critical bed shear stress by a factor $(1+p_{mud})^\beta = (1+0.3)^3 = 2.2$. Including both effects in the digital flume yields sand concentrations that are approximately 4 (for sample J (p_{mud} = 13%)) to 7 (for sample K (p_{mud} = 30%)) times lower than the sand concentrations for sample A (sand only). The observed reduction in sand concentration is much larger (1 to 2 orders of magnitude – see *Figure 4-7*). The effect of mud in these experiments is therefore underestimated by the Van Rijn (2007) transport formulations. This may be caused by the fact that the sediment samples become cohesive for larger mud fractions, such that using a different transport model would be appropriate. Such a distinction in non-cohesive and cohesive transport models was made by van Ledden (2003).

In section 4.2.2, we will evaluate the effect of sand-mud interaction mechanisms as developed by van Ledden on the erosive behavior of the mud fraction. Below, we first explore the effect of applying these formulations on the suspended sand concentration profiles. As shown in Figure 4-10, Van Ledden's (2003) model also underestimates the effect of mud on the sand concentrations, even more than Van Rijn's (2007) model. Including sand-mud interaction in the digital flume yields sand concentrations that are approximately 2 (for sample J (p_{mud} = 13%)) to 3.5 (for sample K (p_{mud} = 30%)) times lower than the sand concentrations for sample A (sand only).
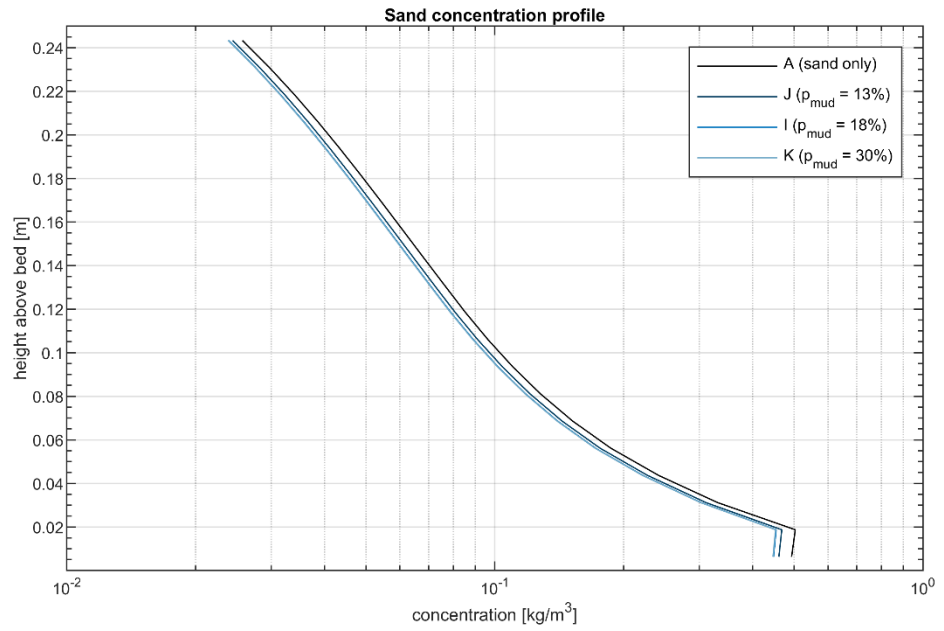
Figure 4-8 Computed sand concentration profiles for sediment samples with different p_{mud}, but without the mud influencing the critical bed shear stress of the sand.
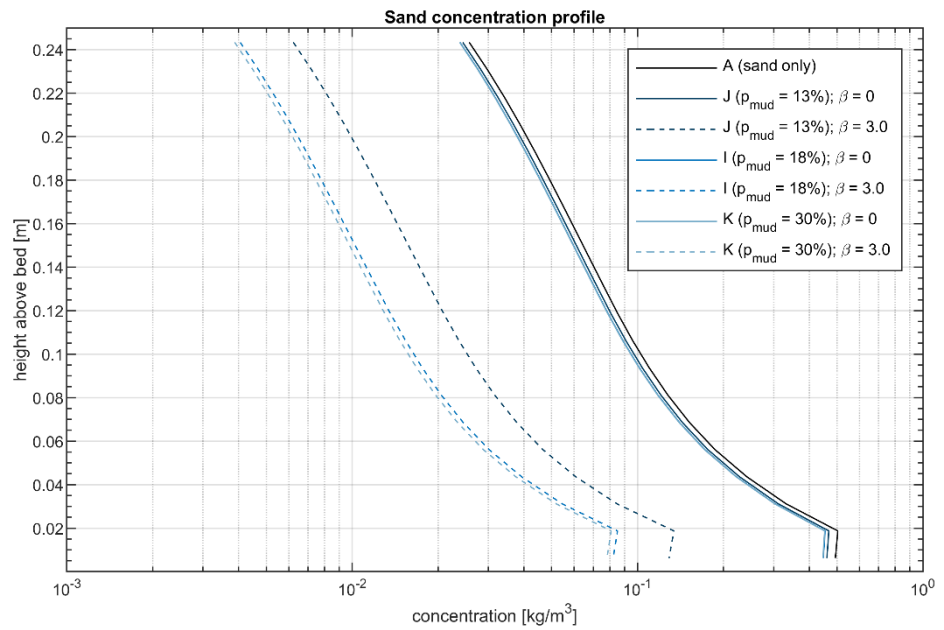

Figure 4-9 Computed sand concentration profiles for sediment samples with different p_{mud}, with and without the mud influencing the critical bed shear stress of the sand via the β parameter.
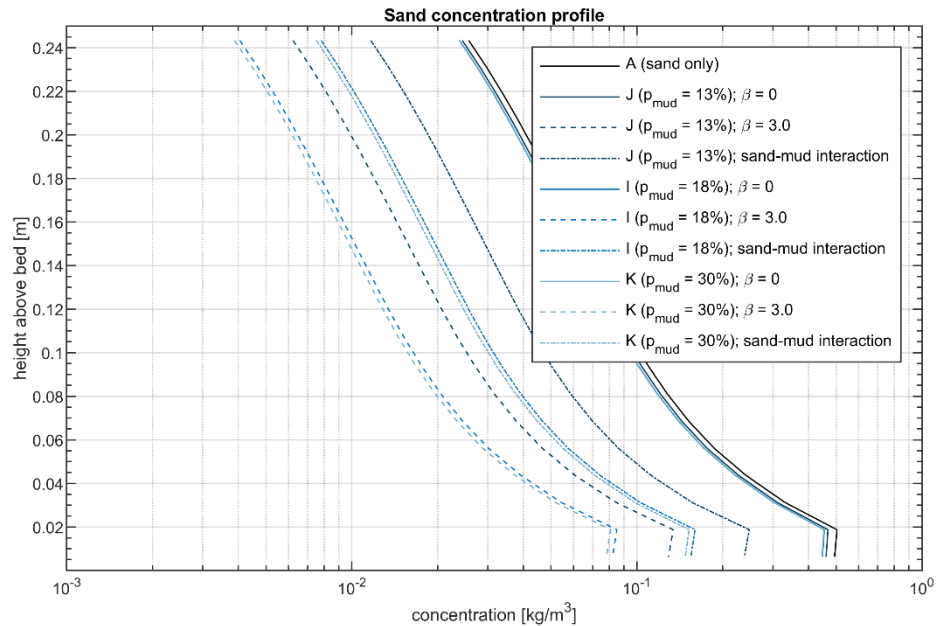
Modelling sand-mud dynamics in Delft3D

31 January 2024

Figure 4-10 Computed sand concentration profiles for sediment samples with different p_{mud}, with and without the mud influencing the critical bed shear stress of the sand via the β parameter, and with and without sand-mud interaction.

4.1.2 Mud concentration profiles

Suspended sand concentrations reach an equilibrium concentration within a short time span, showing that erosion of sand of the test section is in equilibrium with deposition of sand within the flume. In contrast, suspended mud concentrations build up over time. The measured concentration profiles are therefore only representative for one specific moment during the experiment. The time it takes for the mud concentration profiles to reach an equilibrium is studied using the Delft3D model. Figure 4-11 shows the computed mud concentration profiles for a model run with $p_{mud} = 18\%$ and including sand-mud interaction. The computed concentrations are plotted every 30 minutes. The concentration increase (Δc_{mud}) decreases gradually over time. The absolute differences between the first concentration profile (after 30 minutes) and a concentration profile after 1 hour already may differ 20-50%, showing that the measured concentration profiles are very sensitive to the timing of the experiment. This time-dependency of the mud concentration profiles is observed in all scenarios, regardless of the forcing, the bed composition, and the model settings (such as whether sand-mud interaction is applied or not).

Figure 4-11 also shows that for the same model settings, the model is able to closely reproduce the observed mud concentrations (conditions 5, 6), whereas it underestimates the concentrations for condition 3. This implies a dependency of the model performance on the imposed hydrodynamic forcing. In all of the simulations, condition 3 is usually the one for which the model underestimates the sediment concentrations most. Potential reasons for this can be the background turbidity in the flume (which may be higher in reality), the sequence and the timing in which the experiments were executed. For all sediment samples (I, J, K), the hydrodynamic forcing was gradually increased, such that condition 3 was applied prior to the other conditions. Since we have seen that mud concentration profiles develop over time (in the order of hours), it is likely that the measured sediment concentrations are influenced by the hydrodynamic conditions in the previous experiment. Therefore, calibrating the model to the measured concentrations at e.g., condition 7 could result in an overestimation of the erosion rates. However, since the model underestimates the concentrations at condition 3, it is more likely that this is because of a background concentration present in the experiments, prior to the imposed forcing.

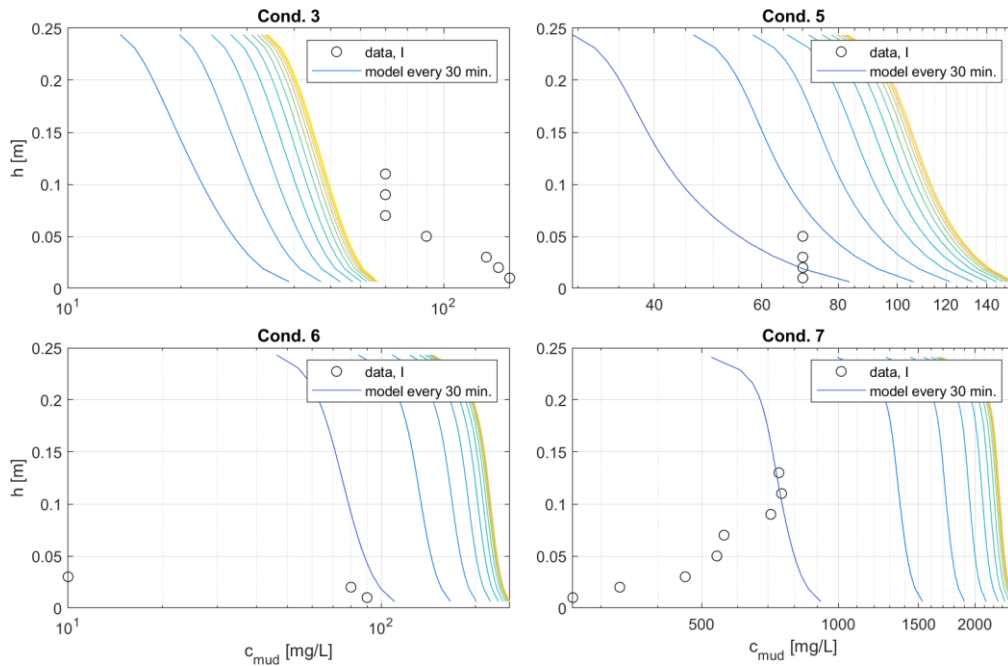Modelling sand-mud dynamics in Delft3D

31 January 2024

MUSA

Figure 4-11 Measured (dots) and calculated (lines) suspended mud profiles for four different hydrodynamic conditions (see Table 3-1). Model results are plotted for every 30 minutes after the start of the simulation (dark blue is 30 minutes after the start of the simulation, yellow colors after > 4 hours). Other model settings: p_{mud}=18% (sample I), calculations include sand-mud interaction.

4.2 Erosion rates

It was discussed in Chapter 2 that in the long-bed experiments, in general, both the erosion rates of mud and those of sand (as can be derived from the total erosion rates) decrease with increasing mud content in the sediment bed. This behavior is independent of the hydrodynamic conditions. In this section, we study the Delft3D parameter space to reproduce this behavior.

4.2.1 Model results without sand-mud interaction

Without sand-mud interaction, sand erosion rates are computed with the van Rijn (2007) formulations (switching off the dependency of sand erosion on mud content, and with $\beta = 3$) and mud erosion with the Partheniades formulations (with a default value M = 10^{-3} kg/m²/s). For both erosion / transport scales with the availability of sand/mud in the bed.

The model results in Figure 4-12 show that the predicted erosion behavior of mud is opposite to the behavior observed in the lab experiments: E_{mud} increases with increasing p_{mud}. This holds for all modelled hydrodynamic conditions. The computed behavior of E_{sand} does agree with the observed behavior. The magnitudes of E_{mud} and E_{sand} are largely overestimated by the model compared to the data. The reason for this is not well understood, since the calculated SSCs are in the correct order of magnitude or sometimes even underestimated by the model. However, here we focus on the observed erosive behavior depending on p_{mud} (decreasing E_{mud} for increasing p_{mud}).

The mismatch in the computed E_{mud} follows from the formulations to compute the erosion rates. E_{mud} is scaled with mud availability only – calculated as $E_{mud} = p_{mud}*E_{mud,100\%}$, while τ and M do not vary with varying p_{mud} – and can therefore only increase with increasing p_{mud} (see also the left panels of Figure 4-14 and Figure 4-15). Similarly, E_{sand} will decrease with increasing p_{mud}, even though the availability of mud may slightly increase $\tau_{crit,sand}$.

The decrease of E_{mud} with increasing p_{mud} can only be explained with a dependency between p_{mud} and $\tau_{crit,mud}$ or M, in which either $\tau_{crit,mud}$ increases or M decreases with increasing p_{mud}.

Modelling sand-mud dynamics in Delft3D
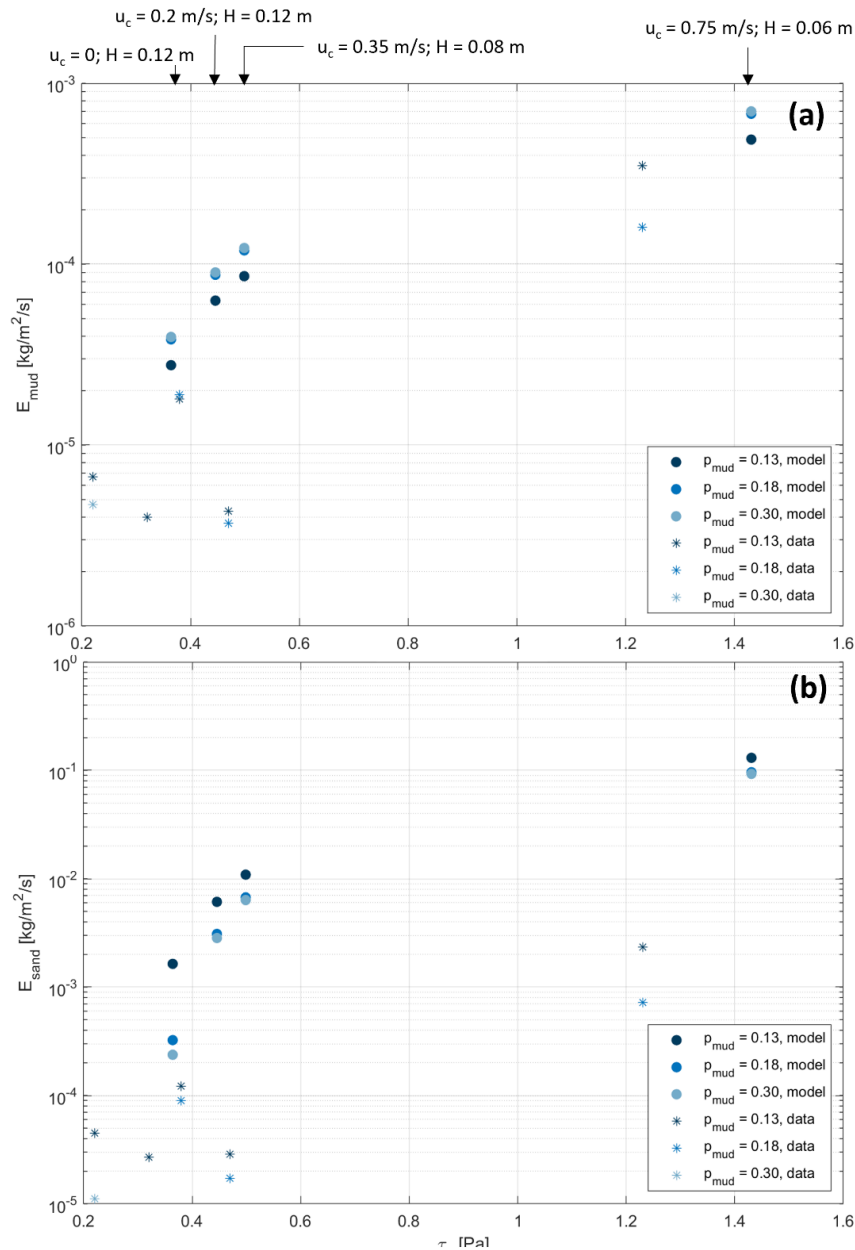
31 January 2024

MUSA

Figure 4-12 Calculated erosion of (a) mud and (b) sand in the digital flume (dots), without sand-mud interaction. The measured erosion in the flume experiments (as shown in Figure 2-5 and Figure 2-6) are plotted as asterisks.

4.2.2 Model results with sand-mud interaction

To determine the interactive sand-mud behavior of our samples correctly, we first revisit the composition and sediment properties (see also Tables 3-6 and 3-7 of Boechat Albernaz et al, 2022). The sediment samples with which the long-flume long-bed experiments have been executed are composed of mud from Noordpolderzijl (NPZ) and fine sand (130 μm). This type of mud contains a very high clay/slit ratio ($p_{2\mu}$ = 25%, $p_{8\mu}$ = 40%, $p_{63\mu}$ = 72%) and has a very high plasticity (PI = 52.8). According to van Ledden's (2003) theory, sand-mud mixtures are non-cohesive or cohesive, depending on whether the clay content is below or above the critical clay content for cohesive behavior ($p_{clay,crit}$ = 5-10%). Herein, clay is defined as the fraction smaller than 4 μm. Since the Delft3D modelling suite accounts for a mud content (and a critical mud content, following the formulations of van Ledden), we convert $p_{clay,crit}$ into $p_{mud,crit}$ based on the clay/silt ratio of our sediment sample. This gives us a $p_{mud,crit}$ = 0.12 to be used as an input parameter in the Delft3D simulations.

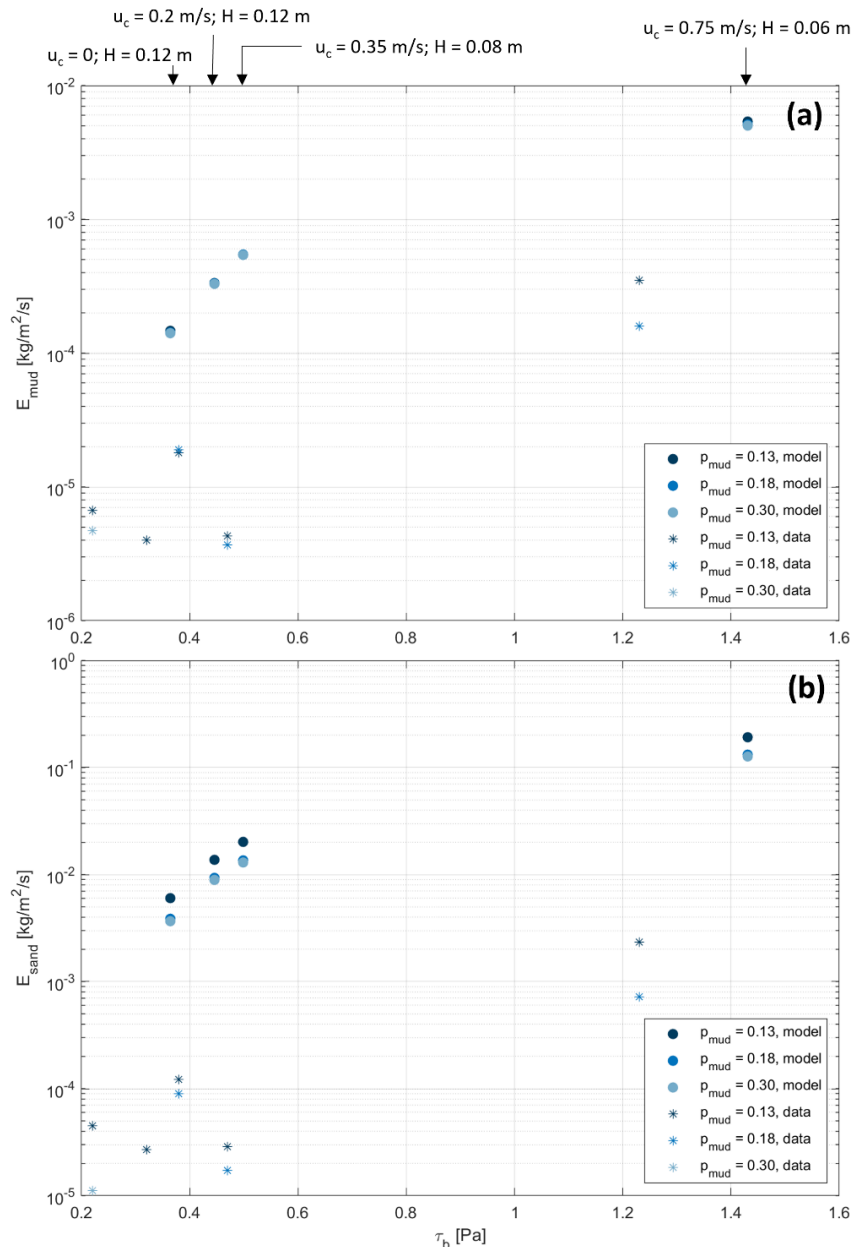Modelling sand-mud dynamics in Delft3D

31 January 2024

Figure 4-13 Calculated erosion of (a) mud and (b) sand in the digital flume (dots), with sand-mud interaction. The measured erosion in the flume experiments (as shown in Figure 2-5 and Figure 2-6) are plotted as asterisks.

Figure 4-13 shows that with van Ledden's (2003) formulations, the predicted behavior of E_{mud} and E_{sand}, does match with the observations, since in the cohesive regime, both E_{mud} and E_{sand} decrease with increasing p_{mud} (see also the right panels of Figure 4-14 and Figure 4-15, where $p_{mud,crit} = 0.3$).

However, the effect of p_{mud} on the magnitude of the erosion is much smaller than observed (see Figure 2-5 for comparison, where we observe that adding a bit of mud largely decreases the total erosion, while this decrease is much smaller in the model).

Moreover, in the modelled scenarios including sand-mud interaction, E_{mud} ranges between 10^{-4} and 10^{-2} kg/m²/s, whereas the observations show a range between 10^{-6} and 10^{-3} kg/m²/s. The modelled scenarios that do not account for sand-mud interaction provide a range between 10^{-5} and 10^{-3} kg/m²/s (which is much closer to reality). These scenarios were executed with an erosion parameter $M = 10^{-3}$ kg/m²/s, while the scenarios with sand-mud interaction were executed with $M = 10^{-5}$ kg/m²/s. The reason for this is the (likely exaggerated) increase in M and E when following van Ledden's formulations for sand-mud interaction, which will be discussed in the next section.

Modelling sand-mud dynamics in Delft3D

31 January 2024

4.3 Erosion parameter M

4.3.1 Overestimation of E at medium p_{mud} with van Ledden (2003)

In the formulations of van Ledden (2003), both τ and M depend on p_{mud}. In the non-cohesive regime, E_{mud} scales with E_{sand}, using an erosion rate M that depends on the sand properties but is independent of the mud content. This value for M is relatively high, which according to van Ledden, matches the observation that fines are easily washed out of a sandy bed. When $p_{mud} > p_{mud,crit}$, M decreases again, until it reaches the value of the erosion parameter M for pure mud.

To better understand the impact of these formulations on the model results, we further analyzed the behavior of van Ledden's sand-mud erosion formulations depending on the parameter choices, and we compare these to the traditional van Rijn (for sand) & Partheniades (for mud) formulations that do not account for sand-mud interaction. While the previous parts of this chapter mainly focused on the erosion of sand-mud mixtures for low p_{mud} values up to the critical threshold for cohesive behavior (since this is the range of the experiments), in this section we focus on the full range of p_{mud} and how these results depend on the choice for sand-mud interaction.

Our results show that the dependency of E_{mud} on p_{mud} greatly varies with the choice for M (erosion parameter for pure mud, i.e. $p_{mud}=1$) when using van Ledden's formulations. The left column in Figure 4-14 shows the erosion rates for sand (E_{sand}) and mud (E_{mud}) computed without sand-mud interaction, and their sum (($E_{sand+mud}$). All cases are computed for a bed shear stress $\tau_b = 0.5$ Pa, The different rows show the effect of the choice for M. The right column shows E_{sand}, E_{mud} and $E_{sand+mud}$ calculated with sand-mud interaction. Here, we observe that when M is in the order of 10^{-3} kg/m^2/s, van Ledden's sand-mud interaction formulations give similar results as the formulations without sand-mud interaction. From this, it is however not clear if these values for the erosion rates resemble reality. When M is in the order of 10^{-4} kg/m^2/s, E_{mud} is largest for intermediate p_{mud} (especially close to $p_{mud,crit}$), but the largest value of E_{mud} along the entire p_{mud} spectrum is still in the same order of magnitude as the largest value of E_{mud} when not accounting for sand-mud interaction. However, further decreasing M to 10^{-5} kg/m^2/s, causes the erosion rate E_{mud} for intermediate p_{mud} to be several orders of magnitude higher than for pure mud ($p_{mud} = 1$). This behavior might be unrealistic and there is insufficient data available to determine the best interpolation method.

The character of E_{mud} is also largely dependent on the critical bed shear stress for mud erosion (τ_{crit}) and gives similar results to the dependency on M (see Figure 4-15). The erosion behavior depends much less on the erosion parameters of pure sand (such as $D_{50,sand}$ for instance), see Figure 4-16. The course of E_{sand} and E_{mud} along p_{mud} does not change with varying $D_{50,sand}$, although their magnitudes do (since the erosion rate for pure sand, $E_{sand;0}$, directly depends on the grain size and E_{sand} is further interpolated from here).

The interpolation between the erosion rate at $p_{mud} = p_{mud,crit}$ on the one hand and at $p_{mud} = 1$ on the other hand may thus lead to an overestimation of the erosion rate of cohesive mixtures. This is particularly the case when the mud erodibility (i.e., M parameter) is low. Ideally, field or lab observations of the erosion rates are available to study whether the erosion rates according to the Van Ledden interaction model are realistic for a certain study site. Since this is generally not the case, users of the Van Ledden interaction model are recommended to perform a sensitivity study of the model results to the sand-mud interaction, especially in case the M parameter is low (< 10^{-4} kg/m^2/s).
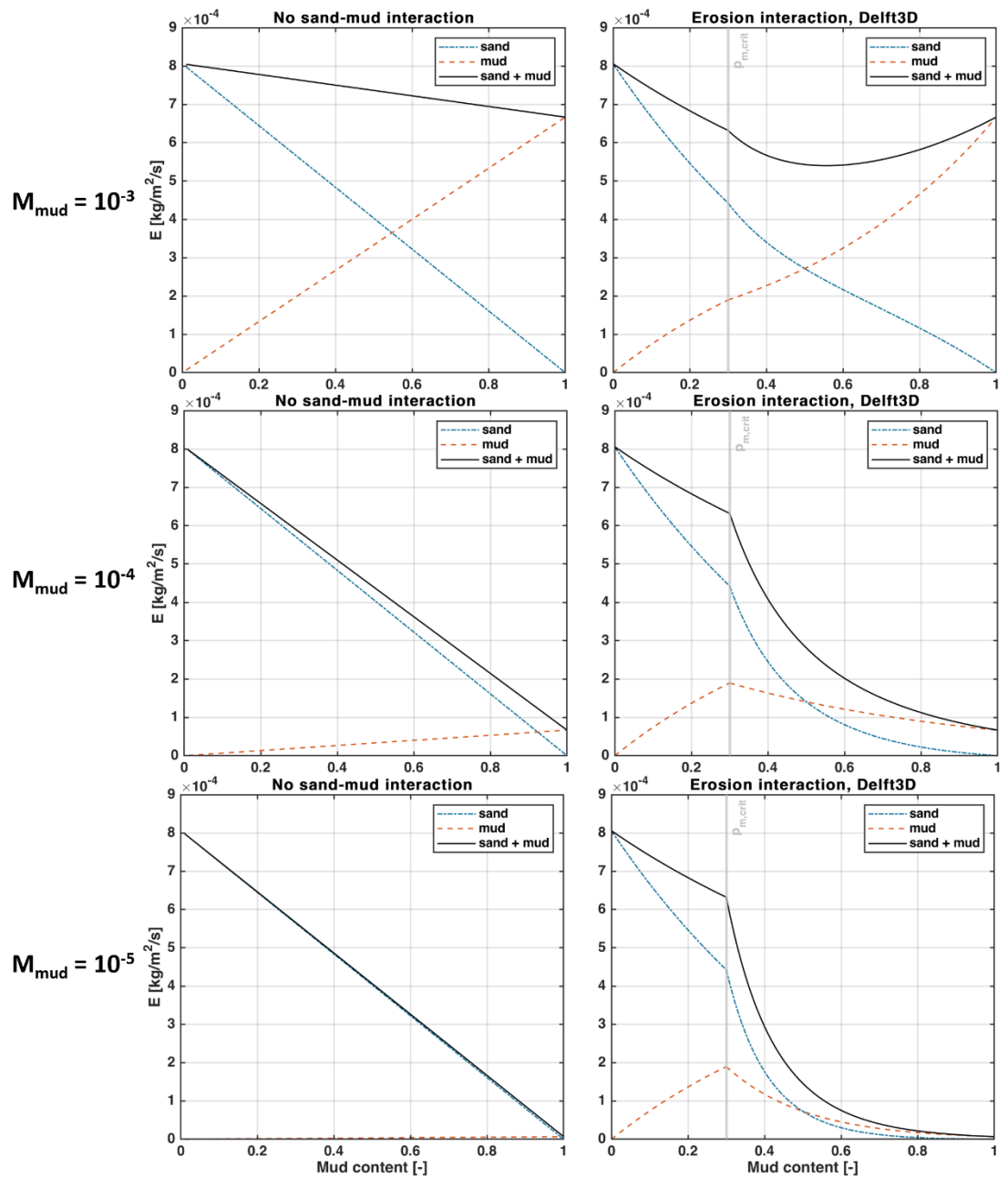
MUSA

Figure 4-14 Comparison of the calculated erosion without (left column) and with (right column) sand-mud interaction, for M=10⁻⁵, 10⁻⁴, 10⁻³ kg/m²/s. Other settings: τ_b = 0.5 Pa, $\tau_{crit,mud}$ = 0.3 Pa, D_{sand}=150 μm, and a critical p_{mud} for cohesive behavior of 0.3.
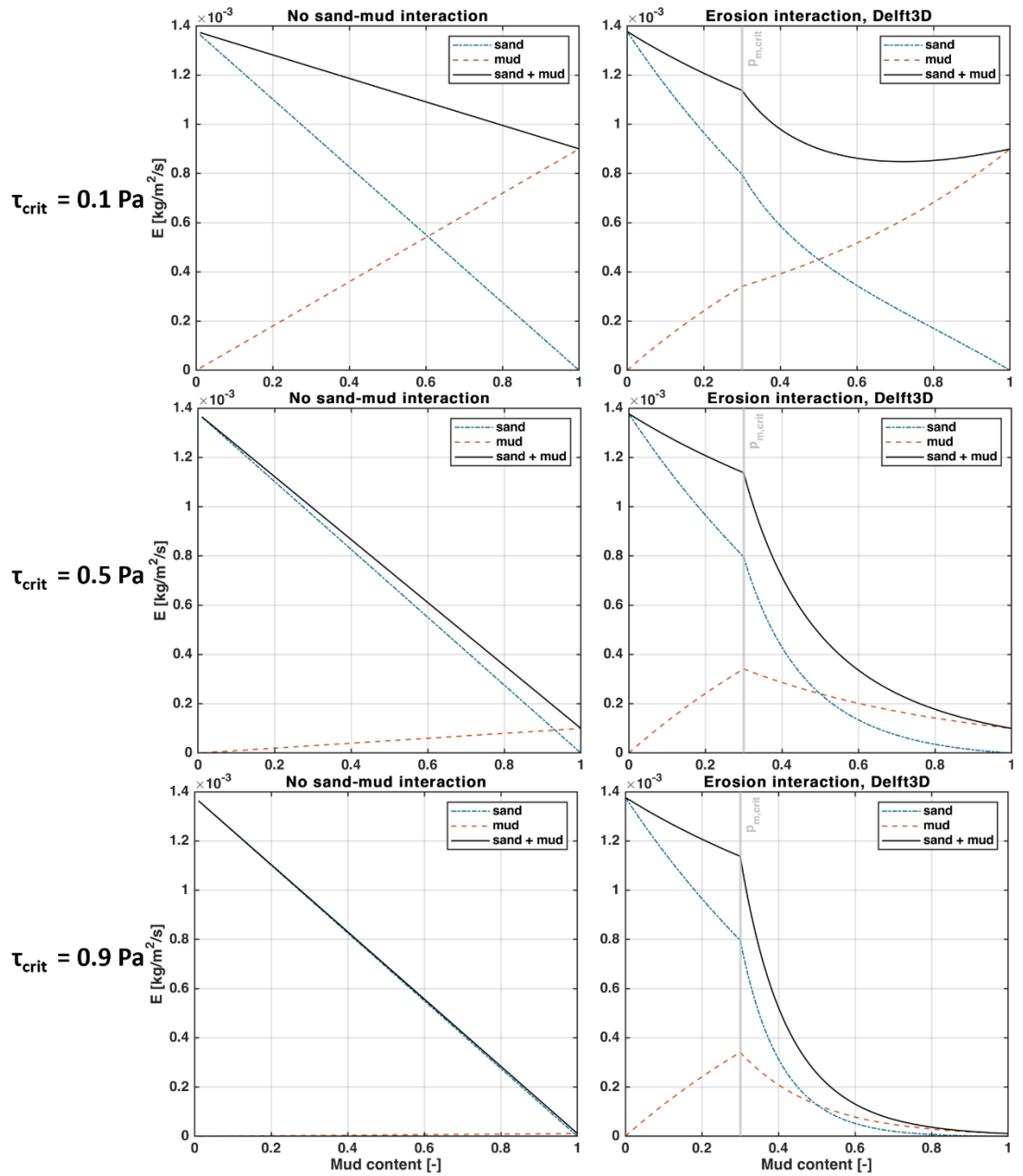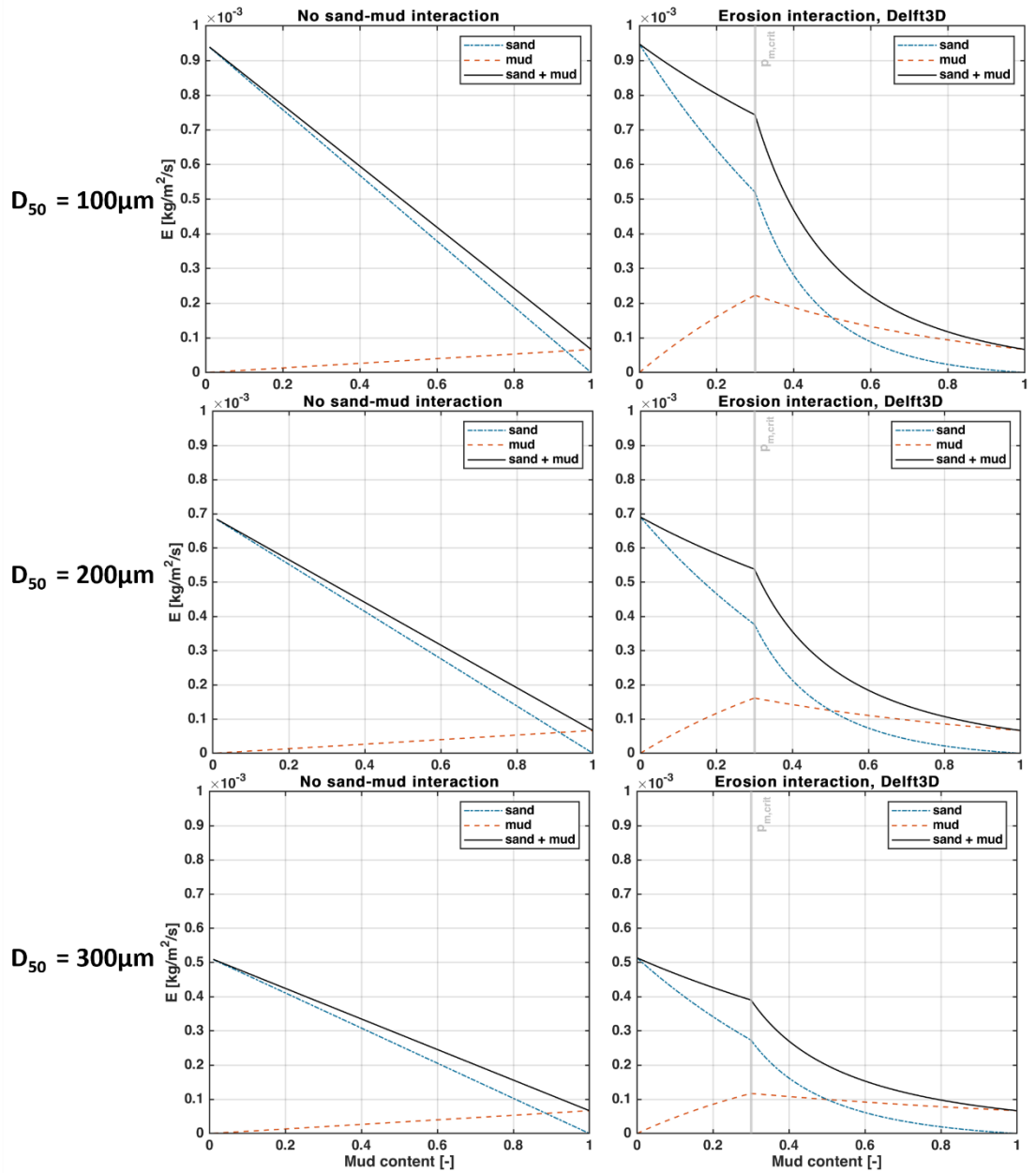
MUSA

Figure 4-15 Comparison of the calculated erosion without (left column) and with (right column) sand-mud interaction, for $\tau_{crit,mud} = 0.1$ Pa, 0.5 Pa, 0.9 Pa. Other settings: $M = 10^{-4}$ kg/m²/s, $\tau_b = 1$ Pa, $D_{sand} = 150 \mu m$, and a critical p_{mud} for cohesive behavior of 0.3.

Modelling sand-mud dynamics in Delft3D

31 January 2024

MUSA

Figure 4-16 Comparison of the calculated erosion rates with (left column) and without (right column) sand-mud interaction, for $D_{50,sand}$ = 100 µm, 200 µm, 300 µm. Other settings: $M = 10^{-4}$ kg/m²/s, $\tau_b = 0.5$ Pa, $\tau_{crit,mud}$ = 0.3 Pa, and a critical p_{mud} for cohesive behavior of 0.3.

Modelling sand-mud dynamics in Delft3D

4.3.2   Methodologies to compute M

Since the sediment properties $D_{50,sand}$ (130 µm), τ_{crit} (~0.3 Pa for all considered sand-mud mixtures), and w_s (0.5 mm/s) have been previously derived from the laboratory experiments (Boechat Albernaz et al., 2023), the M parameter can be calibrated in order to reproduce the observed concentrations and erosion rates in the flume. Herein, we assume that the sediment composition, and therefore also τ_{crit}, does not greatly change during the experiment.

In Section 4.3.1 we have shown that the formulations of van Ledden (2003) tend to largely increase (by ~ 2 orders of magnitude) the erosion rates for intermediate mud contents, around the threshold for cohesive behavior – which is the case for the sediment samples that are considered in the digital flume. Therefore, calculations with sand-mud interaction generally require a much smaller value for M_0 (in which M_0 is the M value for pure mud). We explore the required settings for M in two ways: first, calibrate the modelled sediment concentration to observed sediment concentrations by varying model (and sand-mud interaction) settings to obtain M. Secondly, we compute M based from the OBS measurements, as explained in section 2.1.3. We will show that both methods will provide very different results and we will explain why and which of the two should is most reliable.

Approach 1: Modelled c_{mud}

We analyze the modelled suspended mud concentration profiles by comparing them to the measured profiles. As explained in section 4.1.2, suspended mud concentrations build up over time, making the data of the experiments very sensitive to the exact timing of the measurement. Therefore, here we provide a rough comparison between the model results and the data, in which we mainly look at whether the modeled concentrations within the first 2 hours are in the right order of magnitude. The model results provide the following information:

Sample J (p_{mud} = 0.13)

- Without sand-mud interaction (Figure A-1): M = 10^{-3} kg/m^2/s results in an underestimation of c_{mud} for all conditions of about 1 order of magnitude.
- With sand-mud interaction (Figure A-2): M = 10^{-5} kg/m^2/s underestimates c_{mud} for condition 3 (with a factor of 2), provides good results for conditions 5 and 6, and overestimates c_{mud} for condition 7.

Sample I (p_{mud} = 0.18)

- Without sand-mud interaction (Figure A-3): M = 10^{-3} kg/m^2/s results in an underestimation of c_{mud} for conditions 3, 5 and 6 of up to 1 order of magnitude and a slight overestimation of condition 7.
- With sand-mud interaction (Figure A-4): M = 10^{-5} kg/m^2/s underestimates c_{mud} for condition 3 (factor of 2) and provides good results for conditions 5, 6 and 7.

Sample K (p_{mud} = 0.30)

- Without sand-mud interaction (Figure A-5): M = 10^{-3} kg/m^2/s results in an underestimation of c_{mud} for conditions 3, 5 and 6 (factor ~2-3) and provides good results for condition 7.
- With sand-mud interaction (Figure A-6): M = 10^{-5} kg/m^2/s provides good results for condition 3 and overestimates c_{mud} for conditions 5, 6 and 7 (with a factor 2-3 for conditions 5 and 6, and 1 order of magnitude for condition 7).

From this, we derive two main findings: first of all, we observe differences between the samples, with larger differences between sample I and K (18% and 30 % mud) than between J and I (13% and 18% mud). This suggests that M might vary with p_{mud}, which is to be expected following the sand-mud interaction theory. Secondly, and more strikingly, we observe differences between the conditions within a sample (with equal composition).

Approach 2: OBS data

The measured erosion rates from the lab data (Figure 2-5) are analyzed to derive the M value per condition. Using the Partheniades equation for mud erosion (so disregarding sand-mud interaction) we can derive M as:

MUSA

$$M = \frac{E_{mud}}{\frac{\tau}{\tau_{cr}} - 1} * \frac{1}{p_{mud}}$$

This gives the results in Figure 4-17. Since $\tau < \tau_{cr}$ for condition 2 (with τ_{cr} = 0.3 Pa), this results in negative erosion rates, whereas in reality we do observe an increase in SSC, and thus mud erosion. Therefore, we also perform this calculation for τ_{cr} = 0.2 Pa in Figure 4-18. Here we observe the following:

- M is not constant along the different hydrodynamic conditions, but rather (generally) increases with increasing bed shear stress (except for condition 2, with the lowest bed shear stress).
- In general, but strictly speaking not always, we observe a decreasing M with increasing p_{mud}. The differences can however be very small. This is most pronounced in condition 7 (u=0.75 m/s, H_s=0.06 m).
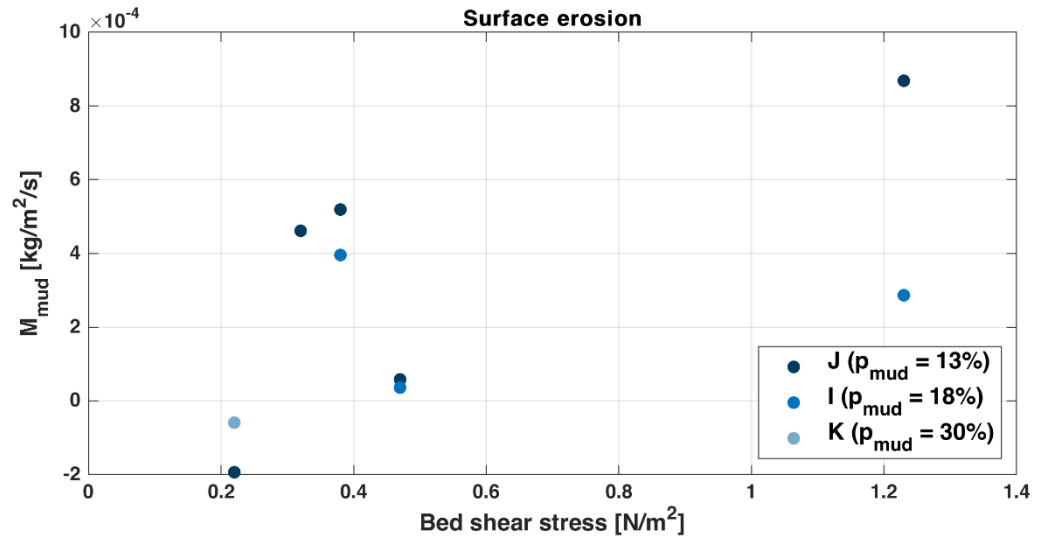- M is generally in the order of 10^{-5}-10^{-4}.

Figure 4-17 Analyzed M_{mud} with the measured values for E_{mud} (Figure 2-5) and the Partheniades equation for mud erosion. Results for surface erosion, with τ_{cr} = 0.3, following Figure 4.3.4 of Boechat Albernaz et al. (2023).
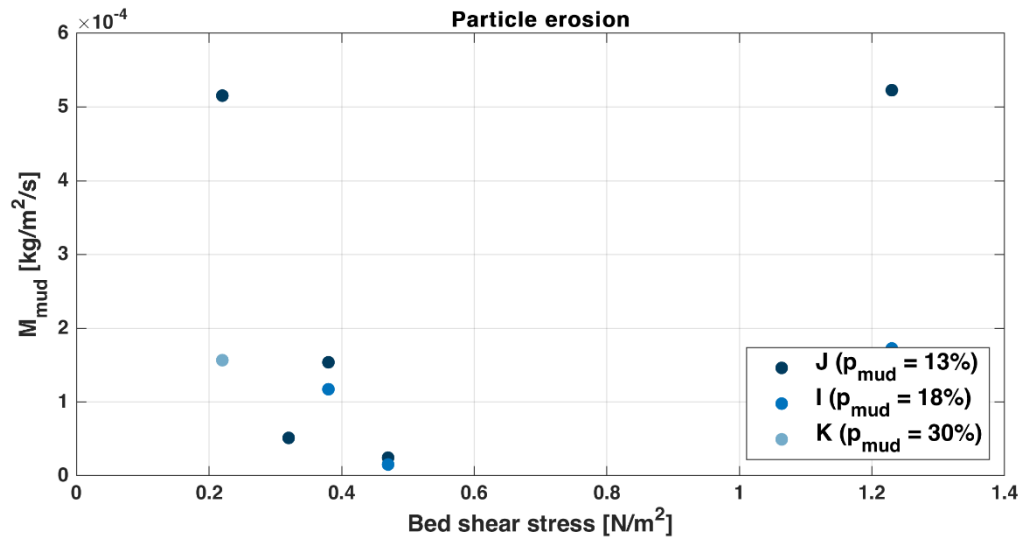

Figure 4-18 Analyzed M_{mud} with the measured values for E_{mud} (Figure 2-5) and the Partheniades equation for mud erosion. Results for "particle erosion", with τ_{cr} = 0.2

Modelling sand-mud dynamics in Delft3D

31 January 2024

MUSA

There is a discrepancy between the M values derived from *method 1* (model calibration, M in the order of 10^{-3} (for condition 7, samples J&K) or larger (all other cases)), and *method 2* (data analysis, M in the order of 10^{-4}). We believe that there are two reasons for this: The first is related to the Partheniades formulation for erosion: including τ_{cr} in the denominator is attractive from a dimensional point of view, but it also introduces inaccuracies in establishing M from erosion experiments, as M then becomes sensitive to small errors in τ_{cr} in near the onset of erosion (which is especially the case for conditions 3, 5 and 6). Moreover, some erosion already occurs at $\tau_b < \tau_{cr}$, which is often referred to as floc erosion (Winterwerp, et al., 2012).

The second and probably most dominant reason is related to the background concentration and timing effects in the flume experiments. When deriving the M parameter from the suspended mud concentration profiles (and especially from their instantaneous magnitude), the result is inevitably influenced by the background concentration in the flume at the beginning of the experiment. Moreover, this background concentration is equal for all tested hydrodynamic conditions, but increases through their sequence (3, 5, 6, 7) since the flume was not flushed in between the experiments. Instead, the hydrodynamic conditions were increased directly after the end on an experiment up-to the desired conditions of the next experiment. This will result in an overestimation of the erosion rates, and therefore also of M, when purely based on this method. Consequently, erosion rates derived from the change in concentration over time (based on the OBS data, and the M parameter that follows from these (Figure 4-17), are probably more realistic than methodologies using the absolute sediment concentration (model calibration).

Modelling sand-mud dynamics in Delft3D

31 January 2024

MUSA

5 Modelling results part 2: Tidal basin model

This chapter presents the results from an application of the formulation for the effects of bed composition and density on sediment erodibility (as presented in Chapter 2, Section 2.2) to a schematized model of a tidal basin (see Section 3.2). First, in Section 5.1 we discuss and compare the overall morphodynamic evolution for different model settings (with and without density effects, and exploring the effects of the input parameters of the density-erodibility formulation). Subsequently, we explore the effects of applying the density-erodibility formulation in a simulation including storm events (Section 5.2).

5.1 Long-term morphodynamic evolution

5.1.1 Phenomenological description

We first analyze the first 45 years of morphodynamic evolution of the tidal basin for a range of scenarios. During this period, only average wave conditions are included in the simulations (i.e., no occasional storms). Figure 5-1 shows the simulated bathymetries and sediment composition after 45 years. The first row of subplots shows the initial settings of all models. The second row shows the results after 45 years of morphodynamic evolution for the simulations without density effects (but with varying large $\tau_{cr,mud}$). The rows below show the results of the simulations with density effects, in which every row explores the sensitivity of the results to a specific input parameter.

If we compare the simulations without density-effects with each other (plots on the 2nd row of the figure), we observe that the imposed critical bed shear stress for erosion of the mud fraction largely impacts morphodynamic evolution. For large $\tau_{cr,mud}$ values (1 Pa, i.e., low erodibility) large shoals are formed on the centrals part of the basin, while shallow muddy intertidal areas evolve along the western and eastern boundaries. Especially the lower intertidal areas seem to be muddy, whereas the upper intertidal areas are sand dominated. For small $\tau_{cr,mud}$ values (0.25 Pa, i.e., high erodibility) only the fringing flats bordering the southern boundary are muddy, whereas the remainder of the basin is predominantly sandy; only a few shoals in the central parts of the basin have mud patches with p_{mud} 0.3.

The results of the simulations with density-effects (plots on rows 3-7 of the Figure 5-1) show much less variability. Most of these results are very similar to those of the simulation without density effects and with $\tau_{cr,mud}$ = 0.5 Pa. The only exception is the simulation with $\tau_{cr,min1}$ = 0.05 Pa and $\tau_{cr,max}$ = 0.75 Pa, of which the results are very similar to the simulation without density effects and high mud erodibility ($\tau_{cr,mud}$ = 0.25 Pa).

5.1.2 Hypsometry

To further quantify the comparison between the scenarios, we have calculated the hypsometric curves after 45 years of evolution. Figure 5-2 shows the hypsometry of the scenarios without density effects (left panel) and compares this to a scenario with the default settings of the density-erodibility formulation (automatic settings set in Delft3D and user defined, which provide identical results showing that the standard settings of the formulation are implemented as stated in Section 3.2.3). Also here we observe that the hypsometry of the simulations with density effects best resembles that of the scenario with $\tau_{cr,mud}$ = 0.5 Pa. In Figure 5-3 we show how the hypsometry varies depending on the user-defined parameters of the density-erodibility formulation. We have tested the parameters within a realistic range. The results demonstrate that while varying $\tau_{cr,max}$ does significantly affect the hypsometry results (and therefore the overall bathymetry), the other parameters hardly do.
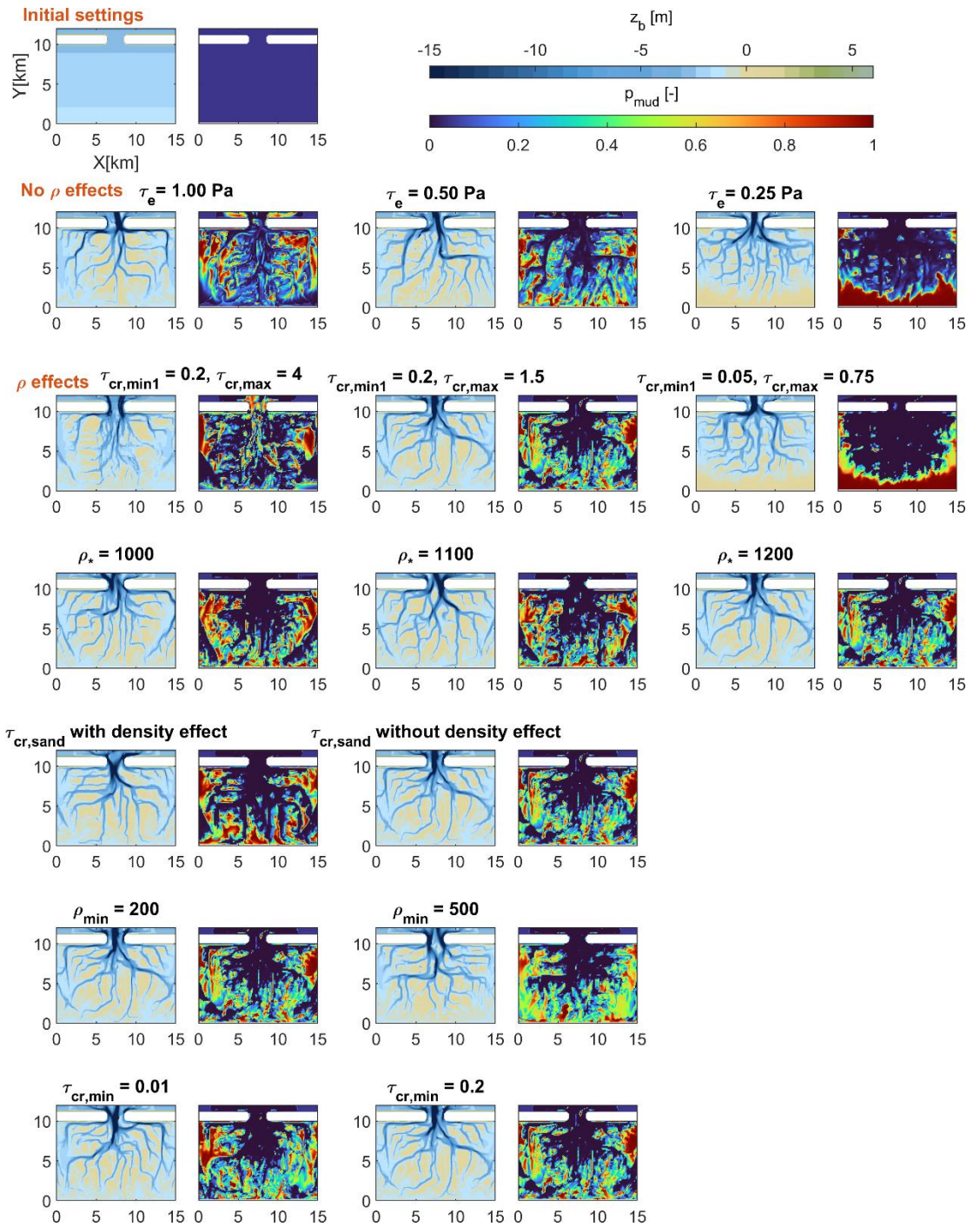
MUSA

Figure 5-1 Modeled morphological evolution (45 years, without storms) for a range of erosion settings without density effects (2nd row), and with density effects (rows 3-7). Every row explores de results-sensitivity to a specific parameter of the formulations (the other parameters are set at default settings, see Section 3.2.3). The plots show computed bed levels (left panel per model realization) and sediment composition (mud content, p_{mud}) of the upper bed (0.1 m, right panel).
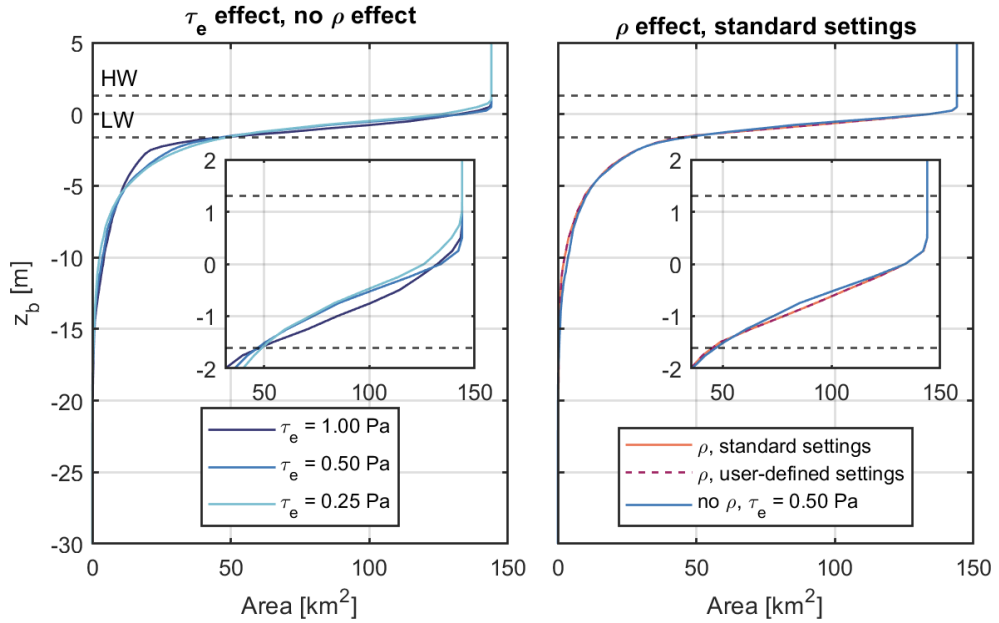
MUSA

Figure 5-2 Hypsometry of the models without density effects (left) and with density effects (right).
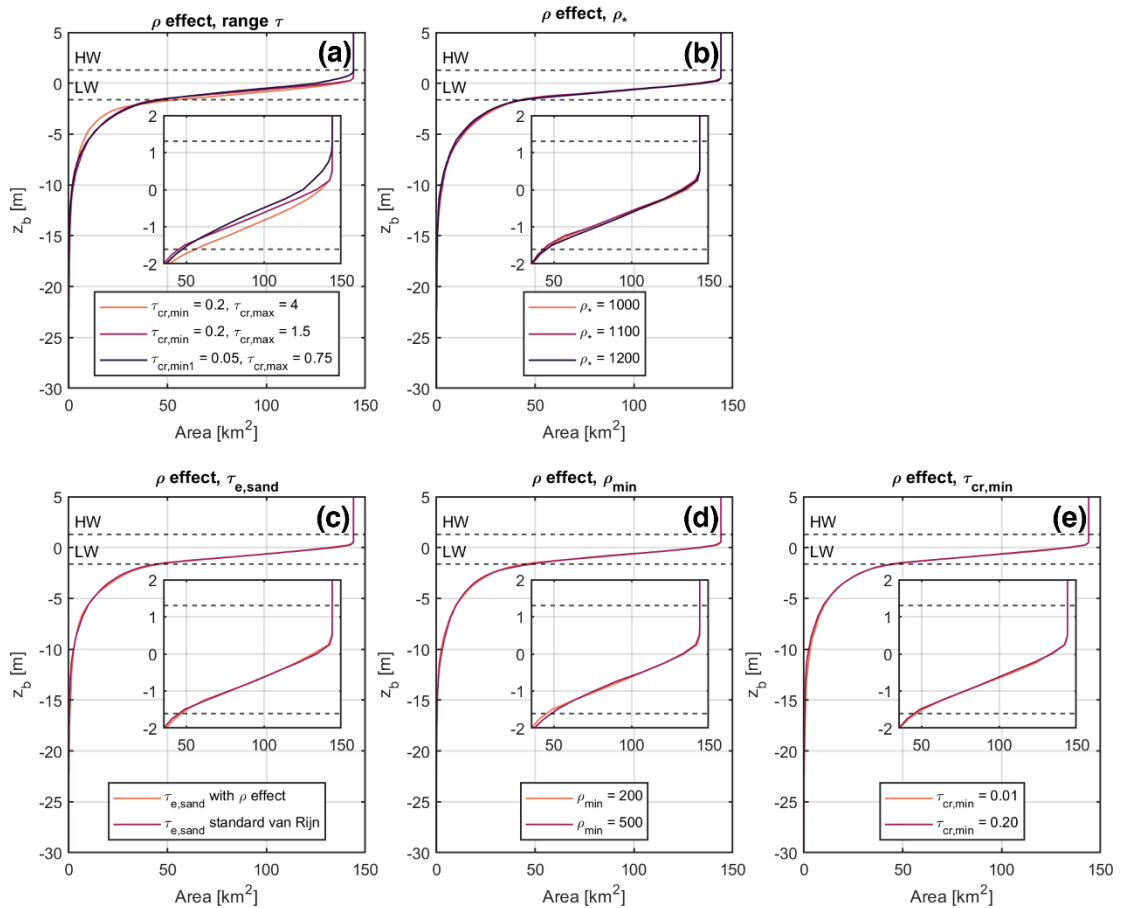

Figure 5-3 Sensitivity of the modelled hypsometry to the parameter settings of the density-erodibility formulation.

Modelling sand-mud dynamics in Delft3D

31 January 2024

MUSA

5.1.3 Sediment composition

The erodibility of the mud fraction has a significant effect on the sediment composition of the bed after 45 years of morphodynamic evolution. To further analyze this, we have determined the total area of 'sandy' (non-cohesive, $p_{mud} < 0.3$) beds, and that of 'muddy' beds (non-cohesive, $p_{mud} > 0.3$). Figure 5-4 shows the sandy and muddy subtidal areas for all scenarios, and Figure 5-5 shows the sandy and muddy subtidal areas.

First, we observe that the total intertidal area is approximately twice as large as the subtidal area. Secondly, the figures show that the relative variability in the sediment composition depending on the parameter setting is much larger in the subtidal than in the intertidal areas. Without accounting for density effects, subtidal areas become muddier with increasing $\tau_{cr,mud}$, while (especially in the scenario $\tau_{cr,mud}$, = 1 Pa) the intertidal areas become sandier. Overall, the variability obtained from the parameter settings in the simulations with density effects is smaller than that obtained from the simulations without this effect. The only exception herein is the (extreme) case of $\tau_{cr,max} = 4$ Pa, which significantly reduces the amount of muddy intertidal area.
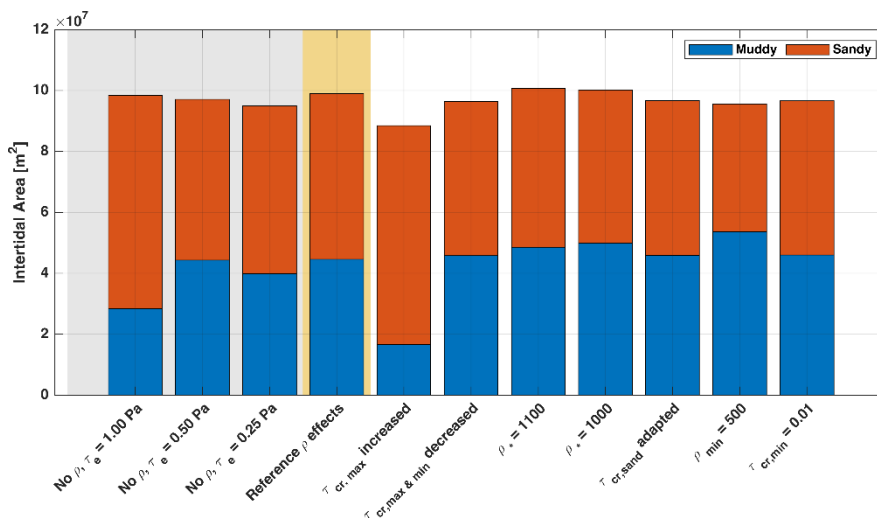

Figure 5-4 Sediment composition of the intertidal areas. The grey box indicates the scenarios without density effects, the yellow box indicates the reference scenario with density effects, to which the other scenarios have to be compared.
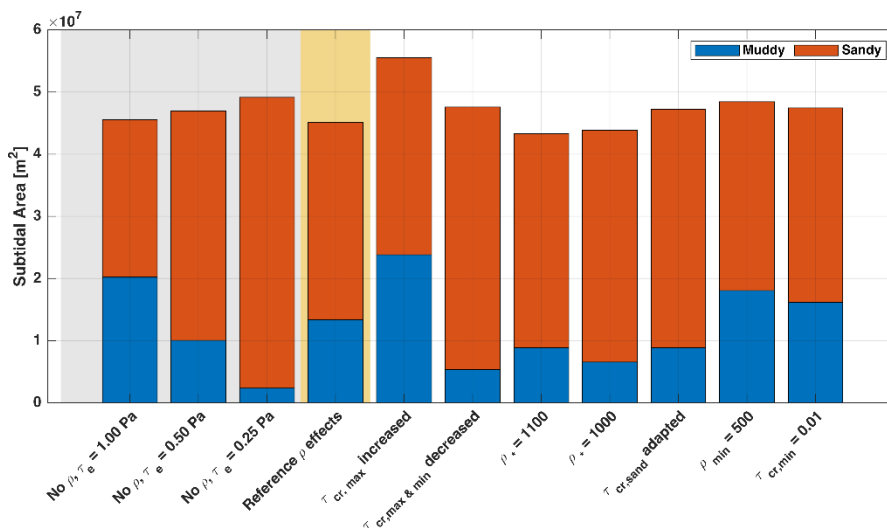

Figure 5-5 Sediment composition of the subtidal areas. The grey box indicates the scenarios without density effects, the yellow box indicates the reference scenario with density effects, to which the other scenarios have to be compared.

Modelling sand-mud dynamics in Delft3D

31 January 2024

Figure 5-6 shows the probability density function of the mud content in the upper bed after 45 years of evolution. The green histograms show the results of the scenarios without density effects and the grey ones of those with density effects. While simulations without density effects tend to have a sharp log-normal-resembling distribution (which is close to reality, see also Colina Alonso et al, (2022)), those with density effects have more evenly spread distributions, excluding the two extremes $p_{mud} = 0$ and of $p_{mud} = 1$. The most distinct case is that of the simulation with $\tau_{cr,min}$,$= 0.05$ Pa and $\tau_{cr,max}$,$= 0.75$ Pa where the pdf nearly approaches a normal distribution.
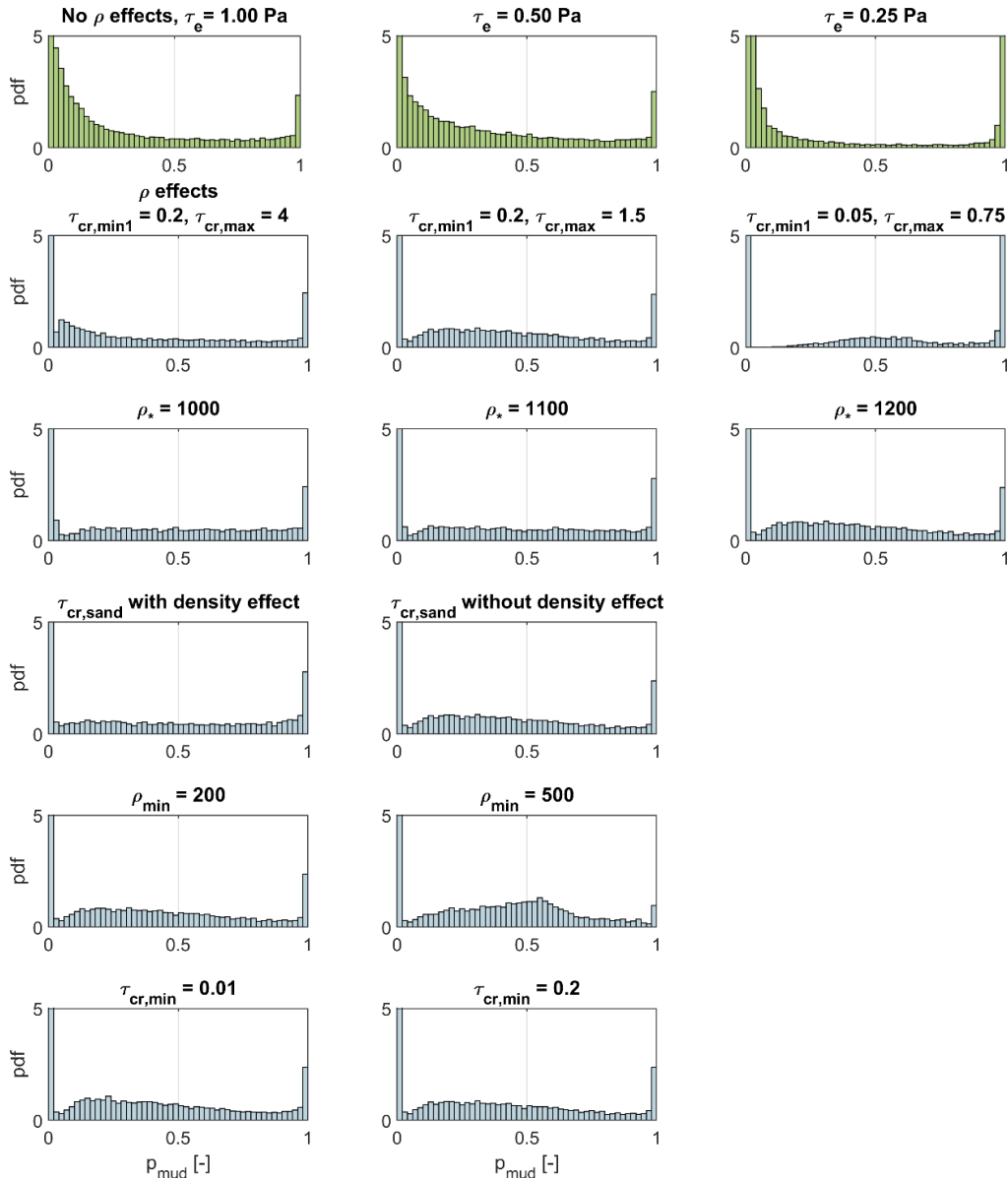

Figure 5-6 PDF of the mud content of the upper layer in the tidal basin (excluding the model domain offshore from the inlet), showing how often specific mud contents occur. The green histograms show the results of the scenarios without density effects and the grey ones of those with density effects (every row explores de results-sensitivity to a specific parameter of the formulations).

5.1.4 Overall sensitivity to parameter settings

To better understand the aforementioned results, we also analyze the computed critical bed shear stress and the occurrence of dry densities per scenario. These results are presented in Figure 5-7. We have seen that most of the results of the simulations with density-effects are fairly similar. This may be the case when the calculated dry-bulk densities, and therefore also the sediment erodibility, is comparable within all scenarios. Figure 5-7 shows however that there are clear differences (see for instance the histograms of $\rho_{min} = 200$ and $\rho_{min} = 500$), and that all densities (500-1600 kg/m^3) widely occur in all scenarios.

We also see that in most scenarios, $\tau_{cr,mud}$ increases to values between 0.5-1.5 Pa on the shoals, for which the mud on these shoals might be able to survive episodic storm events. In simulations without density effects, $\tau_{cr,mud}$ is user defined. When this value is set at 0.5 or even 0.25 Pa, the muddy areas are likely to be eroded during high-energy conditions. When it is set at 1 Pa, it might be able to survive these conditions, but another problem arises: this mud is so poorly mobile that it is difficult to be transported from the channels to the shoals, for which the channels remain muddy and the shoals are largely sandy.
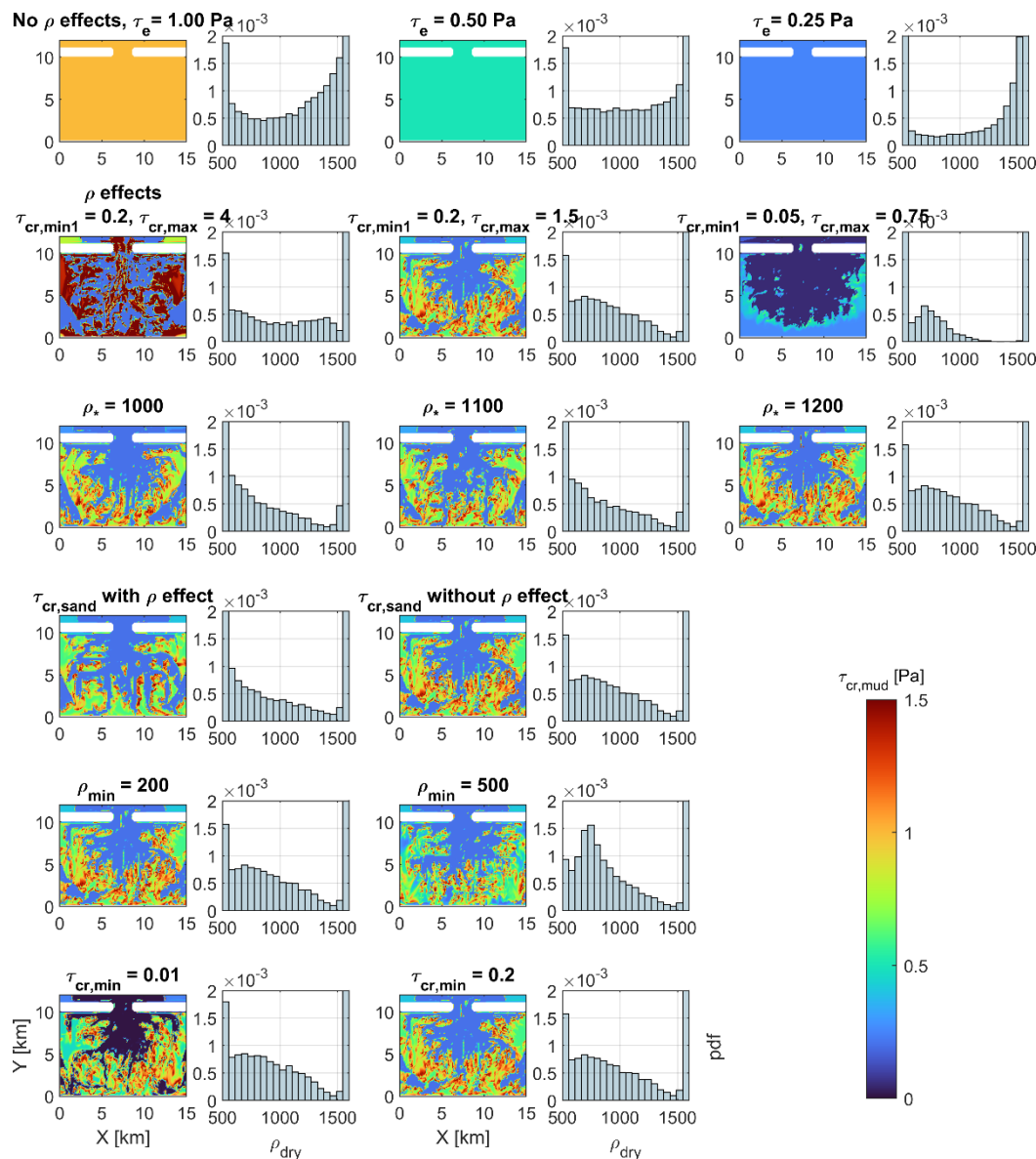

Figure 5-7 Left plots: overview of the critical bed shear stress of the mud fraction in the upper layer after 45 years per scenario (which depends on the sediment composition for the simulations with density effects, and is set at a uniform value at the simulations without these effects, see the first row). Right plots: PDF of the dry bed density of the upper layer in the tidal basin (excluding the model domain offshore from the inlet).

5.2 Response to storm conditions

5.2.1 Without density-erodibility dependence

As previously explained, modelling of morphodynamic evolution including storm conditions and mudflats often results in problems related to the erodibility of the mud fraction: modelling mudflat formation requires mud that is sufficiently mobile to be transported from the channels towards the flats, but this type of sediment is too easily eroded from the flats during storm conditions. An example of the latter is provided in Figure 5-8. Here, we observe that during the last 5 years of the morphodynamic evolution (when storm events are included in the simulations) mud is eroded from almost all flats. If storms were to be included for a longer period of time, eventually all mudflats would disappear (see Δp_{mud} in the right middle panel).
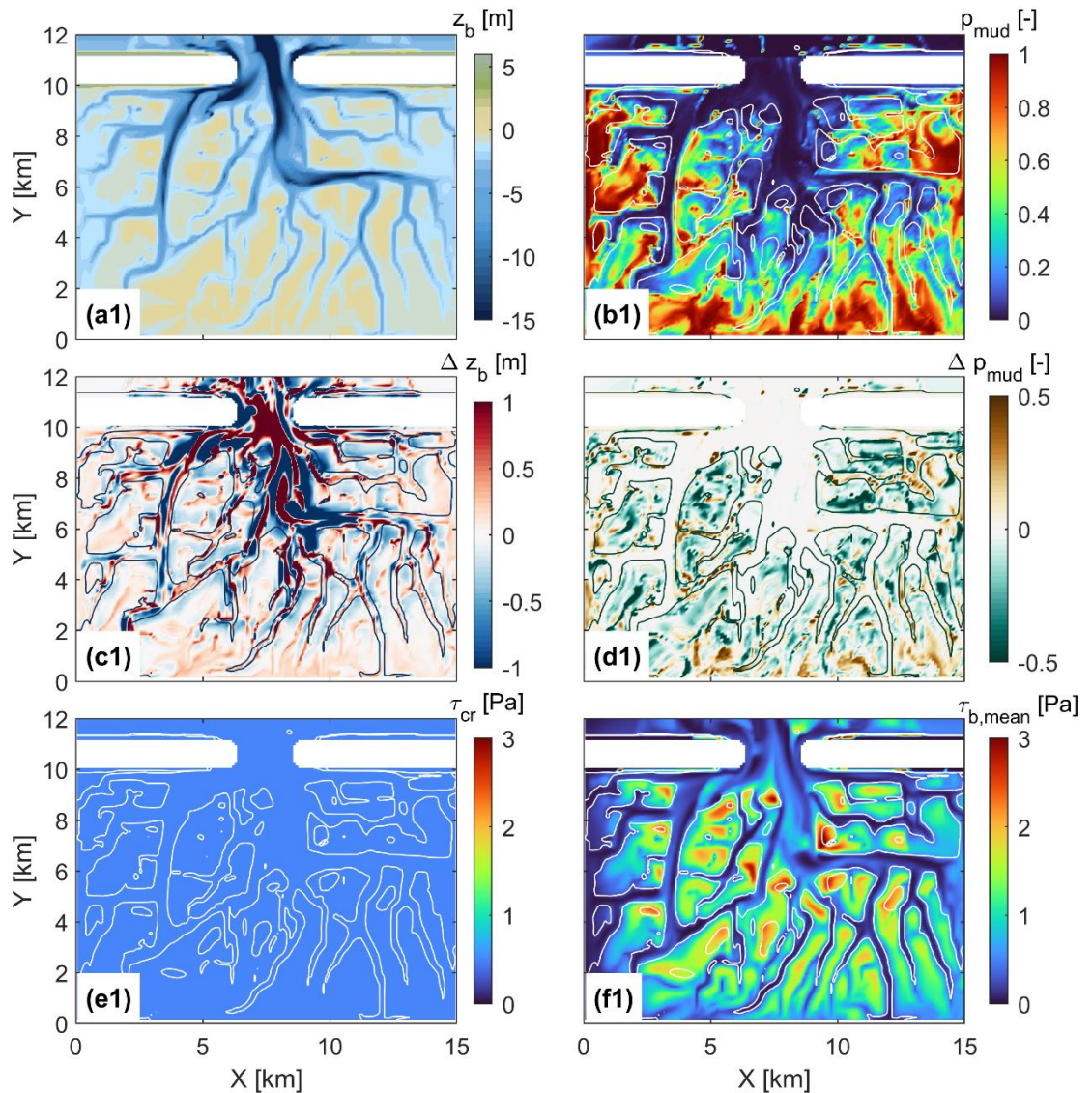

Figure 5-8 Morphodynamic evolution of a simulation without density effects, with $\tau_{cr,mud}$ = 0.5 Pa. Panels a1 & b1: bathymetry & sediment composition after 50 years (the last 5 years include storm events). Panels c1 & d1: difference in bathymetry (positive values in red mean sedimentation, negative values in blue show erosion) & mud content (of the upper 10 cm, positive values show an increase of p_{mud}, negative values show a decrease) after simulating 5 years with storm conditions. Panel e1: $\tau_{cr,mud}$ of the sediment bed, based on the sediment composition in panel b1. Panel f1: average bed shear stresses (of $\tau_{cr,max}$ in Delft3D) during the last 5 years. The contour lines show the bed level at z_b = 1.5 m.

5.2.2 With density-erodibility dependence

Applying the formulation for the density-erodibility formulation seems to largely improve the modelling results with regard to the aforementioned challenge. Figure 5-9 shows the results of a scenario with the standard settings. Even though some flats still erode under the modelled conditions, this is only locally and in general much less than in the simulation without density-erodibility dependence. This shows that the density-erodibility is a promising modelling tool.

Increasing $\tau_{cr,max}$ in the erodibility formulation further does not seem to result in much less mud erosion on the flats, as is shown in Figure 5-10 (with $\tau_{cr,max}$ = 4 Pa): local mud erosion on the flats still occurs, and moreover, mudflat formation is hampered by the immobility of the sediment such that muddy channels evolve.
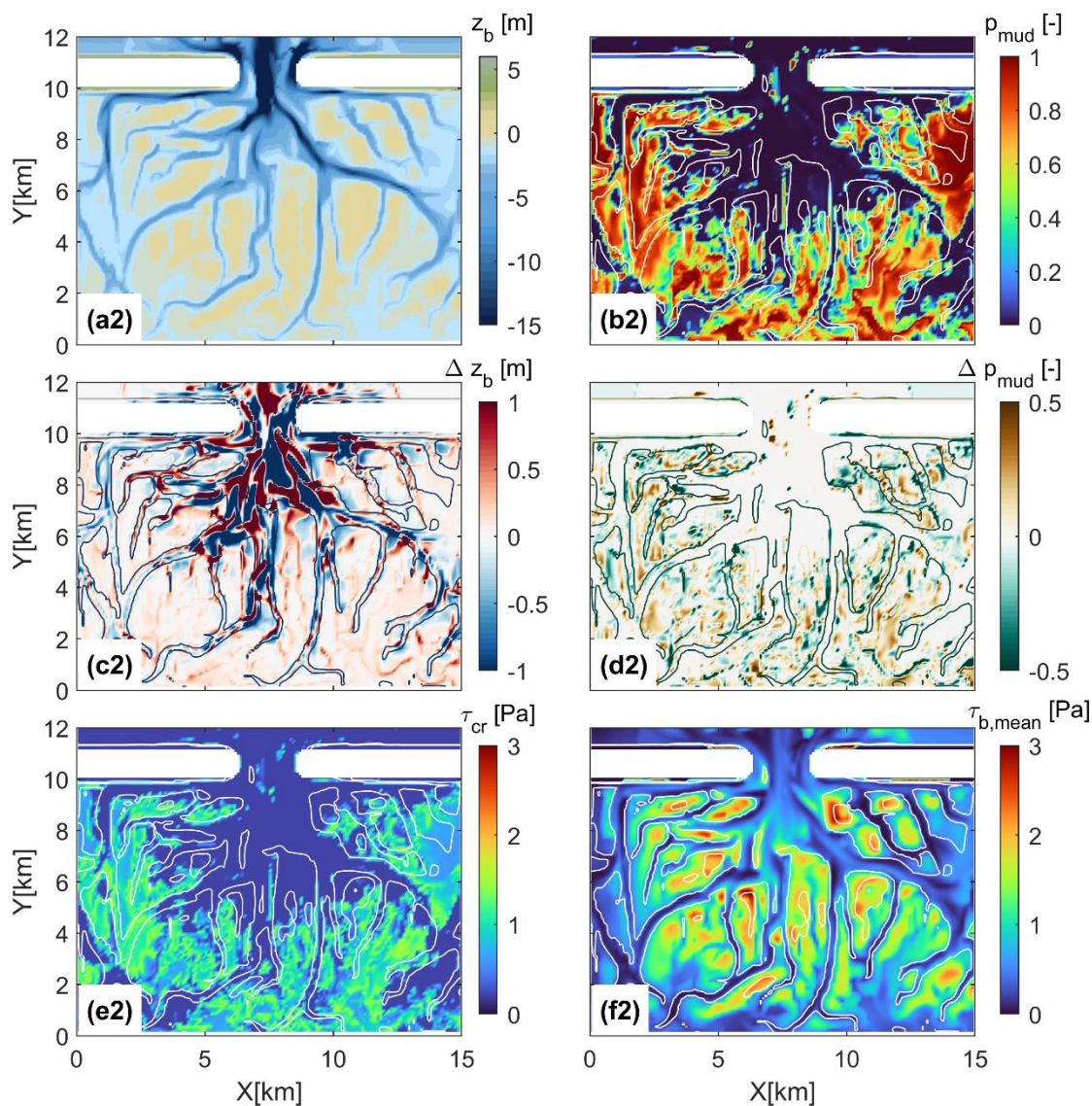

Figure 5-9 Morphodynamic evolution of a simulation with density effects, with the standard settings (among which: $\tau_{cr,max}$ = 1.5 Pa). Panels a2 & b2: bathymetry & sediment composition after 50 years (the last 5 years include storm events). Panels c2 & d2: difference in bathymetry (positive values in red mean sedimentation, negative values in blue show erosion) & mud content (of the upper 10 cm, positive values show an increase of p_{mud}, negative values show a decrease) after simulating 5 years with storm conditions. Panel e2: $\tau_{cr,mud}$ of the sediment bed, based on the sediment composition in panel b2. Panel f2: average bed shear stresses (of $\tau_{cr,max}$ in Delft3D) during the last 5 years. The contour lines show the bed level at z_b = 1.5 m.
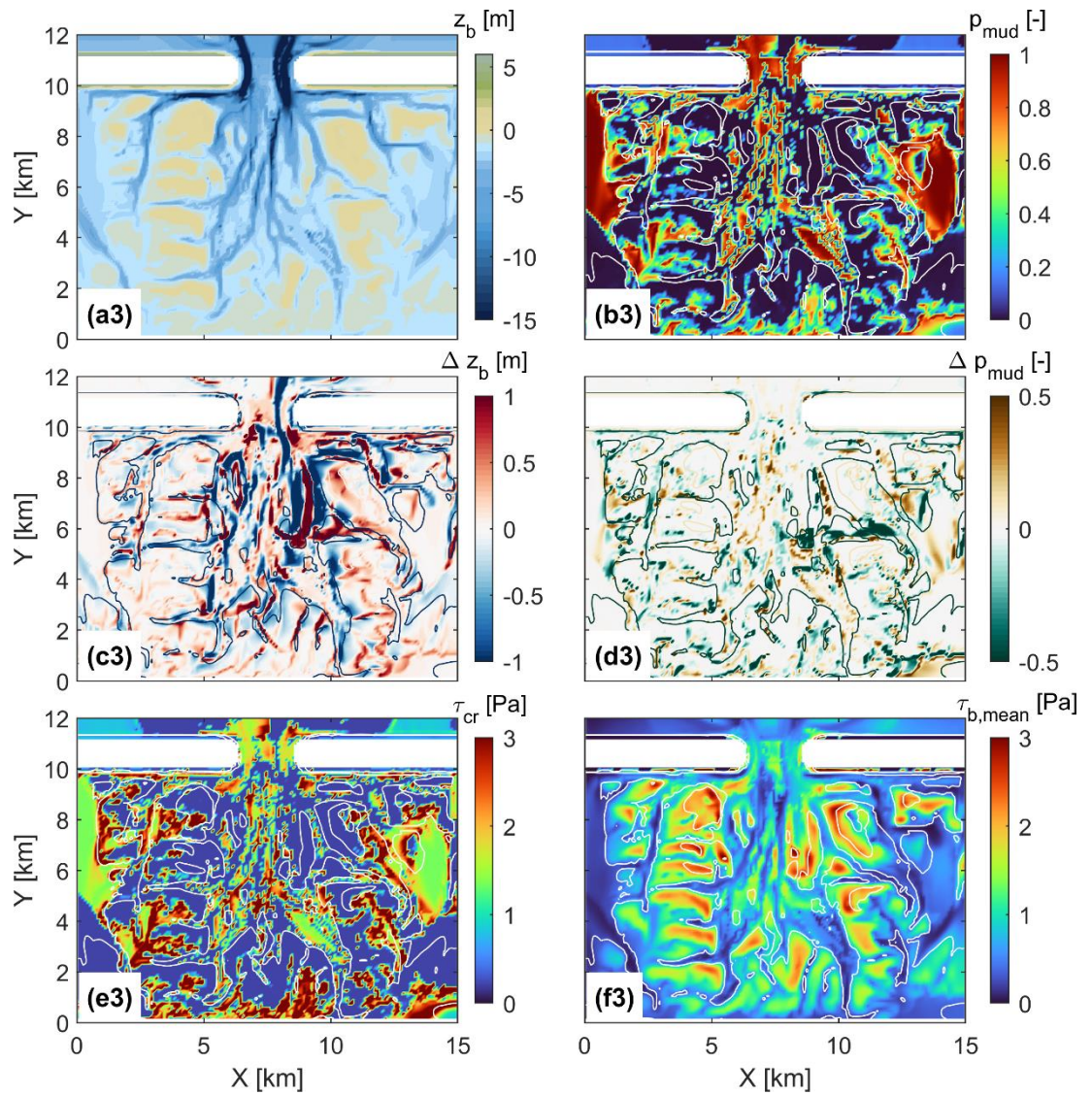
Modelling sand-mud dynamics in Delft3D

31 January 2024

Figure 5-10 Morphodynamic evolution of a simulation with density effects, with $\tau_{cr,max}$ = 4.0 Pa). Panels a3 & b3: bathymetry & sediment composition after 50 years (the last 5 years include storm events). Panels c3 & d3: difference in bathymetry (positive values in red mean sedimentation, negative values in blue show erosion) & mud content (of the upper 10 cm, positive values show an increase of p_{mud}, negative values show a decrease) after simulating 5 years with storm conditions. Panel e3: $\tau_{cr,mud}$ of the sediment bed, based on the sediment composition in panel b3. Panel f3: average bed shear stresses (of $\tau_{cr,max}$ in Delft3D) during the last 5 years. The contour lines show the bed level at z_b = 1.5 m.

Modelling sand-mud dynamics in Delft3D

31 January 2024

MUSA

6 Discussion

6.1 Modelling the erosion of sand-mud mixtures in Delft3D

Often, morphodynamic models that include both sand and mud calculate the erosion, transport and deposition of both sediment types separately and independently, despite overwhelming evidence that erosion of sand and mud is mutually coupled (Jacobs, 2011; Torfs, 1995; van Ledden, 2003; van Rijn, 2020). In this report, we have explored what the effects are of including erosion interaction in the digital flume. This interaction implies that sand and mud interact in the sediment matrix of the sediment bed, and therefore their erosion is coupled. Depending on the sediment composition, a sand-mud mixture can be non-cohesive, in which erosion is defined by the sand skeleton, or cohesive, in which the mud matrix determines the erosive behavior of the mixture. Erosion interaction is implemented in Delft3D using van Ledden's (2003) formulation (with a slight deviation from it, as presented by van Kessel et al, 2012).

In the digital flume model, we aimed at reproducing the findings of the long-bed experiments. We learned from the analysis of these experiments that under the same hydrodynamic conditions, erosion rates are smaller for mixtures with higher mud contents. Our results presented in Chapter 4 show that in order to reproduce this behavior in the numerical simulations, it is necessary to include erosion interaction in the model set-up. Models that calculate sand and mud transport independently, fail to reproduce this behavior (and actually predict the opposite).

Including erosion interaction in simulations however has a potential downside: applying the van Ledden (2003) formulations may lead to an overestimation of the erosion rate of cohesive mixtures. This is especially the case when the overall mud erodibility (i.e., M parameter) is low. Calibration of the erosion rates with field measurements is usually difficult, as it is hard to measure the erosion rate (in the field). Users of the Van Ledden interaction model are therefore recommended to perform a sensitivity study of the model results to the sand-mud interaction, especially in case the M parameter is low (< 10^{-4} kg/m^2/s).

Sand-mud erosion interaction can also be applied to long-term simulations, for instance to predict coastal/estuarine morphodynamic behavior. The effect of these formulations on long-term predictions is out of the scope of this report, but has been documented in detail by Colina Alonso, et al. (2023). Here, it was concluded that including erosion interaction in sand-mud modelling studies is key to correctly reproduce specific characteristics of the sediment bed composition ('*bimodality*'). Moreover, an application of this interaction type to a real-life case in the Ems-Dollard estuary is presented by Arcadis (2023).

Erosion interaction is not the only type of sand-mud interaction that affects the erosion rates of sand-mud mixtures. Sand and mud also interact via *roughness interaction.* Roughness interaction implies that the sediment composition affects the hydraulic roughness of the sediment bed and therefore also the near-bed turbulence and thus the bed-shear stresses. Sandy beds are rougher, generate more turbulence and therefore the bed-shear stresses exerting on these beds are larger than those on muddy beds under the same hydrodynamic conditions. The effect of this type of interaction has not been explored in the digital flume environment in this report. However, it has been previously implemented in Delft3D and its functionality has been tested (see Colina Alonso, et al., 2020 for the guidelines on how to use this in a Delft3D model set-up). It's effects on long-term morphodynamic evolution are presented in Colina Alonso, et al. (2023).

6.2 Modelling erodibility as function of the dry bed density

Results of the short bed flume experiments show that the erodibility of sand-mud mixtures may highly vary depending on the dry bulk density of the sediment mixture. Using this relation in morphodynamic models is complicated by the fact that the dry bed density is often not computed, as it requires to include the sediment consolidation processes. Detailed consolidation models that best resemble reality are computationally expensive, which limits their applicability (especially for the long-term, which is the timescale at which these processes play a role), although simple approached based on rough estimates are possible.

As an alternative, we have implemented a rough estimate of the dry bulk density based on the local mud content in Delft3D (increasing density for a decreasing mud content and increasing sand content). Using the estimated dry bed density, we adopted the relation between the dry bed density and the erodibility of sand-mud mixtures that followed from the flume experiments in the MUSA in Delft3D. This relation basically shows that, starting from pure sand mixture, the erodibility of the mixture decreases with increasing mud content (decreasing density), up to a maximum that is reached around 20-30% of mud, after which it decreases again.

We have seen that applying the implemented density-erodibility dependence in Delft3D enables modelling mudflat formation and mudflat survival during/after storm conditions. This survival is something that has also been observed in the Wadden Sea. Without accounting for the density-erodibility dependence, mudflats may evolve, but are also easily eroded during medium/high energetic condition.

This approach, in which consolation effects are still ignored, thus seems successful in modelling applications of dynamic systems, in which pure mud (p_{mud}~100%) does not get the chance to consolidate over longer periods of time and gain significant strength (since in our application pure mud is still very easy to erode, see Figure 2-9). It is however probably not valid for very low-energy tidal flats with very short inundation periods and frequency. Nevertheless, it is a very promising tool for modelling morphological evolution of sand-mud systems as the Wadden Sea, where storms regularly occur. The physical explanation behind the implemented formulations remains limited, and more (and more extensive) experiments will be needed to improve this.

It is important to note that in this approach, the variability in density (and therefore also of τ_{cr}) is fully attributed to the variability in sediment composition, while in reality also other mechanisms play a role. In mud-dominated environments, τ_{cr} can also largely change by consolidation, compaction and (on inter- and supratidal flats) even drying. This would probably result in a similar spatial behavior of the morphodynamic evolution, but it is still to be tested in future research.

6.3 Relevance of sand-mud modelling in engineering projects

Sand-mud modelling, including the approaches and formulations that have been used in this report, is relevant to a wide spectrum of engineering projects. Several examples are listed below.

- Erosion and strength of the sediment bed:
  - The sediment composition largely alters the erosive behavior of the sediment. We have seen that in general a muddier mixture will have lower erosion rates (in terms of $kg/m^2/s$ or m^3/s). To correctly predict this, one should make use of an erosion-interaction model such as the one by van Ledden (2003).
  - The threshold at which erosion takes place may be relevant to for instance determine the strength of mud in navigation channels. We have seen that this threshold depends on the dry bulk density, which can be estimated based on the mud fraction.
  - The stability of the bed (which depends on the aforementioned mechanisms) may also be very relevant to determine habitat suitability in environmental assessment studies.
- Dredging plumes:
  - If muddy sediment plumes are deposited on top of a sandy bed, accounting for sand-mud interaction is only relevant in case the mud is being mixed into the sandy layer.
  - The magnitude of bed composition change for a given amount of deposition depends strongly on the imposed active/mixing layer height in the model. We therefore advise to perform a sensitivity analysis on this parameter in future studies.
  - When a dredging plume also contains a (fine) sand fraction, this fraction can largely affect the strength of the sediment deposits and its erosive behavior (in terms of erosion rate for instance). This strongly depends on whether sand-mud segregation occurs (prior to deposition).

Modelling sand-mud dynamics in Delft3D

31 January 2024

7   Concluding remarks

This report has focused on the reproduction and application of two main results of earlier MUSA phases in numerical models. Part 1 focused on sand-mud erosion rates derived from the long bed experiments and Part 2 on the dependence of sediment erodibility on the dry bulk density, as derived from the short bed experiments. In this chapter, we summarize the findings in the following conclusions:

Part 1: sand-mud erosion rates

- Suspended sediment concentrations (SSC) in the flume were measured during the flume experiments by an OBS. Based on these measurements (and specifically the increase in SSC over time), erosion rates were determined for different hydrodynamic forcing and different bed samples. An inverse relation was found between the erosion rates and the mud content in the sediment bed.
- The long bed experiments have been reproduced in a digital flume in Delft3D. Hydrodynamic conditions are correctly reproduced by the digital flume.
- The model simulations show that in contrast to suspended sand concentrations, which reach an equilibrium concentration within a short time span, suspended mud concentrations build up over time. The timing and sequence at which measurements are taken therefore largely influences the measured concentrations. Erosion rates can thus only be estimated based on continuous measurements of the concentration and not based on samples that are occasionally taken.
- In order to reproduce the erosive behavior of sand-mud mixtures in the flume, in which the erosion rate decreases with increasing mud content, one must include erosion interaction (van Ledden's model, 2003) in the model set-up.

Part 2: density-erodibility dependence

- We used a relation between the dry-bulk density of the sediment and the critical bed shear stress for erosion based on the results of short bed erosion experiments (Boechat Albernaz et al., 2022; van Rijn et al., 2023b). Starting from purely sandy bed (p_{mud} = 0%, ρ=1600 kg/m^3) the strength of the bed increases with increasing mud content (so the critical bed shear stress increases) up to a certain point (around $\rho \approx$1200 kg/m^3), after which it decreases again. This means that sand-mud mixtures tend to be less erodible than purely sandy or purely muddy mixtures. Note that in reality, also other processes influence the dry bed density (such as consolidation) and that while the derived relation generally holds, exceptions may occur.
- This formulation was implemented in Delft3D. Since the dry-bed density is not determined by Delft3D as long as there is no (computationally expensive) consolidation model being used, the dry-bed density is determined by a simplified formulation based on the sediment composition (in terms of p_{mud} and p_{sand}).
- The performance of this formulation was evaluated in a schematized model of a tidal inlet.
- The implemented density-erodibility formulation enables modelling mudflat formation and evolution, even when periodic storm events occur.
- When we do not account for this dependency, but instead we specify a single constant critical bed shear stress for mud erosion, it is not possible to correctly model mudflat formation and survival under storm conditions:
  - When the critical bed shear stress is low, mudflats evolve, but they are easily eroded and disappear during storms;
  - When the critical bed shear stress is high, mudflats can survive storms, but their formation is hard to model, since the mud is so immobile that it largely remains in the channels (leaving them muddy, while the intertidal flats are sandy).

MUSA

References

Arcadis (2023). Applying the Van Ledden formulation. An Ems-Dollard estuary case study (PPT presentation, 24 november 2023).

Boechat Albernaz, M., van Rijn, L., Schoonhoven, D. & Perk, L. (2022). Results of laboratory experiments; Results Phase 1A & B. MUSA report 11204950_TKI-MUSA_01AB.

Boechat Albernaz, M., van Rijn, L., Schoonhoven, D. & Perk, L. (2023a). Results of flume laboratory experiments; Results of Phase 1C + 1D with combined waves and currents. MUSA report 11204950_TKI-MUSA_03A.

Boechat Albernaz, M., van Rijn, L., Schoonhoven, D. & Perk, L. (2023b). Results of MUSA field measurement campaigns at Holwerd, the Netherlands. MUSA report 11204950_TKI-MUSA_02B_v2.

Colina Alonso, A., van Weerdenburg, R., van Maren, B. & Huismans, Y. (2020). Modelling sand-mud interaction in Delft3D. Deltares report 11205286-010-ZWS-0001.

Colina Alonso, A., van Maren, D. S., Herman, P. M. J., van Weerdenburg, R. J. A., Huismans, Y., Holthuijsen, S. J., et al. (2022). The existence and origin of multiple equilibria in sand-mud sediment beds. Geophysical Research Letters, 49, e2022GL101141. https://doi.org/10.1029/2022GL101141

Colina Alonso, A., van Maren, D. S., van Weerdenburg, R. J. A., Huismans, Y., & Wang, Z. B. (2023). Morphodynamic modeling of tidal basins: The role of sand-mud interaction. *Journal of Geophysical Research: Earth Surface*, 128, e2023JF007391. https://doi.org/10.1029/2023JF007391.

Colosimo, I., van Maren, D. S., de Vet, P. L. M., Winterwerp, J. C., & van Prooijen, B. C. (2023). Winds of opportunity: The effects of wind on intertidal flat accretion. *Geomorphology*, 108840. https://doi.org/10.1016/j.geomorph.2023.108840

Jacobs, W. (2011). *Sand-mud erosion from a soil mechanical perspective* (PhD thesis). Delft University of Technology.

Jacobs, W., Le Hir, P., Van Kesteren, W., & Cann, P. (2011). Erosion threshold of sand-mud mixtures. Continental Shelf Research, 31, S14–S25. doi:10.1016/j.csr.2010.05.012

Le Hir, P., Cayocca, F., & Waeles, B. (2011). Dynamics of sand and mud mixtures: A multiprocess-based modelling strategy. Continental Shelf Research, 31, 135–149. doi: 10.1016/j.csr.2010.12.009

Mitchener, H., & Torfs, H. (1996). Erosion of mud/sand mixtures. Coastal Engineering, 29 (1-2), 1–25.

Scheel, F., Van Ledden, M., van Prooijen, B., & Stive, M. (2012). Simulating the large-scale spatial sand-mud distribution in a schematized process-based tidal inlet system model. NCK-days 2012 : Crossing borders in coastal research : jubilee conference proceedings, 2-6.

Soulsby, R., & Clarke, S. (2005). *Bed Shear-stresses Under Combined Waves and Currents on Smooth and Rough Beds.* Defra project FD1905 (EstProc), Report TR 137.

Torfs, H. (1995). *Erosion of mud/sand mixtures* (PhD thesis). University of Leuven.

Van Kessel, T. (1997). *Generation and Transport of Subaqueous Fluid Mud Layers* (PhD Thesis). Delft University of Technology.

Van Kessel, T., Spruyt-de Boer, A., van der Werf, J., Sittoni, L., van Prooijen, B., & Winterwerp, H. (2012). Bed module for sand-mud mixtures, in framework of BwN project NTW 1.3 mud dynamics. Deltares report 1200327-000-ZKS-0012.

van Ledden, M. (2003*). Sand-mud segregation in estuaries and tidal basins* (PhD thesis). Delft University of Technology.

Van Ledden, M., van Kesteren, W. G., & Winterwerp, J. C. (2004). A conceptual framework for the erosion behaviour of sand–mud mixtures. *Continental Shelf Research 24.*

van Ledden, M., Wang, Z. B., Winterwerp, H., & de Vriend, H. (2006). Modelling sand-mud morphodynamics in the Friesche Zeegat. *Ocean Dynamics*, 56(3-4), 248–265. https://doi.org/10.1007/s10236-005-0055-9

Van Rijn, L. (1993). Principles of Sediment Transport in Rivers, Estuaries and Coastal Seas. *Aqua Publications, The Netherlands*.

Van Rijn, L.C., Colina Alonso, A. & Manning, A. J., (2020). Literature review on sand and mud. TKI MUSA project. Report 11204950-001-ZKS-0002

Van Rijn, L.C., Walstra, D.J.R. & van Ormondt, M. (2004). Description of TRANSPOR2004 and Implementation in Delft3D-Online. WL | Delft Hydraulics report Z3748.10.

Van Rijn, L. (2007). Unified View of Sediment Transport by Currents and Waves. I: Initiation of Motion, Bed Roughness, and Bed-Load Transport. *Journal of Hydraulic Engineering, 133*(6), 649-667.

van Rijn, L. C. (2020). Erodibility of mud-sand bed mixtures. *Journal of Hydraulic Engineering*, 146(1), 1–19. https://doi.org/10.1061/(ASCE) HY.1943-7900.0001677

Rijn, L.C. (2023). SEDCON-model: sediment concentrations and transport due to current and waves. LVRS memo dated 5 March 2023 (www.leovanrijn-sediment.com)

Van Rijn, L.C., van Maren, D.S., van Weerdenburg, R.J.A., Ton, A.M. & Boechat Albernaz, M. (2023b). Synthesis of MUSA experiments, measurements and modelling. MUSA report 11204950_TKI-MUSA_05.

Winterwerp, J. C., & van Kesteren, W. G. M. (2004). Introduction to the physics of cohesive sediment in the marine environment. Amsterdam: Elsevier.

Winterwerp, J. C., W. G. M. van Kesteren, B. van Prooijen, and W. Jacobs (2012), A conceptual framework for shear flow–induced erosion of soft cohesive sediment beds, J. Geophys. Res., 117, C10020, doi:10.1029/2012JC008072

Winterwerp, J.C., Zhou, Z., Battista, G., van Kessel, T., Jagers, H. R. A., van Maren, D.S., and van der Wegen, M. (2018). Efficient Consolidation Model for Morphodynamic Simulations in Low-SPM Environments, Journal of Hydraulic Engineering,144 (8), doi:10.1061/(ASCE)HY.1943-7900.0001477

Zhou, Z., M. Van der Wegen, B. Jagers, and G. Coco. 2016. "Modelling the role of self-weight consolidation on the morphodynamics of accretional mudflats." Environ. Modell. Software 76: 167–181. https://doi.org/10 .1016/j.envsoft.2015.11.002.
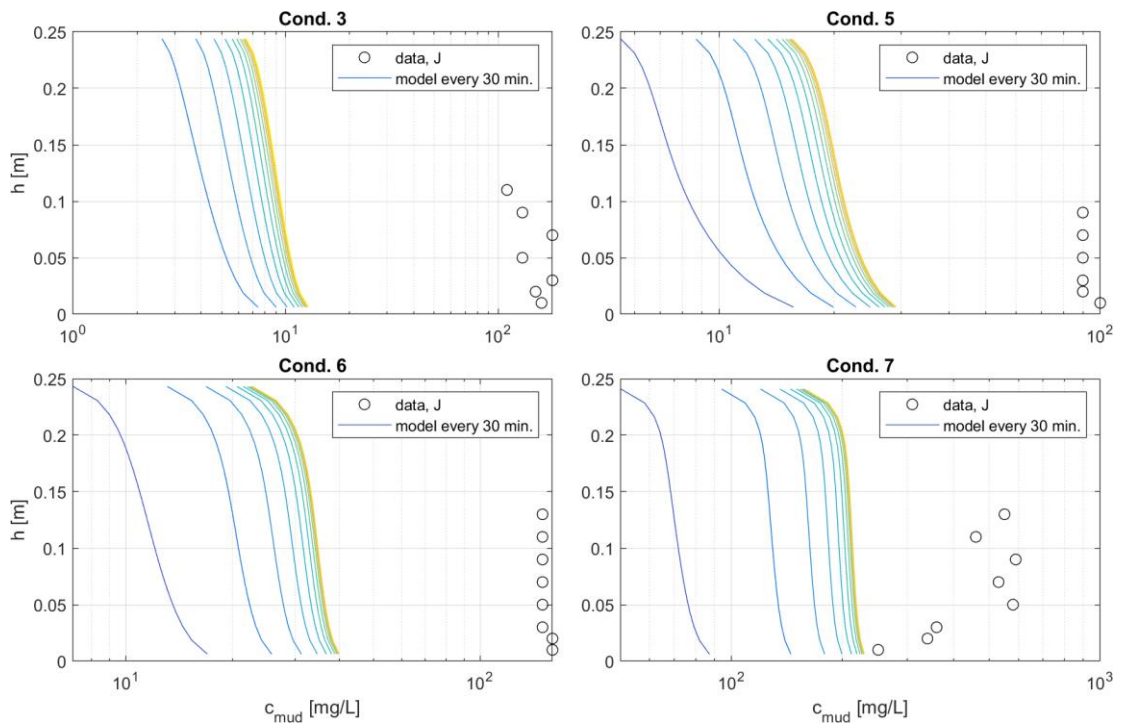
MUSA

A   Mud concentration profiles

Figure A-1 Computed and measured mud concentration profiles, sample J ($p_{mud} = 0.12$), without sand-mud interaction, with $β = 3$.

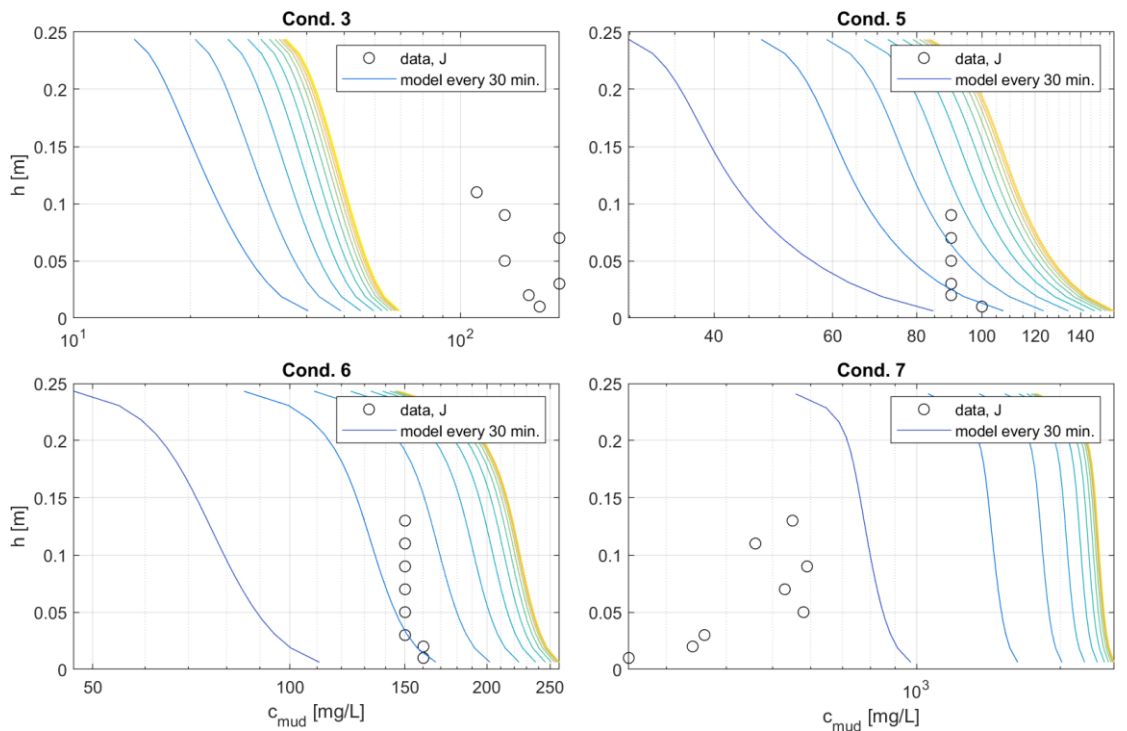*Figure A-2 Computed and measured mud concentration profiles, sample J ($p_{mud} = 0.12$), with sand-mud interaction, with $p_{m,crit} = 0.12$ and $β = 1$.*
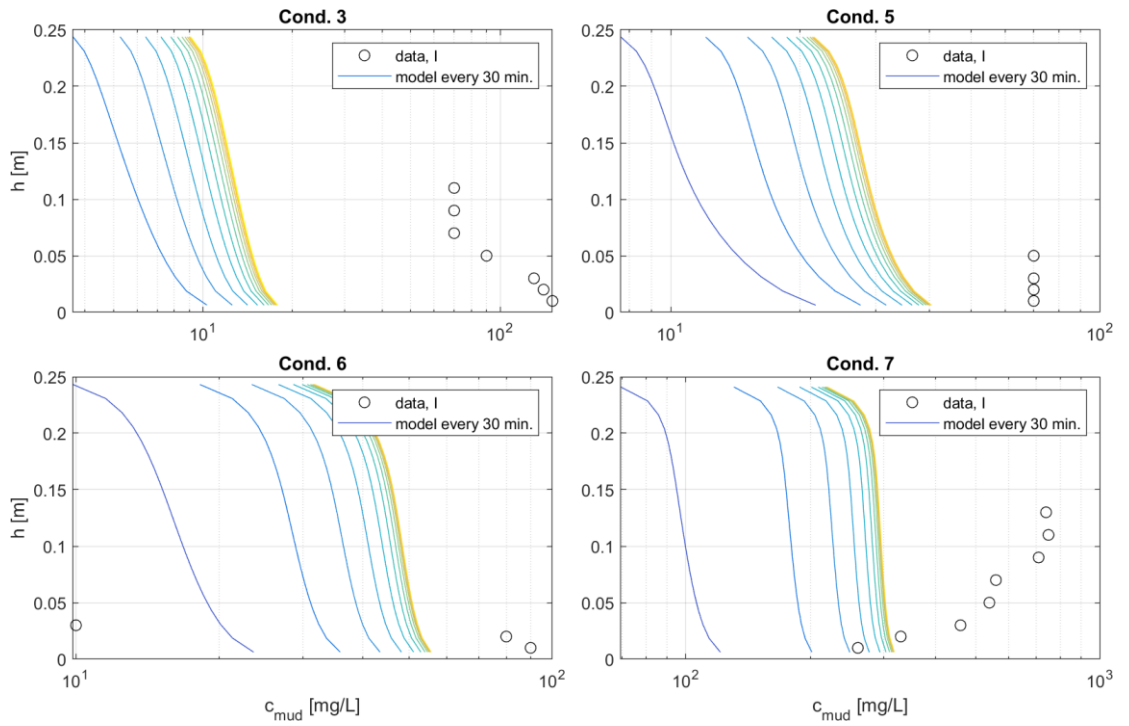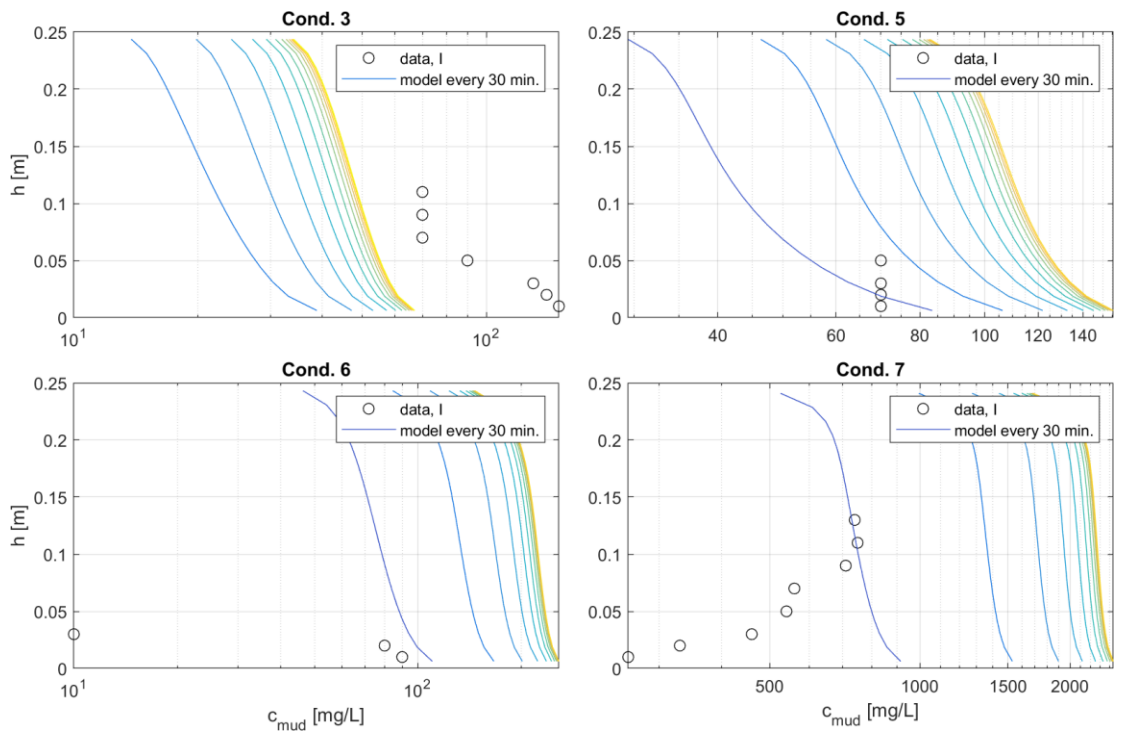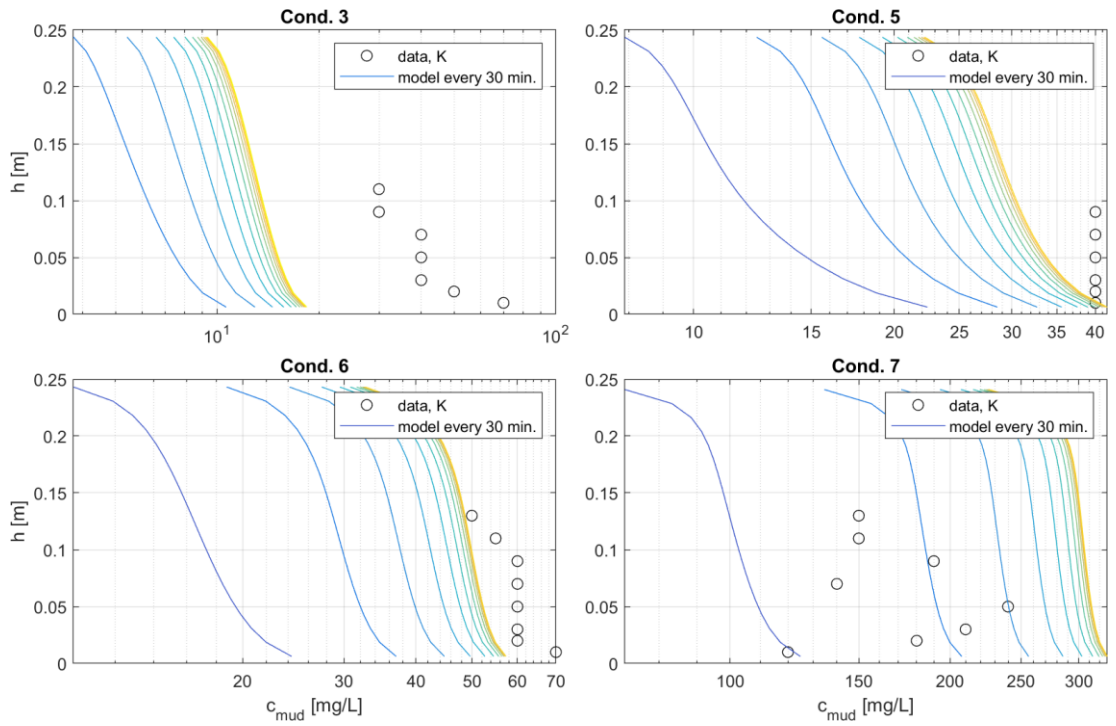
Modelling sand-mud dynamics in Delft3D

31 January 2024

Figure A-3 Computed and measured mud concentration profiles, sample I (p_{mud} = 0.18), without sand-mud interaction, with β = 3.

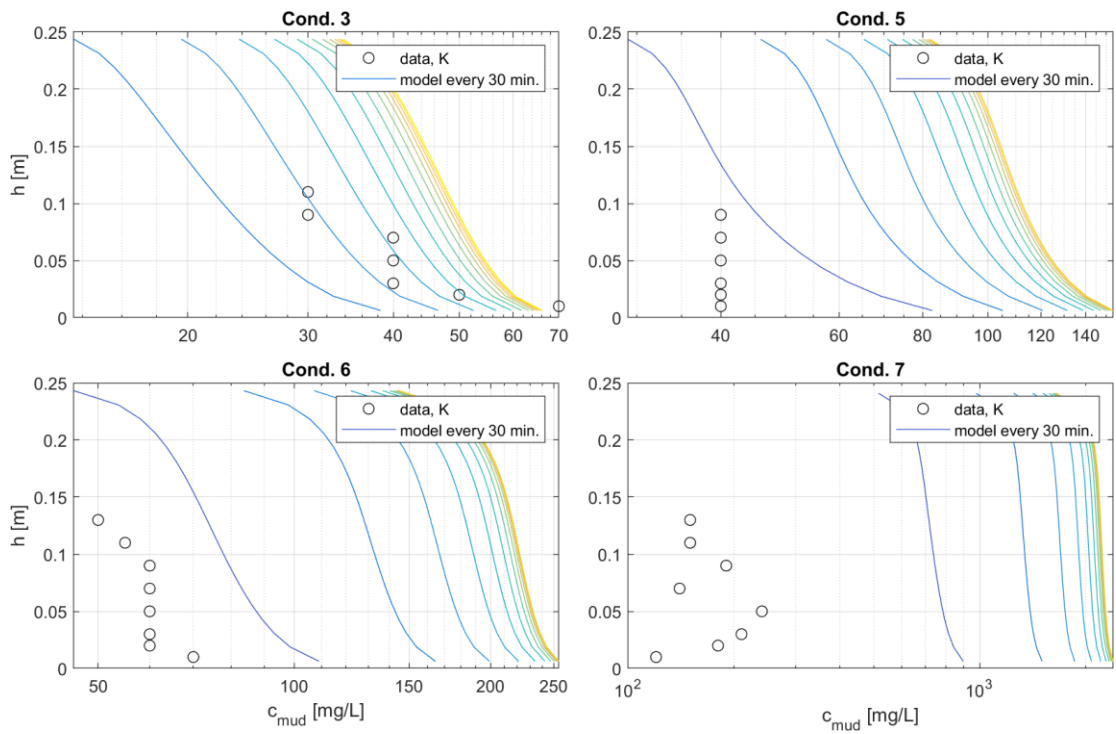*Figure A-4 Computed and measured mud concentration profiles, sample I (p_{mud} = 0.18), with sand-mud interaction, with $p_{m,crit}$ = 0.12 and β = 1.*

Modelling sand-mud dynamics in Delft3D

31 January 2024

MUSA

Figure A-5 Computed and measured mud concentration profiles, sample K ($p_{mud} = 0.3$), without sand-mud interaction, with $β = 3$.

Figure A-6 Computed and measured mud concentration profiles, sample K ($p_{mud} = 0.3$), with sand-mud interaction, with $p_{m,crit} = 0.12$ and $β = 1$.

Modelling sand-mud dynamics in Delft3D
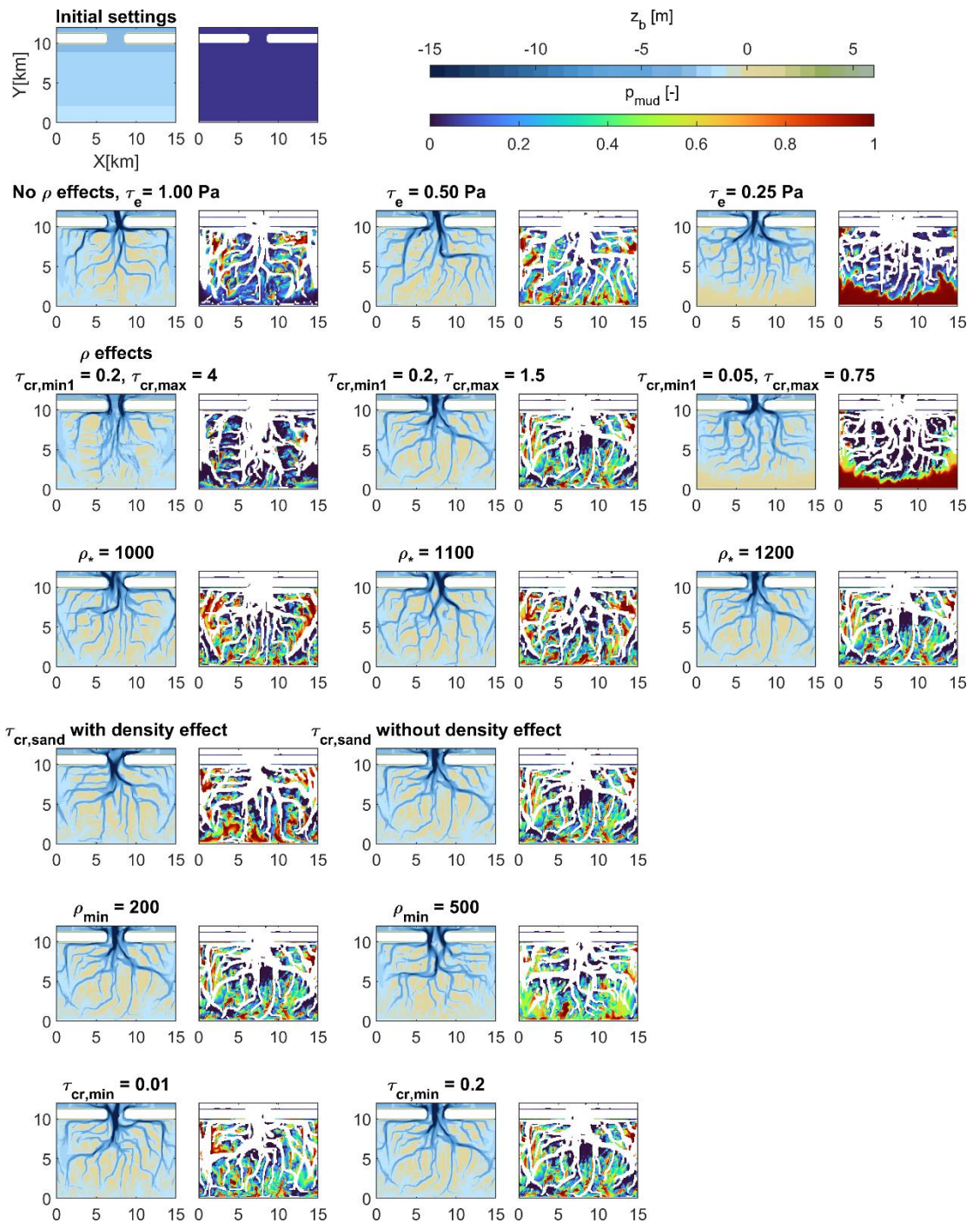
31 January 2024

MUSA

Figure B-1 Computed bed levels in the digital tidal basin and sediment composition of the intertidal areas.
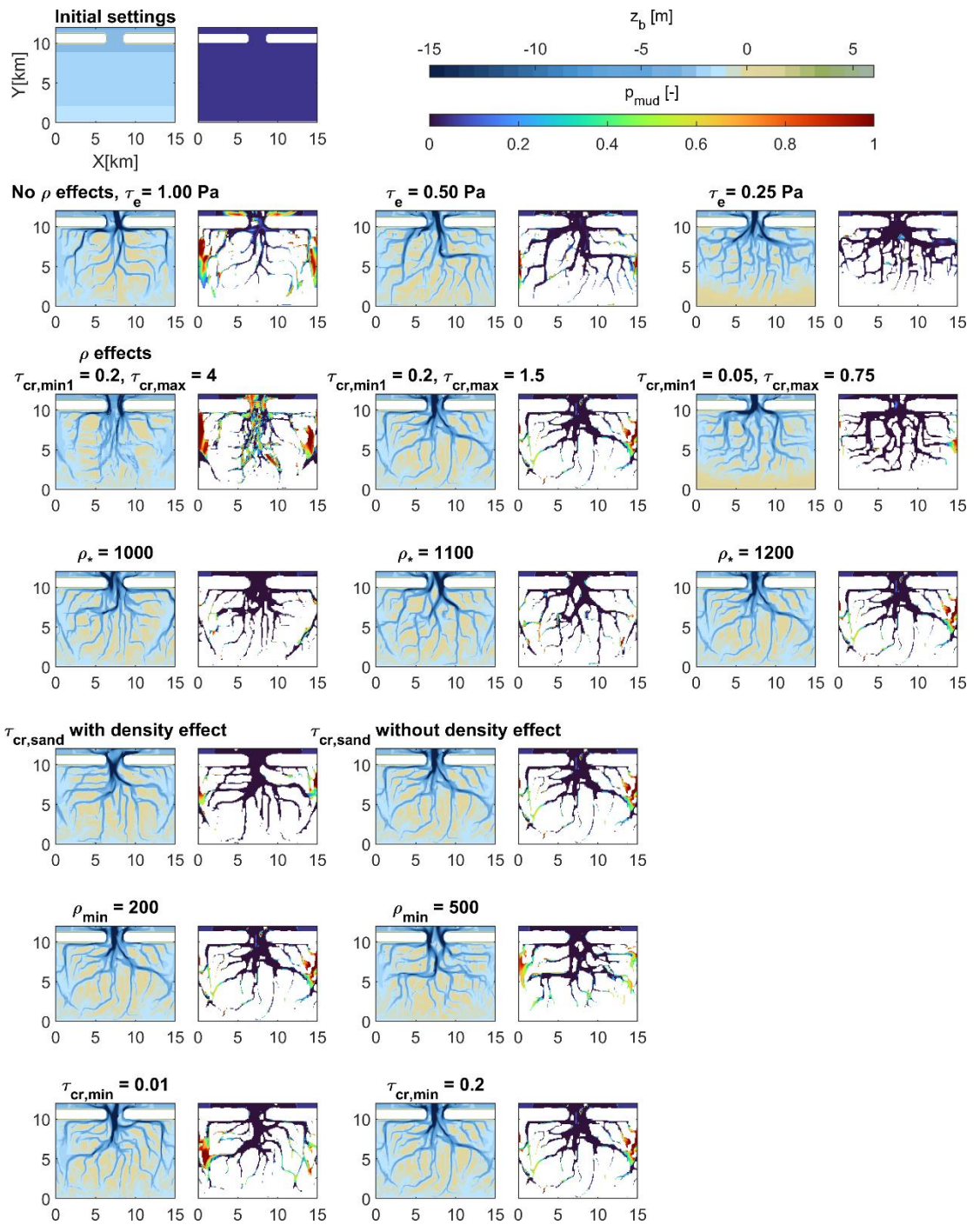
Figure B-2 Computed bed levels in the digital tidal basin and sediment composition of the subtidal areas.

Modelling sand-mud dynamics in Delft3D

31 January 2024

MUSA